Available online at www.sciencedirect.com
SCIENCE DIRECT®
Progress in Materials Science 49 (2004) 713–786
Progress in Materials Science
www.elsevier.com/locate/pmatsci

Influence of interfaces on thin polymer film behaviour

D.G. Bucknall *

Department of Materials, University of Oxford, Parks Road, Oxford, Oxon OX1 3PH, UK

Abstract

In many ways interfaces and surfaces dominate the behaviour of not only bulk polymers but also thin film behaviour. The critical nature that the interface plays on numerous physical properties has stimulated significant effort to understand such behaviour. A number of theoretical models, particularly using mean-field approximations, have been developed to predict critical parameters associated with these interfaces and surfaces. Only with the advance of a number of powerful techniques have the finer details of such theories been able to be critically tested. This paper reviews both the relevant theories and experimental work associated with predominantly polymer–polymer interfaces, with particular emphasis on capillary waves, dewetting, patterning, diffusion and adhesion.

Contents

* Tel.: +44-1865-273-763; fax: +44-1865-273-764.
E-mail address: david.bucknall@materials.oxford.ac.uk (D.G. Bucknall).

0079-6425/$ - see front matter © 2003 Elsevier Ltd. All rights reserved.
doi:10.1016/S0079-6425(03)00038-0

1. Introduction

Polymer surfaces and interfaces play an essential role in many commercial applications of polymers, such as coatings, adhesives, blends, packaging and resists. Understanding the molecular processes taking place at interfaces is, therefore, increasingly important for the wide ranging uses of polymers. For example, the properties of composite materials are dominated by the structure of the interfaces between their constituents, since the interfaces between different phases are more susceptible to deformation, fracture and chemical reactions. In many cases the success of the use of a polymeric material in delivering the required properties depends on the possibility of modifying the interfacial properties. The nature of the interface between immiscible polymers is important to investigate, both because these interfaces provide model systems to elucidate fundamental problems of the statistical mechanics of surfaces and interfaces, and also because an understanding of the microscopic structure of the polymer interface will help to address technological questions connected to the adhesion of polymers and the properties of multiphase polymer systems.

Very few pairs of polymers have any appreciable degree of miscibility with each other. The heat of mixing of polymeric materials is usually positive, so that the energy of a pair of like polymer segments is more negative than that of unlike segments. While the individual amount of repulsion between two unlike monomer

segments can be small, the total repulsion between the unlike polymer molecules is usually quite large due to the large number of monomeric segments per molecule. This will dominate over the entropy of mixing: in fact the entropy of mixing is proportional to the number of polymer molecules [1]. Most polymers are therefore incompatible with each other and form micro-phase separated structures if they are mixed. If two coexisting pure phases A and B, are considered, a question arises about what the forces are that shape the interface between the two different phases. The interfacial composition profile is driven by the energy and entropy of a polymer segment which is determined by conditions in the neighbourhood. The general effect of these factors is to make density gradients in these phase separated structures non-favourable. In the case of polymer systems, the conformational entropy is another important factor and in many cases can dominate. When all these forces are taken into account in a theory that self-consistently balances the various interactions, some conclusions can be drawn about the characteristics of the interface between the phases A and B [1]: the interfacial width varies as $\chi^{-1/2}$ for small χ (χ is the Flory–Huggins interaction parameter); the shape of the interface assumes a hyperbolic tangent function; the surface energy is proportional to $\chi^{1/2}$; the asymptotic properties are independent of molecular weight when there is little or no solvent present.

This article acts as a timely summary of some of the key areas affecting polymer surfaces, interfaces and thin films. Sections 2 and 4 introduce a simple theoretical frame for understanding the interface of thin polymers films and recent experimental results from testing the respective theories. Section 3 provides a brief introduction to some of the more powerful but also more commonly used experimental techniques that have been applied to measure properties of thin polymer films. Section 5 is devoted to recent results on the dewetting of a thin liquid film and on the polymer/polymer systems and on the recent developments to control the instabilities at the polymer interface to produce very well defined patterns. Dewetting of a thin liquid film from a flat surface or in a liquid/liquid system is an important process to study, for the crucial impact it has on various technological applications such as coatings and dielectric layers. Recently, attention has been devoted to the study of the dewetting behaviour of thin polymer films, and in particular to understanding of the spinodal dewetting. This is connected to the fact that polymer films represent ideal systems to study, due to their low vapour pressure and high viscosity, allowing time resolved experiments to be followed on easily accessible time scales.

Diffusion processes are important in many aspects of polymer understanding, including adhesion, welding, and membrane separation. Also, the understanding of diffusion of small-molecule penetrates such as gases and liquids into polymers is of vital importance in many areas, for instance, in order to identify chain architectures and mechanisms that could help develop new polymers for numerous barrier applications. However, the mechanisms that govern the diffusion behaviour are not fully understood despite continued research. Section 6 provides a summary of some of the most recent developments in the experimental and theoretical understanding of polymer–polymer and polymer–small molecule diffusion. The final section reviews the current understanding of the adhesion behaviour of both polymer/polymer and polymer/non-polymer interfaces.

Clearly, all these areas examined are closely related to interfacial phenomena, and we try to restrict our discussions to the current understanding of molecular-level behaviour rather than the cruder more phenomenological understanding. Some of the recent developments in understanding behaviour of these systems have come about by the emergence of some extremely powerful, often atomically, but more commonly molecularly resolved instruments and techniques. This has not only produced confirmation of existing theories, but also provided further developments of new theories. Where possible we have tried to include as many relevant references to published papers, as well as those of reviews that we are aware of.

2. Theory of polymer mixtures

2.1. Introduction to the theory of polymer–polymer systems

A comprehensive treatment of the theory of polymer–polymer systems is outside the scope of this paper and in any case can be found elsewhere [2,3]. Nevertheless, a brief overview is given here by way of an introduction into the areas covered by the subsequent sections [4,5]. Flory and Huggins formulated a lattice model that captures the essential features of the competition between configurational entropy of mixing and enthalpy contributions, and even today this simplified model forms the basis on which most of the discussion on thermodynamics of polymer mixing is based. In this model, a simple cubic lattice in 3-dimensions or a square lattice in 2-dimensions is introduced. Each lattice space can be occupied by a monomer of species A or B, a solvent molecule, or a vacancy. In the model, disparity in size or shape of the chain monomers is not considered. A polymer chain is then represented by a self-avoiding walk on the lattice that must not intersect any other chain, since each lattice site can be occupied only once. The chains are allowed to differ only by their effective degree of polymerisation, expressed by the numbers N_A and N_B which give the number of monomer units that compose a chain.

Other characteristics of the chain, such as chain stiffness, are also disregarded, and therefore the model focuses only on the "universal" aspects of the phase behaviour of a polymer mixture. The next step is to calculate the number of configurations of A-chains (containing N_A monomers) and B-chains (containing N_B monomers) compatible with the given volume fractions Φ_A and Φ_B ($\Phi_A + \Phi_B = 1$), with the constraint that no chain intersections occur (excluded volume). For each configuration ρ, the internal energy has to be calculated:

$$E(\rho) = \varepsilon_{AA} n_{AA} + \varepsilon_{BB} n_{BB} + \varepsilon_{AB} n_{AB} \tag{1}$$

where n_{AA}, n_{BB} and n_{AB} are the number of nearest neighbour pairs of AA, BB and AB in this configuration and ε_{AA}, ε_{BB} and ε_{AB} are the interaction energies between these pairs. Then the partition function Z and the free energy F of the system follow from weighting each configuration with the appropriate Boltzmann factor:

$$Z = \sum_{\rho} \mathrm{e}^{-E(\rho)/k_{\mathrm{B}}T} \tag{2}$$

$$F = -k_{\mathrm{B}}T \ln Z \tag{3}$$

Other quantities can be deduced by derivatives of the free energy of mixing, or by statistical mechanical averages. The problem is that the solution of the above equations is difficult and exact analytic solutions do not exist. To overcome these problems a number of substantial approximations have to be introduced. In estimating the configurational entropy of the chains, most of the excluded volume restrictions are discarded and in the treatment of the interaction energies ε, correlation in the occupancy of neighbouring sites are neglected by making a mean-field approximation. This yields a simple expression for the Gibbs free energy of mixing, given by the Flory–Huggins equation:

$$\frac{\Delta F_{\mathrm{mix}}}{k_{\mathrm{B}}T} = \frac{\Phi_{\mathrm{A}} \ln \Phi_{\mathrm{A}}}{N_{\mathrm{A}}} + \frac{\Phi_{\mathrm{B}} \ln \Phi_{\mathrm{B}}}{N_{\mathrm{B}}} + \chi \Phi_{\mathrm{A}} \Phi_{\mathrm{B}} \tag{4}$$

where the condition that each lattice space is occupied by either monomer A or B implies that $\Phi_{\mathrm{A}} + \Phi_{\mathrm{B}} = 1$, and the Flory–Huggins parameter χ is related to the nearest neighbour pair energy defined by:

$$\chi = z \frac{\left(\varepsilon_{\mathrm{AB}} - \dfrac{(\varepsilon_{\mathrm{AA}} + \varepsilon_{\mathrm{BB}})}{2} \right)}{k_{\mathrm{B}}T} \tag{5}$$

where z is the coordination number of the lattice. The expression of the free energy of mixing gives the free energy per lattice site and for simplicity the volume of one lattice cell can be taken as unity. The enthalpy term, given by $\chi \Phi_{\mathrm{A}} \Phi_{\mathrm{B}}$, neglects any correlation effects in the occupancy of the lattice sites. The probability that in neighbouring lattice sites, A–B pairs occur is simply given by the product $\chi \Phi_{\mathrm{A}} \Phi_{\mathrm{B}}$ of the respective volume fractions. Another approximation concerns the number of monomers that a particular monomer interacts with, which is taken to be equal to the coordination number of the lattice. Clearly, a monomer that is not at the end of the chain has at most $z - 2$ neighbouring monomers from other chains, with two sites being occupied by its neighbours along the chain, and there are at most $z - 1$ neighbours along the chain. This overestimation in the number of neighbours is to some extent corrected in Guggenheim's approximation where z is replaced with $z_{\mathrm{eff}} = z - 2 + 2/N$ when N_{A} is large and equal to N_{B}. However, χ is still overestimated, since interactions of monomers with other monomers of the same chain do not contribute to the de-mixing of different chains [3,4].

The coexistence curve between the one and two phase regions can be calculated from the condition given by $\partial F / \partial \Phi = 0$, so that:

$$\chi_{\mathrm{coes}} = \frac{1}{N} \frac{1}{2\Phi - 1} \ln \frac{\Phi}{1 - \Phi} \tag{6}$$

Phase separation occurs only when χ is bigger than $\chi_{\mathrm{c}} = 2/N$. For a typical polymer of average molecular weight the value of N is very large meaning that χ_{c} is very small.

This very small value of χ_c is the main reason for the strong immiscibility (incompatibility) between polymers blends. If the two-phase region is entered into only slightly, i.e. where the polymers are still close to the coexistence boundary, then demixing only takes place by a mechanism of nucleation of droplets of one phase in the other. If the two-phase region is entered more deeply, i.e. far away from the coexistence curve the interfacial energy vanishes. In this case, it becomes favourable for the system to break up spontaneously into small domains. The threshold is called the spinodal curve in the χ_c–Φ plane and is defined by the equation:

$$\frac{\partial^2 F/T}{\partial \Phi^2} = \frac{1}{N_A \Phi} + \frac{1}{N_B(\Phi - 1)} - 2\chi \tag{7}$$

Negative values of the interaction parameter χ correspond to polymer pairs that are miscible, and this is often related to specific chemical interactions between the two polymers. In most cases the χ parameter is positive. The main reason for this is that the interactions are mainly van der Waals attractions that are proportional to the product of the electronic polarizabilities of both polymers. The χ parameter in the original theory is a constant but recent experimental work has shown that the value χ has a slight temperature dependence. If monomer–monomer local correlations were independent of temperature T, one would expect the interactions to be independent of T and χ to vary as $1/T$. This would mean that the Flory–Huggins parameter χ would be entirely energetic in origin and not entropic. This means that the polymer mixture would phase separate when the temperature was lowered to the upper critical solution temperature. Instead, for some polymer mixtures phase separation occurs when the temperature is raised, the so-called lower critical solution temperature (LCST). This means that χ has a different temperature dependence and has also an entropic component. The properties of the polymer–polymer mixtures are determined by the system minimising the free energy of mixing. Analysis of the free energy of the interface is therefore of fundamental importance in understanding the behaviour of the interface, which in general is normally different from the properties in the bulk. The next section introduces the self-consistent field theory that predicts the interfacial width and the interfacial tension for polymer systems.

2.2. Self-consistent field theory

The self-consistent field theory for interacting polymers was born from an analogy with the classical problem of interacting electrons [6]. The problem of the configuration of a chain surrounding and interacting with other polymer chains is similar to the problem of finding the wave function of an electron in the presence of many other interacting electrons (the so-called Hartree approach). To derive the self-consistent field theory, the first step is to derive a probability function, $q(\vec{r}, \vec{r}^{\,i}, t)$. This is the probability that a chain, that is t steps long, has started at a position $\vec{r}$ and finished at a position $\vec{r}^{\,i}$. For an ideal (isolated) chain, since it is a random walk, it is possible to write a diffusion equation for q:

$$\frac{\partial q}{\partial t} = \frac{a^2}{6}\nabla^2 q(\vec{r}, \vec{r}^{\,i}, t) \tag{8}$$

where $a^2/6$ is the diffusion coefficient with a statistical segment length, a. For the case of a non-ideal chain that is not in free space, the diffusion equation can be considered by including a potential $V(\vec{r})$. In this non-ideal case, the diffusion equation (8) can be written as:

$$\frac{\partial q}{\partial t} = \frac{a^2}{6}\nabla^2 q(\vec{r}, \vec{r}^{\,i}, t) - \frac{V(\vec{r})}{k_B T} q(\vec{r}, \vec{r}^{\,i}, t) \tag{9}$$

which has the same form as the Schrödinger equation. However, with each polymer chain i having a different potential $V_i(\vec{r})$ the solution of Eq. (9) becomes an insoluble problem of coupled differential equations. A mean-field approximation is therefore applied to the system in which each polymer chain of the same type is under the influence of a mean-potential field $\widetilde{V}_j(\vec{r})$. Therefore, if we have two immiscible polymers A and B, the mean-field potential that each polymer type feels for a planar interface, where only the z component is important, is given by

$$\frac{\widetilde{V}_A(z)}{k_B T} = \chi \Phi_B(z) + w(z) \tag{10}$$

$$\frac{\widetilde{V}_B(z)}{k_B T} = \chi \Phi_A(z) + w(z) \tag{11}$$

where $w(z)$ is included to insure incompressibility ($\Phi_A + \Phi_B = 1$), and χ is the Flory–Huggins interaction parameter. The Flory–Huggins interaction parameter is related not only to the chemical attraction (or repulsion) between monomers, but also their volume fraction Φ. The inclusion of an incompressibility term ensures that any two segments are prevented from occupying the same volume. With these expressions for the potential, it is therefore possible to rewrite the diffusion equation, so that the quantities to be determined are the two volume fractions Φ_A and Φ_B. The two volume fractions are related to the distribution functions $q_A(z,t)$ and $q_B(z,t)$ with the following equations:

$$\Phi_A(z) = \frac{1}{N}\int_0^N \mathrm{d}t q_A(z, N-t) q_A(z,t) \tag{12}$$

$$\Phi_B(z) = \frac{1}{N}\int_0^N \mathrm{d}t q_B(z, N-t) q_B(z,t) \tag{13}$$

The integral term in these equations indicates that it is a summation over the number of segments in the chain, up to the total chain length N. The approach that is followed in solving the diffusion equations consists of guessing the functions Φ_A and Φ_B, and solving the equations in order to obtain the values q_A and q_B. With these values for the distribution functions Eqs. (12) and (13) are solved to find better values for Φ_A and Φ_B. This iterative process is repeated until convergence criteria are reached and the volume fraction profiles are obtained. For the interface between two

immiscible polymers of infinite molecular weights, an analytic solution to the diffusion equations exists [1]. In this case the chain segments are assumed to be equivalent and equations for the volume fractions of A and B can then be replaced by simpler expressions:

$$\Phi_A(z) = q_A^2(z) \tag{14}$$

$$\Phi_B(z) = q_B^2(z) \tag{15}$$

The diffusion equations for immiscible polymers become:

$$\frac{a^2}{6}\frac{d^2 q_A(z)}{dz^2} = \chi q_B^2 q_A + w(z) q_A \tag{16}$$

$$\frac{a^2}{6}\frac{d^2 q_B(z)}{dz^2} = \chi q_A^2 q_B + w(z) q_B \tag{17}$$

For the specific conditions when $\Phi_A(z \to -\infty) = 0$ and $\Phi_A(z \to +\infty) = 1$, the solution to Eqs. (16) is given by:

$$\Phi_A(z) = \frac{1}{2}\left(1 + \tanh\left(\frac{z}{w}\right)\right) \tag{18}$$

where the interfacial width (w) is given by:

$$w = \frac{a}{\sqrt{6\chi}} \tag{19}$$

and a is the average statistical segment length. Given the complexity of the mathematical arguments in the mean-field approximation, Eq. (19) is surprisingly simplistic, but highly useful. Clearly, from an experimental point of view, the Flory–Huggins parameter for any polymer pair can be determined simply by measuring the interfacial width between them. Alternatively, for a polymer pair with a known χ parameter the interfacial width can easily be predicted. The interfacial tension can also be evaluated from the Flory–Huggins parameter using the equation:

$$\gamma = k_B T \rho a \sqrt{\frac{\chi}{6}} \tag{20}$$

where $1/\rho$ is equal to the monomer unit volume. By putting in typical values for χ and an average value of a in Eq. (19), it can easily be seen that theoretical predictions of the interfacial width between two immiscible polymers is typically smaller than 10 nm. As we show subsequently care needs to be taken with using this equation (see Section 4). As the interfacial widths are predicted to be of nanometer length scale techniques to measure this width must therefore have an appropriate resolution as well as an ability to distinguish between the two phases. A number of very powerful techniques have been applied to studying such immiscible polymer interfaces and these are discussed in Section 3.

3. Experimental techniques

In this section an introduction to some of the main techniques used to investigate polymer interfaces, surfaces and thin polymer films will be outlined, with an emphasis on the neutron reflection technique, which is arguably one of the most powerful techniques for such studies. Recently, various reviews have been published on the various techniques which have been used to study polymer interfaces [7–11]. Whilst individual techniques have certain advantages, often they come with a number of their own difficulties and disadvantages. We do not discuss these issues in detail here, since comparison between the techniques is provided in the reviews mentioned above.

3.1. Reflectivity techniques: neutron (NR) and X-ray (XR) reflectivity

Neutron reflectometry is ideally suited to studying surfaces and interfaces between immiscible and partially miscible polymers because of its inherent sub-nanometer resolution [12]. Although recent reviews of the theory (see Ref. [12] and the comprehensive book by Lekner [13]) and application to polymer interfaces [14,15], have been published it is worth describing the basic principles. The reason neutrons have been so widely used for studying polymers is essentially because in many ways neutrons are an ideal probe. The length-scales probed by the reflection experiment are sensitive to structural features perpendicular to the plane of the film with length scales between 0.5 and 500 nm [7,16,17]. Two other key advantages of neutrons which make them particularly suited for studying organic materials is firstly their penetration power is large so it is straightforward to study buried interfaces, and secondly, the large difference in neutron scattering length density between deuterium and hydrogen. This latter property means that by isotopic substitution it is possible to highlight whole molecules or parts of molecules, without unduly disturbing the underlying physical and chemical properties. This is of course not strictly true in all cases but can easily be accounted for in the experimental design [18].

Experimentally, the measured reflectivity represents the ratio of the reflected intensity from the sample to that of the incident intensity. By inspection of the appropriate reflection equations it is possible see that the reflectivity a high wave vector (k) limit is simply related to the Fourier transform of the derivative of the scattering length density profile [13,19]. The practical implication of this relationship is that if a reflectivity profile can be measured to a high enough wave vector, it would be possible to simply Fourier transform the reflectivity data (i.e. R versus k data) into a real space profile to obtain the required scattering length density versus perpendicular distance i.e. a chemical composition profile. Apart from a few limited cases [18], in practice it is not possible to use Fourier transformations to derive the composition profile due to the limited k range that can often be reached experimentally. In practical terms, data analysis relies on fitting the reflectivity data using neutron optical formulisms, which can calculate reflectivity from any proposed model [20,21]. To appreciate how this may be achieved it is necessary to understand how neutrons propagate through and interact with a medium.

Since all scattering centres that are small compared with the wavelength of the neutrons, the effect of the medium can be represented by a pseudo-potential [22–24]. By solving the Schrödinger equation using this potential, the value of the reflectance, r, and therefore the reflectivity, R ($= |r|^2$), can be determined. Consider the simplest case of a bulk sample which has a scattering length density, b/V, in contact with a vacuum, where it is also assumed that the interfacial width between these bulk media is zero. For this system, the perpendicular component of the wave vector within the material k_i is equal to $\sqrt{k^2 - 4\pi(b/V)}$, where k is the wave vector in the vacuum. When $4\pi b/V > k^2$, k_i is imaginary, which means that the neutrons can only propagate into the material as an evanescent wave, giving rise to total external reflection, and the reflectivity is equal to unity. When $4\pi b/V < k^2$, then the neutrons refract into the media and the reflectivity is given by the well known Fresnel expression:

$$R = |r|^2 = \frac{k - k_i}{k + k_i} \tag{21}$$

For high values of k, the reflectivity has the limiting value of $R \sim \pi^2 (b/V)^2 k^{-4}$, which shows that the reflectivity drops off very rapidly with increasing wave vector. In real systems, the interfacial width is either rough or diffuse, i.e. no longer zero, and so the reflectance of the ideal interface (denoted r_F) is modified by introducing a roughness factor, so that the reflectance is r is given by $r_F \, e^{-2kk_i\sigma^2}$, where σ is the Gaussian width of the interface. The principles for calculating the reflectivity for the interface between two infinite media can easily be extended to systems consisting of one or more layers between two infinite media. In these layered systems, it is necessary to determine a reflectance for each layer which includes terms for thickness and roughnesses for each individual layer, and there are a number of methods for calculating the total reflectivity from these multiple reflectances [13].

In practice, data analysis has a number of difficulties, associated with straight inversion of the reflectivity data into a composition profile not being possible in a majority of cases, as discussed above. In addition, if the sample contains more than two unknown compositions then the composition profile cannot be determined uniquely [21]. This implies that NR is not suitable to analyse films of completely unknown compositions. It should instead be considered as a powerful tool for characterising the structure of thin films at high resolution when their make up is either already known at some coarse level or one has some knowledge of the materials from which they are composed. There are a number of approaches including using polarised neutron reflectivity (PNR) [25], and speckle holography [26,27], which allow composition profiles to be obtained unambiguously, but these methods may not be applicable to all systems. NR is at its most powerful when samples are specifically made for the technique, in particular when using isotopic labelling such as deuteration, which is widely used in polymeric systems. An example of typical reflectivity profiles for bilayers consisting of deuterated polystyrene (dPS) with thicknesses varying from 6 nm (top curve) to 480 nm (bottom curve), on thicker films of poly(methyl methacrylate) (PMMA) is shown in Fig. 1 [28]. In this figure the reflectivity data are plotted as a function of the momentum transfer q_z

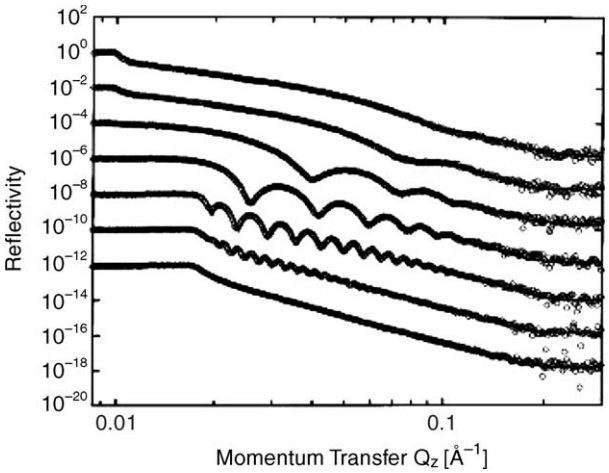

Fig. 1. Examples of NR curves with fits for bilayers of dPS/PMMA with a thick PMMA layer at the bottom and different thickness of deuterated PS on the top, from very think (top curve) to very thick (bottom curve). Reproduced with permission from Ref. [28].

($q = 4\pi\lambda^{-1}\sin\vartheta$, which is related to the wave vector by a factor of 2π) and the solid lines are fits to the data derived from a multilayer model.

The closely related technique of X-ray reflectivity (XR) can also be applied to study the surfaces and interfaces in some polymer systems. In contrast to neutrons, XR experiments are sensitive to the average electron density fluctuations along the sample normal. The general experimental and analysis approach is analogous to the NR case with many of standard optical equations identical for both techniques, but with the neutron scattering length density being replaced by the electron density. The technique can be used if enough contrast in electron density between the polymer phases is present such as may be produced between polystyrene (PS) and bromonated PS (PBrS) [29]. However, recent work by Seeck et al. using Fourier analysis has demonstrated that very little contrast is required to extract highly detailed information [30], which may stimulate wider use of the XR technique to systems where it was not previously believed enough contrast existed to make the experimental results of value. For a comprehensive review on the XR and its application, the book by Daillant and Gibaud is recommended [31].

3.2. Off-specular scattering

Specular reflectivity measurements have made a dramatic impact on the study of polymer surfaces and interfaces. As we have seen above, specular NR and XR is only sensitive to the structure perpendicular to the surface of the sample. In order to obtain information on the in-plane structure, the radiation scattered out of the specular direction have to be studied [10,31]. In this case, the diffraction vector is oriented at some off-normal angle with respect to the surface giving components of the diffraction vector parallel and perpendicular to the surface.

While the use of X-ray diffuse scattering is quite an established technique and many results have been published with some examples of the data presented in the Section 4, the use of neutrons for studying lateral morphologies of surfaces and interfaces has not been exploited to the same extent. The main reason for this is due to the weak intensity of neutrons available from current neutron sources. Despite this relatively poor intensity in the off-specular direction an example of the importance of using off-specular NR in the context of a polymer/polymer interface is described in Section 5.

3.3. Ion beam techniques

This technique uses medium energy (MeV) ions to determine depth-concentration profiles. The ions are either scattered at the surface or within the sample, and the particles emitted from nuclear reactions or fragments from collisions are detected. The ion beam is most often produced using a van de Graff accelerator, which is then used to probe the polymer sample. A number of ion beam techniques have been used extensively for studying polymer surfaces, interfaces and thin film [32–37]. The techniques which have been used most commonly for these studies of polymer films are forward recoil spectrometry (FReS) [9,38–65], nuclear reaction analysis (NRA) [66–79] and to a lesser extent Rutherford backscattering (RBS) [80]. More extensive technical details and substantial reviews of their application, together with a comparison between these techniques have been published elsewhere [8,9,81].

Perhaps the ion beam technique which has had the most impact to depth profile studies is FReS, which is also referred to in some cases as elastic recoil detection analysis (ERDA). The basic principle of the technique is that a $^{4}He^{+}$ beam scatters both ^{2}H and ^{1}H, and the energy of these elements are detected in the forward direction. By carefully measuring the energy of these scattered particles relative to the energy of the primary ion beam, it is possible to evaluate the depth profile. RBS uses the same primary ion beam scattering events but measures the ejected particles that are backscattered. Backscattering is most effective from heavier elements so depth profiling of hydrogen is not typically possible. Due for the need for higher mass elements, RBS has not found as wide spread use in polymer research as FReS, but nevertheless has been used where available contrast between polymers exists. In NRA the ion beam interaction with the sample causes a nuclear reaction and it is the detection of the reaction products that are used for profiling. The most common form of NRA is the use of a $^{3}He^{+}$ beam to detect deuterium within samples. The $^{3}He^{+}$ ion of known energy implants into the sample and reacts with any deuterium atoms (^{2}H) it encounters in the sample to form a $^{5}Li^{+}$ intermediate product which decays into an α-particle (^{4}He) and a proton ($^{1}H^{+}$) and releasing exactly 18.353 MeV. As the proton recoils out of the sample surface it looses energy proportional to the depth of the deuterium which caused the reaction with the $^{3}He^{+}$ ion. This means that the further into the sample the deuterium at was, the more the proton will loose energy, so that the detected energy of the proton is reduced from the initial 18.353 MeV. Therefore by detecting the resulting energy of the ejected proton it is possible to obtain a direct observation of the deuterium depth concentration profile. Varia-

tions of this technique using $^{15}N^-$ to detect ^1H [82], or $^1H^+$ to detect $^{19}F^-$ [83], have both been applied to measuring concentration profiles in polymers. The resolution of these techniques in general is not as good as that of NR, with a resolution better than approximately 10 nm often difficult to obtain. This results from cascade mixing effects, which are generated by the forward collision of the target atoms by the primary ion beam [66]. NRA is for polymers a sample destructive technique, due to charging, cascade mixing, and chain scission effect. This has the combine effect of limiting the resolution but also means kinetic properties of the sample cannot be measured on exactly the same area of sample.

3.4. Secondary ion mass spectroscopy

Secondary ion mass spectroscopy (SIMS) uses the mass detection of secondary ions created by implantation and sputtering from charged ions (the primary ions). If the primary ion current density is low the technique is very sensitive to the first few nanometers of the surface since the primary ions do not penetrate to any great depth below the sample surface. This technique is known as static SIMS (SSIMS), which often has a time-of-flight detection system (TOF-SIMS). TOF-SIMS uses a pulsed primary ion beam so that the time taken for the secondary ions to reach the detector can be timed with respect to the individual primary ion pulses. Depth dependent information can be achieved through dynamic SIMS (DSIMS), which has been widely applied to studying polymer systems (see for example Refs. [9,43,63,67,84–94]). In DSIMS, the surface is continuously sputtered by scanning with a high energy ion beam over a given area and the ejected ionised atomic or molecular fragments are analysed in a mass spectrometer. The ion beam effectively shaves off a thin layer of material ($\sim$2 nm) on each scan and the analysis of the secondary ion fragments from successive layers in the growing crater which is formed by the sputtering provides a method of depth profiling. The depth resolution is determined by molecular mixing caused by ballistic collisions associated with the primary ion beam implantation and molecular fragmentation processes. In typical DSIMS instruments used for polymer studies, an approximately 5–20 keV primary ion beam and a 25 nA current, is used to sputter the surface. The primary ion source varies with both atomic (i.e. Ga^+, Cs^+, O^-) or polyatomic (i.e. SF_6^-) ions used depending on the required fragments to be observed.

A more recent adaptation of SIMS techniques is the use of the neutral species that are also ejected from the surface during sputtering by the primary ions. The neutral species are ionised after ejection from the surface using a laser of suitable wavelength and detected using a normal mass spectrometer system. This relatively new variant of SIMS is called secondary neutral mass spectroscopy (SNMS). Depending on the type of instrument it is possible to use a focussed primary ion beam which enables lateral imaging of the sample to be undertaken. An example of this is shown in Fig. 2 showing the secondary ion intensity false colour images of a PS–dPMMA blend compatibilised by a PS–b-PMMA diblock copolymer to restrict the phase domain size [95]. Some of the more sophisticated DSIMS instruments also allow so-called 'imaging DSIMS', whereby the depth profiling capability of DSIMS is coupled with

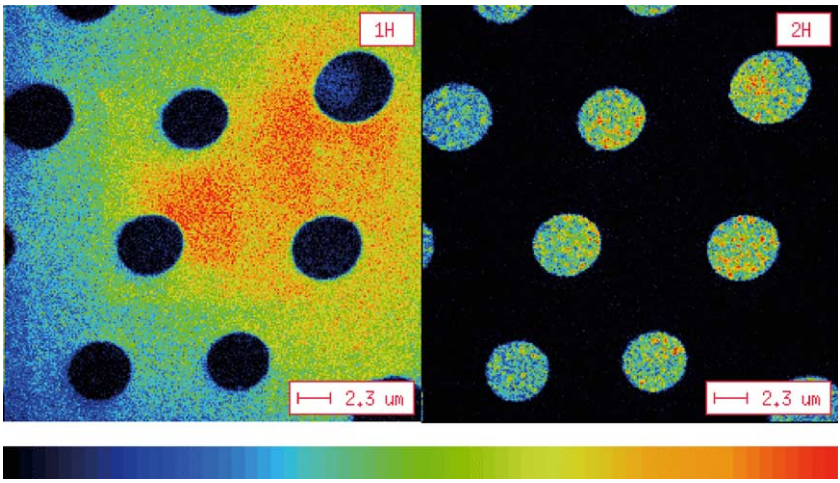

Fig. 2. SIMS image taken using a Cameca nanoSIMS 50 of the surface of a thin film of a compatibilised immiscible polymer blend of dPMMA ($M_w = 160$ kg/mol, $M_w/M_n = 1.06$) and PS ($M_w = 1112$ kg/mol, $M_w/M_n = 1.15$) were mixed in equal parts by mass and compatibilised by 6% (by mass) with a PS–b-PMMA symmetric diblock copolymer (M_p: 85 kg/mol, $M_w/M_n = 1.08$). The ^{1}H (left hand image) and ^{2}H image are shown [95].

a good lateral resolution, and allows 3-D mapping of atomic or molecular species to be extracted.

3.5. Other techniques

A number of other techniques have been widely applied to studying polymer surfaces and interfaces [32,64,96,97]. Perhaps the most commonly used traditionally have been optical microscopy [98], transmission electron microscopy (TEM) [84,99–107], and scanning electron microscopy (SEM) [96,108–113]. Care has to been taken using the electron microscopy techniques to prevent altering the sample either during preparation or through vacuum or electron damage when imaging. The methods required to minimise or even prevent these effects from occurring are well established and microscopy has proved to be a very rapid and reliable method of sample analysis, particularly using SEM to image surface features. Atomic force microscopy (AFM) by comparison to electron microscopy is a relatively new technique it has nevertheless become very popular and has been applied extremely widely in the study of polymer surfaces (see for examples Refs. [32,64,96–98,114–121]). Although the development of AFM to study polymers was initially hindered by misinterpretation of the data (like many early work with new techniques), the technique is now mature and very robust and has been applied widely to study surfaces with remarkable detail. It is an extremely powerful technique since the imaging can be conducted under ambient conditions and does not require vacuum or dry environments to operate. This means it has been able to measure systems in situ which could include

under a liquid or at elevated (or reduced) temperatures. For most studies the technique is used to quantify surface topographic features, but variants of the AFM technique do allow spatially resolved surface chemical composition to be determined. Another approach to chemical analysis, which has been applied to studying polymer surfaces is X-ray photoelectron spectroscopy [122–127], which has no lateral resolution, but is very sensitive to the surface of the polymer down to a depth of approximately 3–5 nm. Perhaps the primary limitation to this technique is the requirement that the sample needs to be under high vacuum and this has distinct implications, as mentioned before, in sample preparation and handling. Alternatively, IR methods such as attenuated total reflection Fourier transform (ATR-FTIR) or imaging FTIR can be applied. In imaging FTIR, the standard diameter of an IR beam is reduced to micron levels and rastered across the sample to build up a lateral IR image typically with a resolution of approximately several microns.

Ellipsometry is a sensitive optical technique that measures the change in the state of the polarisation of light upon specular reflection from a planar interface in order to obtain information about the structure of the interface. Specifically, the ellipsometer is used to determine the thickness and refractive index of a film on a surface. Measurements can be made in any transparent medium, such as vacuum, gases and liquids, and can be performed on any reflecting medium or transparent surface, like metals, semiconductors and polymers. The technique is also non-invasive and a dynamic experiment can be carried out in situ. In fact with a monochromator, the wavelength can be fixed to allow a continuous monitoring of the optical properties of samples. Spectroscopic phase modulated ellipsometry is a technique for the characterisation and measurement of the optical properties of surface and adsorbing films, and uses a beam of elliptically polarised white light to reflect off a highly reflective surface that supports the polymer layer. Reviews on this technique have recently been published [128–130].

4. Immiscible polymer/polymer interfaces

4.1. Interfaces between incompatible polymers

One of the most intensively studied incompatible blends is the PS/PMMA system, where values of the interfacial width between these two polymers have been determined using a range of different techniques. NR studies of PS/PMMA interfaces performed independently by Anastasiadis et al. [131] and Fernandez et al. [132] found the interfacial width to be 50 Å. This value was independent of the film thickness and polymer molecular weights used. The temperatures used for annealing the samples were 170 and 120 °C for the two studies, respectively, which are both above either of the two polymers' the glass transition temperature. More recently, work by Sferrazza et al. also obtained an interfacial width of 50 Å if the layer thicknesses are over a critical value [28]. Independent ellipsometry investigations gave an interfacial width between 30 and 90 Å for polymers with molecular weights of 180,000 g/mol PS and 151,000 g/mol PMMA at an annealing temperature of

between 140 and 170 °C [133]. TEM gave an interfacial width value of 50 ± 30 Å, for 180,000 g/mol PS and 151,000 g/mol PMMA annealed at 140 °C. The TEM measurement of the interfacial width was obtained by cutting the sample perpendicular to the interface and staining one of the components to provide the contrast [134], although the resolution is limited by the sample preparation. Interfacial tension measurements have also been performed by different groups giving an interfacial width between PS and PMMA of 26–49 Å for different combinations of molecular weights used. However this technique does not yield the interface width directly and provides no information on the profile [135].

Although PS and PMMA interfaces have been widely studied, other immiscible polymer pairs have also been investigated extensively. For example, Genzer and Composto [54] have studied the interface profile between 1,4-polybutadiene (PB) and dPS using low-energy FReS and NR and obtained an interfacial width of 6 nm, which supports previous studies on this system [136]. Stone et al. [137] have investigated the interface formation of PS and chlorinated polybutadiene with XR and X-ray diffuse scattering and observed an interfacial width of 4.7 nm. The experimental results for different amorphous polymer–polymer interface combinations have been extensively reviewed by Schubert and Stamm [7] and Jones [138] (also see references contained therein). Most of these studies have been limited to the interface between amorphous immiscible, due in part to their ease of sample preparation and also because of limitations of the techniques used. However, in a recent series of papers, Bucknall and co-workers have shown that by overcoming some of these technical issues narrow interfacial widths are also observed for amorphous–crystalline (PS/polyethylene (PE)) and crystalline–crystalline (polypropylene (PP)/PE) polymer pairs [139–144].

The experimental interfacial widths obtained for incompatible polymers [138], such as PS–PMMA, are broader than the value predicted by the self-consistent field theory developed by Helfand and Tagami [1]. An understanding of the reason for the discrepancy is fundamental for developing a better understanding of the properties of polymer interfaces. In fact, Helfand's theoretical prediction for the interfacial width between two strongly immiscible polymers is very well established on theoretical grounds. Let's take again the well studied system of a PS and PMMA blend. For these polymers the theoretical interfacial width w between PS/PMMA can be determined using the expression $w = a/\sqrt{6\chi}$. With a reference volume equal to the volume of a PS repeat unit, a χ value of 0.04, and statistical segment lengths for PS and PMMA as $a_{PS} = 6.7$ Å and $a_{PMMA} = 7.5$ Å, the calculated interfacial width is $w = 29$ Å [145]. This value contrasts to the measured value of approximately 50 Å for the PS/PMMA interface, a value which is independent of the M_w and film thicknesses used. A possible explanation for the difference between the experimental and theoretical result was suggested by Shull et al. who postulated that the experimental result agrees with the theoretical prediction if a correction to the interfacial width due to capillary wave fluctuations is considered [145]. Clearly, this has important implications in applying theories or testing experimental results, so what follows is an introduction to the general capillary wave theory.

4.2. Theory of capillary excitations

As mentioned above the discrepancy between the self-consistent field theory and the experimental results for the immiscible polymer blends, could be connected to the fact that the theory neglects contributions from thermally excited fluctuations at the interface. Extension of the basic results of the theory to polymer systems is straightforward. An intuitive approach to the broadening of fluid interfaces due to thermal fluctuations was initiated by Buff, Lovet and Stillinger (BLS) [146–153]. The following outlines their approach, except for the fact that the interfacial plane is not assumed to be infinite.

A dividing surface $\zeta(x,y)$ between two fluid phases of mass density equal to ρ_1 and ρ_2 is considered, where ζ is a measure of the vertical distance of the surface from the x–y (interface) plane. The reversible work, W, to create the dividing surface $\zeta(x,y)$ is given by:

$$W = (\rho_1 - \rho_2)\int\int_A \left[\left[\int_{\zeta(x,y)} U_l(z)\,\mathrm{d}z\right] U_l(z)\,\mathrm{d}z\right]\mathrm{d}x\,\mathrm{d}y + \gamma\int\int_A (1+\zeta_x^2+\zeta_y^2)^{1/2}\,\mathrm{d}x\,\mathrm{d}y \tag{22}$$

where γ is the interfacial tension between the phases, U is the external potential acting on a unit mass of fluid, z is the height perpendicular to the x–y plane, A is the area of the interfacial plane, and ζ_x and ζ_y are the x and y derivatives of $\zeta(x,y)$, respectively. The potential energy term in the expression of W is computed relative to that of a flat (planar) interface at $z=0$. For simplicity, the assumption that the system is square in the interfacial plane is assumed, so that $A = L^2$ where L is the length of a side of the square. For the surface $\zeta(x,y)$, the collection of the points with coordinates equal to $(x,y,\zeta(x,y))$, can be represented in terms of decoupled, harmonic surfaces waves, so that:

$$W = \sum_k A(k)\,\mathrm{e}^{\mathrm{i}\vec{k}\vec{s}} \tag{23}$$

with $\vec{s} = x\hat{i} + y\hat{i}$, and the sum is extended to all wave vectors k. $\zeta(x,y)$ is the sum of a group of waves each having a wave vector k. If the external potential varies sufficiently slowly, the approximation $U(z) \approx gz$ can be made, where the "gravitational" constant is defined by $g \equiv (\partial U/\partial z)_{z=0}$ and where U is chosen such that $U(0)=0$. By introducing this approximation into Eq. (22), it is possible to obtain:

$$W = \gamma A + \sum_{k,k^i} A(\vec{k})A(\vec{k}^i)\int_0^L\int_0^L \mathrm{e}^{\mathrm{i}(\vec{k}+\vec{k}^i)\vec{s}}\left[\frac{1}{2}(\rho_1-\rho_2)g - \frac{1}{2}\gamma(k_x k_x^i + k_y k_y^i)\right]\mathrm{d}x\,\mathrm{d}y \tag{24}$$

With the periodic boundary conditions, $\zeta(0,y) = \zeta(L,y)$ and $\zeta(x,0) = \zeta(x,L)$, the allowed values of the wave vector k are:

$$\vec{k} = \frac{2\pi}{L}(n_x\hat{i} + n_y\hat{i}), \quad n_x, n_y = 0, \pm1, \pm2, \ldots \tag{25}$$

and this yields the following expression for W:

$$W = \gamma A + \sum_{k,k^i} \left|A(\vec{k})\right|^2 \left[\frac{1}{2}(\rho_1 - \rho_2)g - \frac{1}{2}\gamma k^2\right] A \tag{26}$$

The mean values of ζ and ζ^2 for a given set of amplitudes $A(\vec{k})$ are:

$$\bar{\zeta} = \frac{1}{A}\int_0^L \int_0^L \zeta \,\mathrm{d}x\,\mathrm{d}y = A(0) \tag{27}$$

$$\bar{\zeta}^2 = \frac{1}{A}\int_0^L \int_0^L \zeta^2 \,\mathrm{d}x\,\mathrm{d}y = \sum_k |A(k)|^2 \tag{28}$$

Since ζ represents the fluctuations of a flat interface about the $z = 0$ position, it implies that if $\bar{\zeta} = 0$ then $A(0) = 0$ and the summation may be restricted to non-zero values of k. In addition, k is forced to have non-zero values, and is limited to maximum and minimum values, $k_{\max}$ and $k_{\min}$, which are both fixed by physical considerations. For a wave to have physical meaning in a molecular system, $k_{\max}$ must be bounded by $2\pi/l_{\mathrm{m}}$ where l_{m} is the minimum wavelength definable at the interface (such as the interfacial width determined by the mean-field theory for a plane interface). The probability that a given set of $A(\vec{k})$ occurs through a thermal fluctuation is proportional to $\mathrm{e}^{-W/k_{\mathrm{B}}T}$, where T is the absolute temperature and k_{B} is the Boltzmann constant. By averaging over all $A(\vec{k})$ values, the mean square capillary wave dispersion can be calculated:

$$\sigma_\zeta^2 \equiv \left\langle \vec{\zeta}^2 - \langle \bar{\zeta} s\rangle^2 \right\rangle = \sum_{k>0} \left[\frac{L^2}{2k_{\mathrm{B}}T}(g\Delta\rho + \gamma k^2)\right]^{-1} \tag{29}$$

where $\Delta\rho = \rho_1 - \rho_2$. Transforming the summation over all $\vec{k}$ to an integral with the aid of the relation $1 \equiv \Delta n_x \Delta n_y = (L/2\pi)^2 \Delta k_x \Delta k_y$ it is possible to obtain:

$$\sigma_\zeta^2 = \frac{k_{\mathrm{B}}T}{2\pi^2\gamma} \int\int_{\frac{2\pi}{L} \leqslant k \leqslant \frac{2\pi}{l_{\mathrm{m}}}} (\xi^2 + k^2)^{-1}\,\mathrm{d}k = \frac{k_{\mathrm{B}}T}{4\pi\gamma} \ln\left(\frac{\xi^2 + \left(\frac{2\pi}{l_{\mathrm{m}}}\right)^2}{\xi^2 + \left(\frac{2\pi}{L}\right)^2}\right) \tag{30}$$

where $\xi^2 \equiv \Delta\rho g/2\gamma$ (gravitational cut-off of the spectrum). In the limit of an interface of infinite extent ($L = \infty$), Eq. (30) gives the BLS result. It also follows that the major contribution of capillary waves to the interfacial width comes from waves corresponding to small k values, i.e., to large wavelengths.

It is also necessary to consider the effect of other external fields acting on the interface. For a sample consisting of two thin layers of different phases on a substrate, terms associated with van der Waals forces between different phases are also important. The length scale of the capillary fluctuations can then be expressed by:

$$\Delta_{CW} = \frac{k_B T}{4\pi\gamma} \ln \frac{k_M^2 + q_{grav}^2 + q_+^2 + q_-^2}{k_m^2 + q_{grav}^2 + q_+^2 + q_-^2} \tag{31}$$

where q_g is the gravitational cut-off as seen before and q_+ and q_- are the contributions from the two interfaces, denoted '+' and '−'. The upper limit of the wave vector, k_M, is linked with the atomic size. For polymers, a good assumption is that this upper limit is derived from the intrinsic interfacial roughness, $\Delta_0 (= \sqrt{2\pi} w)$, so that $k_M = (2\pi/\Delta_0)^2$. The value of Δ_0 is determined by the self-consistent field theory for the case of the two immiscible polymers using Eq. (19). The lower wavelength limit (k_m) is derived from a dimension related to the limit of the wavelength detectable by the technique used. For neutrons, for example, the coherence length of the neutron is used so that $k_m = (2\pi/\lambda_{coh})^2$. As will be seen below, by combining this term with the intrinsic interfacial width extracted by the self-consistent theory, a general formula for the width modified by the capillary wave amplitude can be obtained.

4.3. Combining theory and experiments

In the last few years, there have been notable advances in understanding the fundamental properties of interfaces between immiscible polymers. Using NR, Schubert and Stamm measured the interfacial width between d-PS and h-PMMA for various molecular weights of the polymers [154]. The range of M_w was varied between 6600 and 145,000 g/mol for the PMMA layer and fixed at 700,000 g/mol for the d-PS film. These workers found that the interfacial width changed between 55 and 33 Å in this molecular weight (M_w) range. The values of the interfacial widths measured were corrected using an over simplified approach of subtracting in quadrature the measured roughness of the sample as made. The main conclusion of their work was that for the PS/PMMA system, the results obtained were consistent with the mean-field theoretical predictions without need of capillary wave corrections. A series of reflectivity experiments on bilayers of PS and PMMA were also performed by Sferrazza et al. changing various conditions, such as the M_w, the thickness of the layers, the annealing temperature and the time of annealing at a fixed temperature [28]. Of particular interest was the study of the effect of long-range van der Waals forces on the polymer interface, which were clearly detected when the film thicknesses were varied. For the air/PS/PMMA/substrate system studied by Sferrazza et al., the characteristic gravitational length was taken as 2 mm, which has to be compared with the neutron coherence length, which is of the order of microns. The gravitational term was therefore not relevant for a determination of the interfacial width with neutron reflection and can be neglected. The van der Waals part of the external potential, given in Eq. (31) by q_+ and q_- (where q_- is the contribution coming from the PMMA/substrate interface and q_+ derives from the air/PS interface) introduces a dispersive capillary length given by:

$$a_{dis}^2 = \frac{4\pi\gamma l^4}{A} \tag{32}$$

where l is the film thickness and A is the Hamaker constant for the interactions between the substrate and the air across the thickness of the polymer. The Hamaker constant can be estimated from the refractive index and dielectric constant data of the materials using an approximation based on the Lifshitz theory [155]. Where the thin PS film is between two semi-infinite media, i.e. PMMA and air, a Hamaker constant of 2×10^{-20} J is obtained [28]. For PS films in the thickness range of 50–500 Å, the dispersive capillary length may be estimated as falling between 300 Å and 3 μm. Thus for films in this range of thickness, the dispersive capillary length rather the neutron coherence length (which is of the order of microns) dominates the capillary wave expression. For a film with a thickness larger than ~1000 Å, the capillary wavelength is larger than the neutron coherence length and therefore the neutron coherence length becomes the cut-off for the capillary waves. The total interfacial roughness is therefore expressed by the following relation, where it is assumed that the contributions to the interfacial width due to the intrinsic width and to the capillary wave broadening add in Gaussian quadrature:

$$\Delta^2 = \Delta_0^2 + \langle\Delta\zeta^2\rangle = \Delta_0^2 + \frac{k_B T}{4\pi\gamma}\ln\frac{(2\pi/\Delta_0)^2}{(2\pi/\lambda_{coh})^2 + (2\pi/a_{dis})^2} \tag{33}$$

where Δ_0 is the intrinsic roughness, λ_{coh} is the neutron coherence length and a_{dis} is a dispersive capillary length. The $\langle\Delta\zeta^2\rangle$ term is the capillary wave contribution to the interface and can be thought of as if the interface were a membrane in a state of tension and can be characterised by a bare interfacial tension γ that sustains a spectrum of waves, each of which has an average energy determined by an equipartition of energy. From inspection of Eq. (33) is it important to note that the capillary wave contribution to the measured interfacial width varies logarithmically with the film thickness.

In a series of neutron reflection experiments, Sferrazza et al. measured the interfacial width of bilayers of d-PS on h-PMMA, where the bottom PMMA layer was between 400 and 900 nm and the top d-PS film layer was varied between ~5 and ~2000 nm [28]. Fig. 3 shows the interfacial width (in this figure it is plotted as interfacial roughness) as a function of the d-PS layer. It is clear that for thinner d-PS films the value of the interfacial roughness depends on the film thickness, and it is approximately logarithmic as expected from Eq. (33). This logarithmic dependence persists up to d-PS layer thicknesses of ~100 nm, after which the data clearly levels off to a value of ~2 nm (for thicknesses bigger than ~100 nm the neutron coherence length is dominant). Using Eq. (33), Sferrazza et al. fitted the data by varying the intrinsic interface width Δ_0 and the interfacial tension γ, giving the solid line shown in Fig. 3. The value of the neutron coherence length was fixed at 20 μm and the best fits to the experimental data were obtained when values of $\Delta_0 = 9.3 \pm 1.4$ Å and $\gamma = 2.7 \pm 0.3$ mJ m^{-2} were used.

An interesting counterpoint to this study is the investigation by Doerr et al. of the surface roughness of liquid perfluorohexane, cyclohexane, decane and ethanol thin films adsorbed on silicon wafers as a function of film thickness [156]. The systems were investigated by XR, diffuse scattering and grazing incidence diffraction. The film thicknesses used for these films were in the range of 20–250 Å. The surface

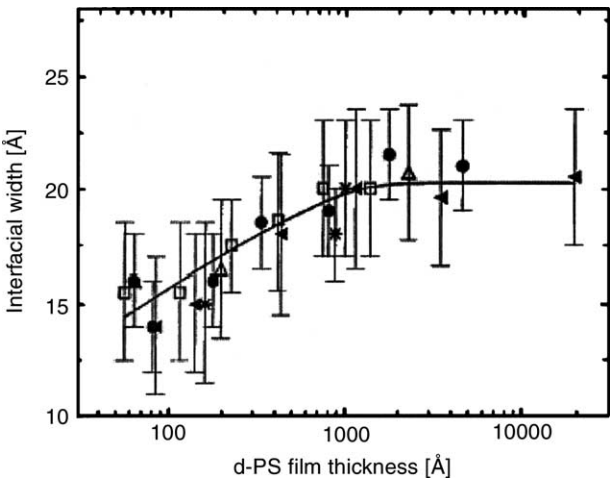

Fig. 3. Experimental interfacial roughness of d-PS/PMMA as a function of the dPS film thickness for various polymer combinations of high molecular weight. The solid line is a fit to Eq. (33). Reproduced with permission from Ref. [28].

roughness obtained from the reflectivity data are shown in Fig. 4, where the roughness is displayed as a function of the film thickness [157]. The observed logarithmic increase of the roughness with d was predicted by the inclusion of capillary wave roughening of the surface which has a van der Waals cut-off given by $q_l = a/d^2$, where d is the thickness of the film and $a = (A_{\text{eff}}/2\pi\gamma)^{1/2}$ (A_{eff} is the effective Hamaker constant and γ is the interface tension). For thicker films the experimental roughness is larger than that predicted by the capillary wave prediction which is plotted as the solid line. This can be understood by considering that retardation effects must play a role for thicker films, lowering the value of the Hamaker constant and in turn yielding an increased surface roughness.

As observed for liquid surfaces, polymer surfaces also contain a spectrum of capillary waves. Wang et al., showed the effect of the interactions with the substrate on the spectrum of capillary waves at the polymer surface [158]. In this study, thin films of PS and polyvinyl-pyridine (PVP) on silicon substrates were investigated using both specular and diffuse X-ray scattering. For these measurements the thin polymer films had thicknesses between 35 and 1600 Å. The effect of geometric confinement within these thin films was seen to suppress the capillary wave spectrum at the surface. The intensity of the scattering obtained for the different polymer film thicknesses as a function of the transfer momentum, q_x, in the sample is shown in Fig. 5. By analysing both the specular and off-specular scattering intensity, the roughness of the surface was determined as a function of the thickness of the PS layer (see inset of Fig. 5). It is observed that the mean square roughness, σ^2, of the film surface increases logarithmically with increasing film thickness, as expected. A difference between the capillary wave amplitude prediction and the experimental data was observed when the wave-number cut-off extracted from the diffuse

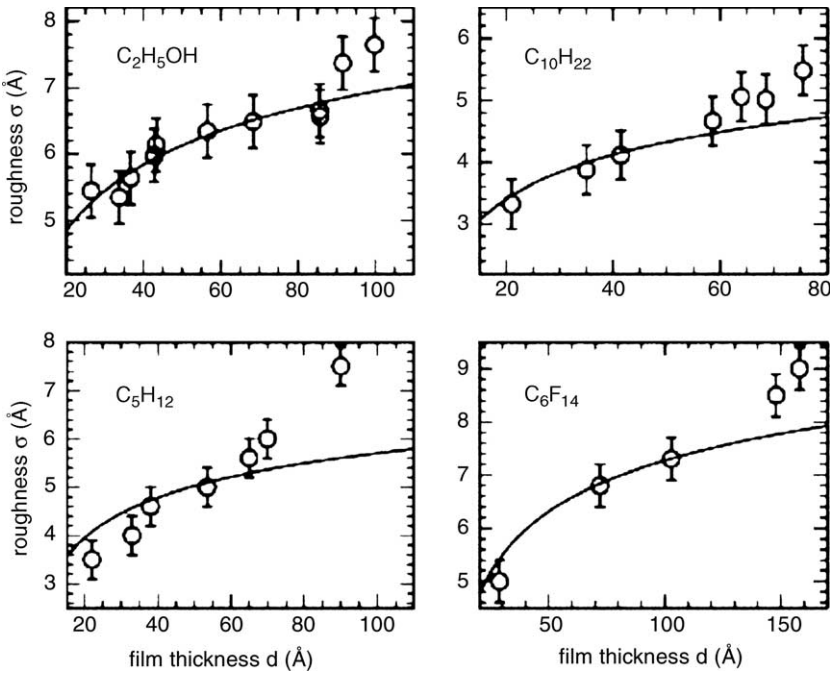

Fig. 4. Surface roughness for different liquid films obtained from XR. The solid lines are calculation based on the capillary wave theory. Reproduced with permission from Ref. [157].

scattering was plotted as a function of the film thickness for both series of PS and PVP samples. This prediction was calculated using pure van der Waals interactions without inclusion of viscoelasticity, i.e. the bulk shear modulus of the viscoelastic polymer is assumed to be zero. The prediction gives the behaviour of $q_{l,c} = a/d^2$, which clearly disagrees with the experimental data indicating the importance of the interaction with the substrate. For PVP, the difference between the experimental data and the capillary waves prediction is even more pronounced. This is perhaps not surprising since PVP interacts strongly with the silicon substrate and therefore the viscoelastic nature of the film becomes important. The unusual non-liquid like behaviour of these films is clearly caused by strong geometric confinement induced by the substrate interaction. This is also supported by the fact that for polymers that do not interact with the substrate, Tolan et al. have shown that the capillary waves at the surface are not suppressed [159]. The strong interaction and therefore the strong confinement at the silicon oxide interface could therefore be the source of the viscoelastic behaviour observed by Wang et al. for these films.

4.4. Approaching criticality

As has been shown so far, the equilibrium interfacial width in polymer systems is substantially broader than the mean-field prediction, and the origin of this broad-

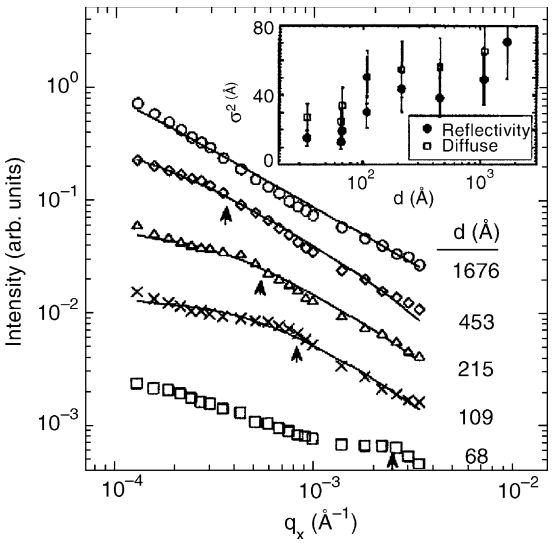

Fig. 5. Diffuse scattering from polystyrene films on silicon substrates of different film thicknesses. In the figure the transverse scans along q_x for a fixed value of q_z of 0.2 Å^{-1} are shown. The lines are fits to the data. The inset shows the roughness σ^2 as a function of the thickness of the polymer film for both specular and off-specular scattering. Reproduced with permission from Ref. [158].

ening is thermally excited capillary waves. It is also clear that in confined systems the spectrum of capillary waves excited is modified, and that this has a substantial effect on their contribution to interfacial width in thin films. A logarithmic dependence of the interfacial width as a function of the film thickness is observed when long range dispersive forces dominate. In this case, an effective potential for an interface at a distance L from the wall is of the form $V(L) \propto L^{-m}$, where m is an exponent ($m > 2$ for such systems). However, the relative long range van der Waals forces and short range "truncation forces" are important factors in influencing the capillary wave spectrum. This is particularly true for systems which are close to the critical point where the width is a considerable fraction of the film thickness. Short range interactions, between the monomeric unit and the surfaces, can also be important, where the effective potential for an interface at a distance L from the wall is of the form $V(L) \propto e^{-kL}$. For short range surface fields, the width of the apparent profile in a thin films increases like $\sqrt{D}$ where D is the film thickness. The surface fields give rise to a lateral correlation length, $\xi_{\|}$, which acts as a long wavelength cut-off for the spectrum of capillary waves. The parallel correlation length incorporates two contributions, from short range distortions of the interfacial profile near the wall, as well as long range surface fields. This lateral correlation length is given by:

$$\xi_{\|} = \xi_b e^{kD/4} \tag{34}$$

where ξ_b is the bulk correlation length and $1/k$ is a transverse length. The correlation length is proportional to the thickness of the film, which can be understood at a

qualitative level by considering the energy cost of truncating the local interfacial composition profile between the coexistence phases by the film boundaries. This truncation effect depends on the thickness of the film, so that for thicker films the effect is weaker since the boundaries are more distant from the average position of the interface. In the presence of an interface in this situation a new contribution to the capillary wave, that is the Hamiltonian function, has to be considered. This term arises form the two walls and is given by $V_{\text{walls}}(z_0) \propto e^{-[k((D/2)+z_0)]} + e^{-[k((D/2)-z_0)]}$ where z_0 is the equilibrium position of the interface. The effect is to attenuate any fluctuations of the interface far away from its equilibrium position i.e. when $z_0 = 0$. Clearly, for a confined interface it is meaningless to consider capillary waves larger than the correlation length $\xi_{\|}$, since this is the largest length over which a correlation in z_0 persists. For a confined interface therefore, the interfacial width is given by:

$$\left(\frac{w}{2}\right)^2 = \xi_b^2 + \xi_b \frac{D}{4} \tag{35}$$

This equation means that the interfacial width is proportional to the square root of the total thickness of the film. Kerle et al. have studied the interface width of binary mixture of two different mixtures of polyolefins [74,160]. The polymers used were random copolymers, in each of which the monomers have structure either (–C_4H_8–) and (–$C_2H_3(C_2H_5)$–) randomly positioned along the chains. Partial deuteration of these polymers was necessary to allow the polymers to be distinguished using NRA depth profiling. Kerle et al. prepared films between 80 and 1200 nm thicknesses, consisting of mixtures of these polyolefin random copolymers, and annealed the

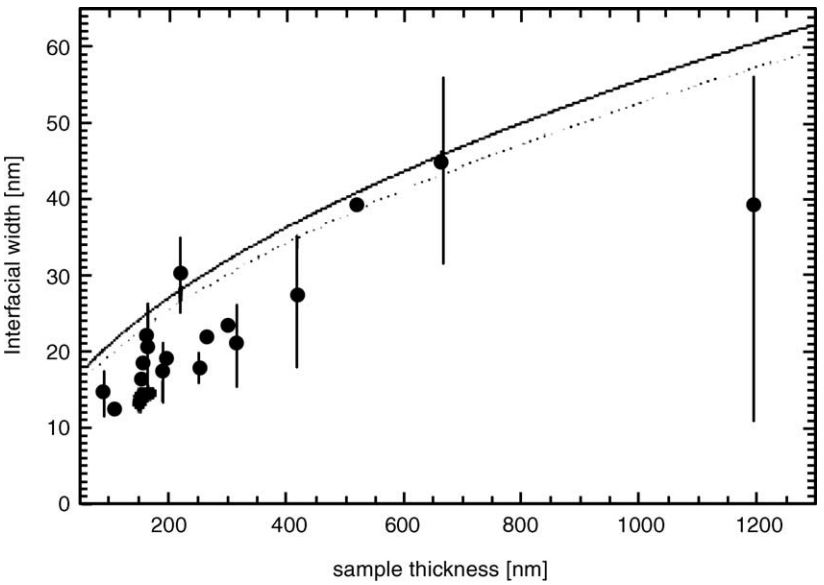

Fig. 6. The interfacial width w as a function of the thickness for a blend of olefinic copolymers at a temperature of 356 K, extracted from NRA experiments. The curve corresponds to a fit using Eq. (35). Reproduced with permission from Ref. [160].

samples at a temperature T_0 of 356 K [160]. At this temperature, which is below T_{cb} but above T_w, the polymer mixtures underwent phase demixing. The interface formed between the phases was parallel to the surface and demonstrated surface roughness. The interfacial width obtained as a function of the total thickness is shown in Fig. 6, with widths predicted using Eq. (35). These predictions were obtained by using the standard mean-field estimate for the correlation length in polymer blends, with ξ_b in the range of 10.6–11.8 nm. It is clear (see Fig. 6) that Eq. (35) qualitatively predicts the experimental data for the interfacial thickness. Kerle et al. [74] suggested that another effect which could contribute to the experimental interfacial width observation is the increase in surface energy due to the phase separation with a preferential attraction of one of the phases to either of the two surfaces. This energy increase would then suppress the interfacial width even further. Another point worth considering, is that for a film thickness D of around 600 nm, the correlation length of the system is of the order of 1 cm, which is comparable with the lateral dimension of the sample used by Kerle et al. In this case one would expect a levelling off of the interfacial width for sample thicknesses larger than 600 nm. The limited set of data in this region seems to indicate this behaviour, and is similar to the asymptotic behaviour in the interfacial width of PS/PMMA observed by Sferrazza et al., for film thicknesses above the lateral coherence of the neutrons [28].

5. Instability in thin polymer films

The wetting and dewetting of surfaces by thin liquid films are well-known phenomena that have been studied for some time (see for example [161]). Recently, a lot of attention has been paid to the study of the dewetting behaviour of thin polymer films [162–188]. Polymer films represent ideal systems to study such physical phenomena due to their low vapour pressure and high viscosity, which allows time resolved experiments to be undertaken. The dewetting behaviour of thin polymer films has also attracted substantial technological interest due to the widespread use of polymers in for example coatings and packaging where film integrity is essential. Polymer systems are more complicated than non-polymeric ones, due to their long chains. Although dewetting occurs in many fluid systems, the behaviour of polymer films have demonstrated some unique effects. For example, for films of thickness less than the bulk equilibrium size of their constituent molecules, spontaneous dewetting can take place [170]. This opens up the possibility of investigating polymer mobility in thin films [171–173]. The study of dewetting and how to control it using polymer chains attached by one end to an interface (polymer 'brushes') has also been investigated [176]. This makes the study of their wetting and dewetting phenomena quite an exciting field in soft condensed matter.

5.1. Mechanisms of dewetting in polymer systems

One of the first systems used to investigate the dewetting of thin polymer films was PS. The initial studies of the dewetting of thin PS films on silicon substrates was

performed by Reiter [162] who showed that the dewetting of thin films proceeds via three stages. In the first stage, the films breaks up into randomly distributed holes, this is followed by growth of the holes so that the rims eventually merge creating cellular structures. Finally, the resulting ribbons between the enlarged holes become unstable and break up by Raleigh instabilities to form an ordered array of droplets. These initial studies showed that the average distance between the holes depends on l^2, where l is the thickness of the film. More recently, it has been shown that in general the dewetting of a thin polymer film can develop in two different ways, either by nucleation and growth of holes or by amplification of surface fluctuations. Nucleation and growth of holes can take place, initiated by nuclei in the form of dust particles or other surface heterogeneities. This mechanism is called 'heterogeneous nucleation'. The growth of the holes causes the accumulation of polymer along the hole perimeter, building up rims around them, until these rims eventually break up into droplets. This process has been studied recently for the bilayer of PS and PMMA by Qu et al. [179]. The second possible dewetting mechanism is caused by the instability of the film against thermally excited capillary waves at the surface or interface and no nuclei are needed for the dewetting to start. This instability is analogous to spinodal decomposition processes and the mechanism is therefore often referred to as 'spinodal dewetting'. For thin films with thicknesses less than approximately 100 nm, the van der Waals forces are expected to play an important role, and the instability against excited capillary waves becomes very sensitive to the thickness of the film [168,183]. In the spinodal dewetting mechanism [167,168,186–190] a dominant capillary wave amplitude mode at a polymer surface or interface grows exponentially with time with a characteristic wavelength that depends on the thickness of the film, until the instability ruptures the film. Once the film ruptures and holes form the dewetting process then proceeds in the same way to the growth of the holes and rims described above.

In the process of spinodal dewetting, thermally excited capillary waves at a fluid interface are amplified by dispersion forces which are essentially Rayleigh–Taylor instabilities [191]. The condition for marginal stability is given when the free energy cost of an interface perturbation arising from the increased interfacial energy is balanced by a lowering of the free energy due to the dispersion force. The dispersion forces acting across a thin film, of thickness h, may be expressed in terms of a Hamaker constant A. The excess free energy per unit area due to a sinusoidal perturbation of wave vector q and amplitude ς_q is equal to $A\varsigma_q^2/8\pi h^4$. Thus, if the Hamaker constant is positive, the capillary waves lead to an increase in the system's free energy and the dispersive forces in this case stabilise the interface against capillary wave fluctuations. On the other hand, if the Hamaker constant is negative, the growth of long wavelength capillary waves leads to a lowering of the system's free energy and the onset of instability occurs, with the wave vector for marginal stability q_c given by $q_c = (|A|/2\pi h^4\sigma)^{1/2}$, where σ is the interfacial tension. At early times, the dynamics of the instability can be solved by a linear approximation [172,190]. For a thin liquid film A on a liquid substrate B the mode that leads to dewetting is called the 'peristaltic mode', where the displacements of the free surface and the fluid/fluid interface are in anti-phase. It should be noted that for a system composed of two

different polymers, then in general the interfacial tensions are typically an order of magnitude smaller than the polymer surface tensions, in which case it is the interfacial tension that dominates the behaviour. Similarly, in a pure peristaltic mode the ratio of the amplitudes of the displacement of the surface and the displacement of the interface is equal to the ratio of the surface tension to the interfacial tension so for a polymer/polymer system we expect the displacement of the surface to be much smaller than the displacement of the polymer/polymer interface. In the liquid/liquid case, the expression for the rise time of the unstable mode takes the form:

$$\tau_{\mathrm{m}} \sim \frac{h^6 \eta_{\mathrm{B}} \sigma}{L|A|^2} \tag{36}$$

where L is the thickness of the substrate film, h is the top film thickness, and σ is the interfacial tension. For a liquid film on a solid substrate, dissipation processes in the substrate become important or dominant, so that the rise time takes the form:

$$\tau_{\mathrm{m}} \sim \frac{h^5 \eta_{\mathrm{A}} \sigma}{|A|^2} \tag{37}$$

where η is the viscosity of the bottom or top film depending on the situation [172,190].

The main predictions of the theory are that the wavelength of the fastest growing wave at the interface or surface is proportional to the square of the thickness of the film. The rise time of the amplitude of the wave is also predicted to increase with the inverse of the nth power of the thickness, where n depends upon the type of substrate on which the thin film is deposited. For the fluctuations at the surface or interface to be amplified with time, the value of $1/\tau_q$, given by the equation above must be negative, and this happens if the Hamaker constant is negative. In this case, fluctuations at the surface or interface should be amplified until rupture of the film takes place. When the Hamaker constant is negative spinodal dewetting has been predicted to be the main mechanism for dewetting for ultra-thin films.

Theoretical approaches to describe spinodal dewetting have been reported by a number of authors [190,192–195]. Brochard-Wyart et al. [172,190] for example have predicted that the characteristic wavelength depends on the square of the film thickness; and that the rise time of the amplitude of the fastest mode is related to the nth power of the thickness, with n between 4 and 6, depending on the viscosity of the polymers. Experiment results have been published on the dewetting of polymer films due to instability against capillary wave excitations. For example the studies by Reiter et al., have shown that the dewetting of thin polystyrene films on silicon substrates develop circular holes patterns in the PS films, where the number density of the holes are proportional to the square of the film thickness [162,169,174], which are in agreement with the spinodal dewetting predictions. The process of spinodal dewetting in thin film geometry is valid also for other systems. A nice example is a recent study on thin liquid metal films, published by Bischof et al., using optical microscopy and scanning electron microscopy [196]. In this case, the instability of the liquid film against the growth in amplitude of surface waves with a characteristic wavelength was observed. More recently Herminghaus et al. have shown that for

thin gold films as well as thin liquid crystal films the spinodal dewetting and nucleation mechanisms are present [197].

A general problem with these types of study is that the theory of dewetting predicts modulations of the surface or interface with a wavelength proportional to the square of the thickness but this does not describe the actual break-up of the film and is strictly only valid for the early stages of the process, which lead to the rupture of the film. For example, for the spinodal dewetting of a polymer–polymer system it is the instability of the films against capillary wave excitations at the interface that is important and the early stages of the phenomenon are difficult to investigate in detail, since the interface of interest is buried. Recently work which overcomes these limitations has been published by Sferrazza et al. who have used off-specular neutron scattering to study the wave amplification of capillary waves at the buried PS and PMMA interface [185].

5.2. The free energy of the system

Spinodal dewetting of liquid films was predicted theoretically well before it was observed experimentally. The two mechanisms of dewetting were developed by Vrij [192] and Ruckenstein and Jain [193], who predicted the spontaneous rupture of a free liquid film would result in a dewetting pattern of 'hills and gullies' with a characteristic wavelength, λ. This characteristic wavelength is connected to the free energy per unit area, which is the excess free energy per unit area needed to bring two interfaces from infinity to a distant l apart. For a polymer film on a substrate two interfaces exist, which are the substrate/polymer and the air/polymer surfaces. In general, the stability of the film with respect to dewetting depends on the free energy per unit area, which for a macroscopic film that is thicker than a few micrometers, is equal to the sum of the capillary and gravitational energies. For microscopic films, the long range forces are dominant in the expression for the free energy. In this case, these long range forces introduce a correction to the capillary energy if the thickness of the film becomes very small, and a new term to the free energy has to be added, which tends to zero for larger thickness l. If the thickness l is larger than the molecular size, the van der Waals free energy term per unit area is given by:

$$W(h) = \frac{A}{12\pi h^2} \tag{38}$$

To better understand the properties of the film as a function of the free energy, it is important to sketch the free energy per unit mass as a function of the film thickness for stable, metastable and unstable films [168]. For the stable films (Fig. 7, curve (1)) the free energy is always positive and the global minimum is at a distance corresponding the infinite thickness. For unstable films (Fig. 7, curve (2)) the free energy has a minimum at a distance $h = h_i$, and therefore the system can gain energy if it changes its thickness to h_i. However, if the initial thickness is larger than h_i the film will dewet. This can be understood since it is known that spinodal dewetting can happen if the second derivative of the free energy is negative at an initial thickness of the homogeneous film. Fig. 7, curve (2) is a characteristic plot of such a situation and

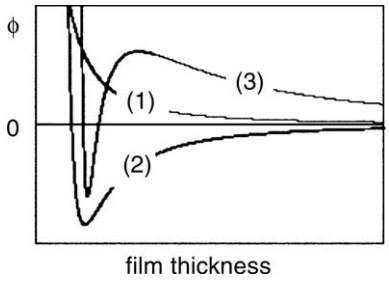

Fig. 7. Sketch of the free energy per unit mass as a function of the film thickness for (1) stable, (2) unstable and (3) metastable films. Reproduced with permission from Ref. [168].

therefore represents an unstable film. Fig. 7, curve (3) represents a different situation in which a region exists for very small film thicknesses where the second derivative of the free energy is negative. For larger thicknesses only nucleation processes can cause the dewetting, so Fig. 7, curve (3) therefore describes the metastable case [168].

The sign of the Hamaker constant is important for the dewetting process. Consider a two phase system in which medium A is more polarizable than medium B, and the Hamaker constant is negative. As described above, the stability of the film depends on the free energy per unit area $F(h)$. When the second derivative of the free energy per unit area is zero ($F''(h) = 0$), a thickness h_i is defined so that $h_i^2 = k^{-1}a$, where $k^{-1} = \sqrt{\gamma/\rho g}$. Two regimes can be defined from the sign of $F''(h)$. In the first regime, for film thicknesses between h_i and h_c (where h_c is given by $k^{-1}\vartheta_E$ and ϑ_E is the contact angle determined by the minimisation of the free energy of the drop) the films are metastable and the dewetting proceeds by nucleation and growth. In this case $F''(h) = 0$. For films of thickness which are less than h_i thick they are unstable since $F''(h) < 0$. The thermal fluctuations at the interface between the two phases are amplified until the upper film breaks into droplets. The amplitude of the unstable mode grows exponentially with a rate given by $\exp(t/\tau)$, where τ is the grow time and is characteristic of the respective mode and of the corresponding wavelength λ. In the second regime 'spinodal dewetting' occurs, where the film instability is driven by van der Waals forces. In this case, the characteristic wavelength, which is proportional to the square of the thickness, occurs after a minimum value of τ. For times longer than the amplitude of the characteristic wavelength has reached the thickness of the film and holes are created. Therefore τ is normally called the rupture time.

For the first regime, i.e. h is between h_i and h_c, Brochard-Wyart et al. have predicted different behaviour for the growth of the holes depending of the relative viscosities of the two phases [172,190]. For systems where the viscosity of the bottom layer is larger than that of the top, the bottom layer behaves like a solid and different regimes are possible, depending on the viscosity of the top liquid. The top liquid A may be viscous and have a small contact angle (viscous regime), or it may have a low viscosity and a large contact angle (inertial regime). For both cases the dewetting velocity is constant and for the viscous regime the growth velocity is controlled by the competition of capillary forces and viscous flow of the A phase. In this case, the

velocity scales as the cube of the contact angle and does not depend on the viscosity of the substrate. The width of the rim grows as the square root of time and the radius of the holes grows linearly with time. In the inertial regime the velocity of the rim is proportional to the spreading coefficient S. For the case of a substrate with a lower viscosity than the top layer, three regimes are possible, a viscous regime, a viscous–inertial regime, and a purely inertial regime. For the viscous case, if the thickness of the film is larger that the size of the rim, a constant growth velocity for the rim is predicted depending on the viscosity of the substrate. If the thickness of the film is comparable to the size of the rim, the radius of the holes does not increase linearly with time and the velocity depends on time t as $t^{-1/3}$. For the viscous–inertial case, the growth of the holes depends instead on $t^{6/7}$. The purely inertial regime is similar to the high viscosity case.

All these predictions have been the subject of various experimental studies by different authors [178,179,182,198,199]. For instance, Martin et al. have studied poly(dimethylsiloxane) (PDMS) films on top of poly(fluoroalkylmethylsiloxane) (PFAS) [199], whilst Faldi et al., used polycarbonate (PC) on a rigid substrate of poly(styrene-co-acrylonitrile) (SAN) [198]. Lambooy et al. studied the dewetting between thin PS films and a PMMA substrate [178], which was subsequently followed up by Qu et al. [179]. In all these studies, different combinations of molecular weights were used for the polymers, giving the possibility of probing different viscosity regimes as described above. An interesting technique was applied by Lambooy et al. [178] to study the buried interface between PS and PMMA, where the shape of the interface near a growing hole was studied by AFM. The samples were annealed for different lengths of time above the glass transition during the dewetting process and then quenched below the glass transition. After measuring the PS surface, the top PS layer was subsequently removed by immersing the samples in cyclohexane. After locating the same spot on the sample, another AFM image was taken, of the remaining PMMA surface. By combining the two images it was possible to produce a 3-dimensional map of the PS rim around a growing hole (see Fig. 8).

5.3. Spinodal dewetting in thin films—recent experimental results

In the last few years, experiments devoted to the investigation of the spinodal dewetting have concentrated on the characterisation of the mean distance of holes to verify the proportionality of λ with the square of the film thickness (see for example the original work of Reiter [162]). However, the mean distance of holes calculated from the area density is not necessarily equal to the characteristic spinodal dewetting wavelength. Jacobs et al. showed that the characteristic wavelength requires correlation between the sites of holes and this may be significantly smaller that the mean distance of holes, since not all the troughs of the fastest growing mode will necessarily lead to a generation of holes [189]. Recently, theoretical predictions of the rupture of thin polymer films producing different classes of dewetting pattern have shown the dependence on the form of the free energy [194,200]. The resulting morphologies of the simulated patterns closely resemble experimental results.

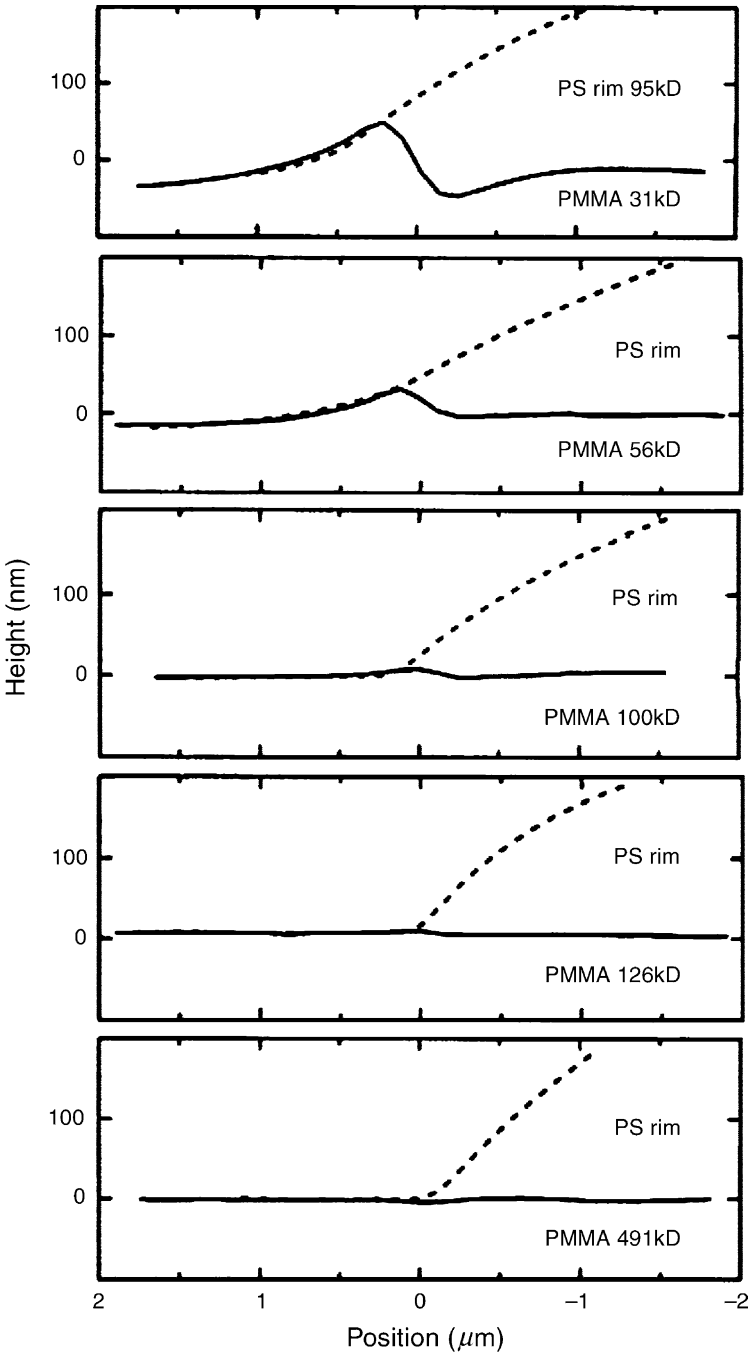

Fig. 8. Cross-section through AFM images taken at the same holes before (- - -) and after (—) the removal of the PS top layer, for PS and PMMA of different molecular weight. Reproduced with permission from Ref. [178].

More recently the dewetting of a thin PS layer on an oxide coated silicon substrate was studied by Seemann et al. to elucidate the relation between the dewetted pattern and the effective potentials shown in Fig. 7 [167,168]. In this work, the interplay between short- and long-range interfacial forces was determined to understand the process of nucleation, spinodal dewetting and thermal nucleation of holes. Their work also showed that the assumption of additivity of dispersion potentials in multilayer systems gives good results. Fig. 9 shows the AFM images for films of different thickness on top of thick and thin silicon oxide layers. It is clear that for thinner films with a thickness of 3.9 nm on top of very thick 191 nm silicon oxide that the characteristic pattern of spinodal dewetting is observed with a characteristic wavelength (Fig. 9a). The wavelength values extracted were plotted as a function of the film thickness in Fig. 9d. It was observed that the characteristic wavelength of the system increased with the thickness of the PS layer as predicted for spinodal dewetting. Seemann et al. also performed XR measurements on these samples and they observed that a thin PS layer of 1.3 nm persisted underneath the dewetting pattern. The same characteristic wavelength was observed for dewetting of PS on thin silicon oxide layers of around 2 nm but only for initial PS thicknesses smaller than 4.1 nm (see Fig. 9d). Thicker films showed

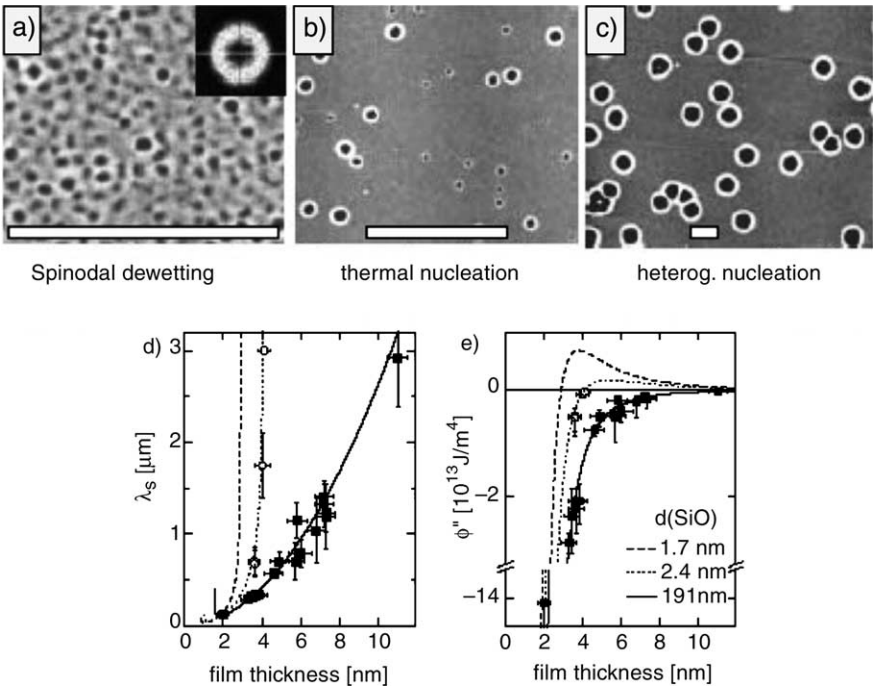

Fig. 9. AFM images of the dewetting for a PS layer of molecular weight of 2000 g/mol and for different thickness of the films ((a) 3.9 nm, (b) 4.1 nm and (c) 6.6 nm) indicating the different regimes of the dewetting processes. The characteristic wavelength of the systems as a function of the PS films is also shown as well the second derivative of the interfacial potential. Reproduced with permission from Ref. [168].

the classical dewetting pattern of holes (Fig. 9c), which was derived from nucleated holes. The material that was on the interior of the hole accumulates in the surrounding rim seen as a bright circle in the AFM picture. While the van der Waals potential could explain the morphological behaviour of the film with the second derivative of the potential a function of the film thickness, it cannot explain the global minimum of the potential at the equilibrium thickness. To explain this, a short range potential was introduced by Seemann et al., which was of the type of Lennard-Jones interparticle potential [168]. For thinner polymer films, the van der Waals potential had to be modified due to the thin silicon oxide layer, since the van der Waals potential of the PS film is composed of two terms: one for the SiO_x layer and the other for the bulk Si (corrected by the presence of the SiO_x thin layer). By considering this corrected potential and the short range term Seemann et al. were able to reconstruct the potential that could explain the observed patterns. From the reconstructed potential for all their systems, they were able to calculate the dependence of the spinodal wavelength as a function of the thin PS film (see Fig. 9d). They also made another interesting observation that the nucleation is responsible of the break-up of the holes if the second derivative of the free energy is positive. Close to the change in sign of the second derivative, they observed that thermal activation was sufficient to overcome the energy barrier for nucleation. This thermal nucleation is another mechanism of dewetting characterised by a continuous break up of holes in contrast to normal dewetting in which the holes appear in a distinct time window (see Fig. 9b).

Seemann et al. also performed interesting studies on the profile of the liquid front of the holes of a dewetting PS system using AFM [167]. They showed the existence of an undulating behaviour of the film on the liquid side. By analysing the hole shape using the AFM, they observed that just after the rim on the wetting side there is a distinct dip. On the dry side of the rim, the rim shape is dominated by the receding contact angle of the liquid on the surface. On the wet side, however, the contact angle is zero and the rim merges with the liquid with the initial thickness of the film. This was predicted theoretically to happen by an undulation that decays with the distance from the rim. An interesting point of this study is the difference of the shape of the rim and the trough when the M_w of the PS layer was changed. They observed that the trough may even be completely suppressed when the M_w increased from 2000 to 600,000 g/mol. It was observed that even if the viscosity increased over five orders of magnitude between these limiting molecular weights, the rim shape for the low molecular weights were always similar but the high molecular weight samples were different. This is an interesting point considering that the lowest molecular weights were below the entanglement molecular weight. This observation suggests that the shape of the rim is related to an increase of the viscoelastic properties of the system. A similar study performed by Reiter also demonstrated a different shape and behaviour of the rim [166]. In this investigation Reiter showed that thin films do not need to be purely liquid in order to allow the dewetting. He observed dewetting of thin PS films at a temperature close to the glass transition temperature of 103 °C indicating that hole formation could be caused by the relaxation of internal stress accumulated during sample preparation and by confining the polymer to films with thicknesses lower that the radius of gyration.

Reiter has also studied the dewetting of a thin PS film on a PDMS coated substrate [166]. The PDMS was used to screen the heterogeneities of the substrate and provide a homogeneous surface of low surface tension for the PS. Reiter measured the diameter of the holes formed as a function of the time at the early stages of the dewetting process for very low and high M_w PS. The dewetting process was observed to occur after a few minutes. Since the two polymers showed the same dewetting behaviour and the viscosity of the two systems varied by several orders of magnitude, this strongly suggests that viscosity does not play a major role in determining the rate of the hole formation. By measuring at temperatures close to the T_g, where the reptation time of the polymer is of the order of 1 year, Reiter could also exclude viscous flow on the time scale of the experiment. This implies that the gain in interfacial energy is probably balanced by dissipation mechanisms in the quasi-solid film, similar to plastic deformation processes. Fig. 10 shows an example of the hole and rim formed for this PS–PDMS system, which is clearly different from the observed shape of the rim seen by Seemann et al. [168]. While at the beginning of the process no rim was observed, an asymmetric rim shape was observed at the later stage. Reiter also showed that the height of the rim is proportional to the diameter of the hole, and this linear relationship indicates that the polymer is not flowing like a liquid. A key feature of this work is that the annealing temperature was close to the T_g of the polymer, where the polymer is highly elastic and therefore viscous phenomena are not responsible for the observed behaviour. This implies that the capillary forces may be sufficiently strong to plastically deform the thin film and semi-glassy polymer layer.

More recently, Reiter et al. have investigated the evolution of the morphology in thin PDMS films between a silicon wafer and a bounding liquid [187]. These studies showed that by increasing the compatibility between the film and the bounding liquid by adding a few surfactant molecules, the instability of the layer was driven faster and the characteristic wavelength was shorter. Fig. 11 shows the results of the dewetting of PDMS films using different liquids that clearly demonstrate the different morphologies. Reiter et al. used these different spinodal patterns to determine that the value of the interfacial tension was small. In general, 'liquid–liquid' dewetting is a more complicated situation since the 'liquid–liquid' interface is easily deformed and must be considered during the dewetting process. This presents a challenge from the

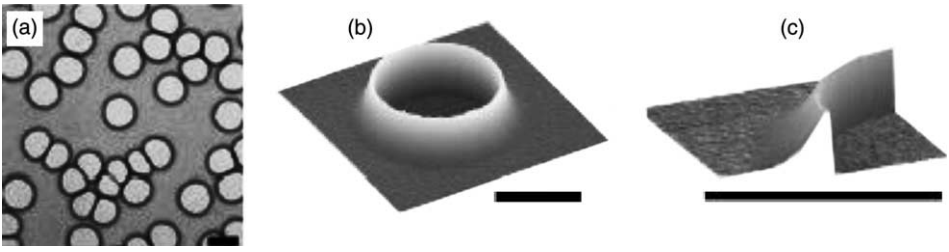

Fig. 10. An example of typical AFM and optical microscopy pictures of holes and the rim from a dewetting PS film. The rim is clearly asymmetric. Reproduced with permission from Ref. [166].

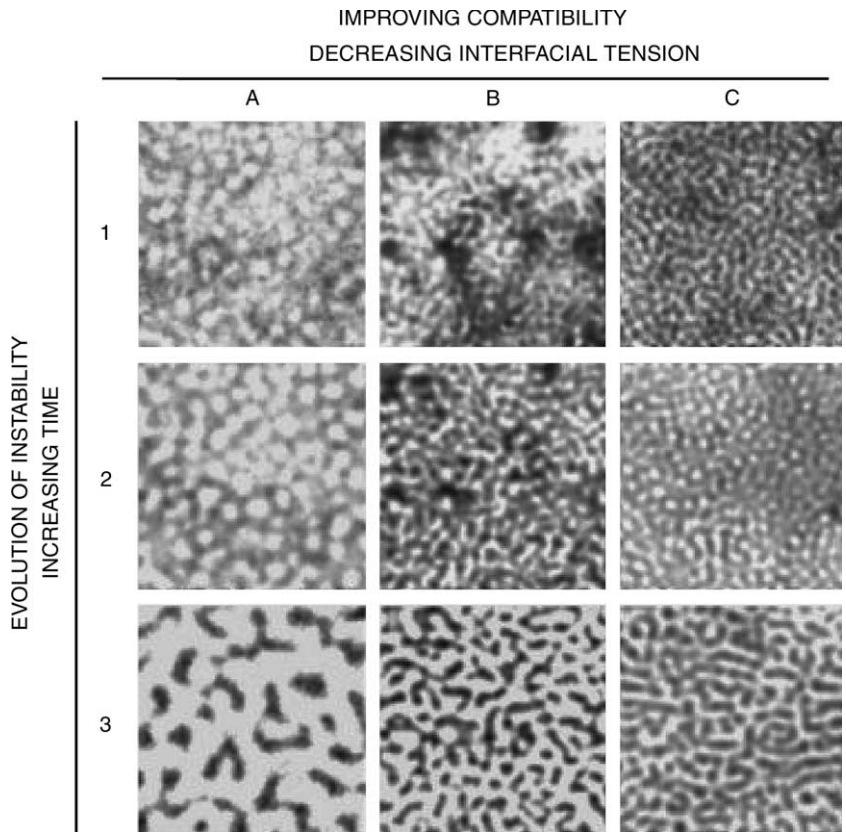

Fig. 11. Different morphologies at different time scales for a thin layer of PDMS under bounding liquids that have different level of compatibility with PDMS. Reproduced with permission from Ref. [187].

experimental point of view in particular at the early stages of the dewetting, since the interface of interest is buried. This is particularly important since the interface between the two phases has, in general, a lower interfacial tension than the surface tension. Recently, Sferrazza et al. studied the early stages of the spinodal dewetting of thin PMMA on top of PS layer in the melt [185]. Higgins and Jones have subsequently investigated the late stages of the spinodal dewetting using the same system [188]. A system in which the PS is a thick layer now at the bottom (on a silicon substrate) and the top layer is a thin PMMA layer, has an Hamaker constant of $A \approx -1.7 \times 10^{-20}$ J. The theoretical considerations introduced in the previous section indicate that the fluctuations at the interface between the two polymers should now be amplified until rupture of the film takes place. The theoretical treatment describes the early stages of dewetting before ruptures takes place. A study of this early stage is therefore an important step towards the understanding of spinodal dewetting. Since the interface is buried, to monitor the development of the unstable mode at the interface between the two polymers the interface, Sferrazza et al. used off-specular

neutron scattering [185]. Off-specular scattering is sensitive to the in-plane structure of the surface or interface, while specular scattering is sensitive to the change of refractive index in the direction perpendicular to the interface. The characteristic size of the fluctuations in the plane of the interface can be extracted from off-specular neutron analysis. The change of its intensity with time can be connected with the characteristic rising time of the unstable mode. Clear features were visible from the reflectivity measurements as a function of the time for the PMMA–PS system. For annealing times between 0 and 6 h, specularly reflected interference fringes due to the bottom layer were visible, corresponding to a PS thickness of around 130 nm (fringes corresponding to the top dPMMA layer were also clearly visible). The intensity of these fringes decreased with increasing annealing time and they were still present up to 6 h, although quite reduced in intensity. After 6 h, a clear difference in the reflectivity was visible, with the top dPMMA fringes disappearing. Clearly in order to provide a more searching test of the theory it would be desirable to study the growth of capillary waves in a way that discriminates between modes of different wavelength. This was achieved by Sferrazza et al. [185] using measurement of the off-specularly reflected neutron intensities. The diffuse scattering for different annealing times as a function of the angle from the specular position for a sample is shown in Fig. 12. The data for the unannealed sample shows a rapid and monotonic fall in intensity from the specular peak. After annealing, however, a prominent shoulder appears which grows in size with increased annealing time. The inset shows the excess scattering relative to the unannealed sample plotted against the scattering

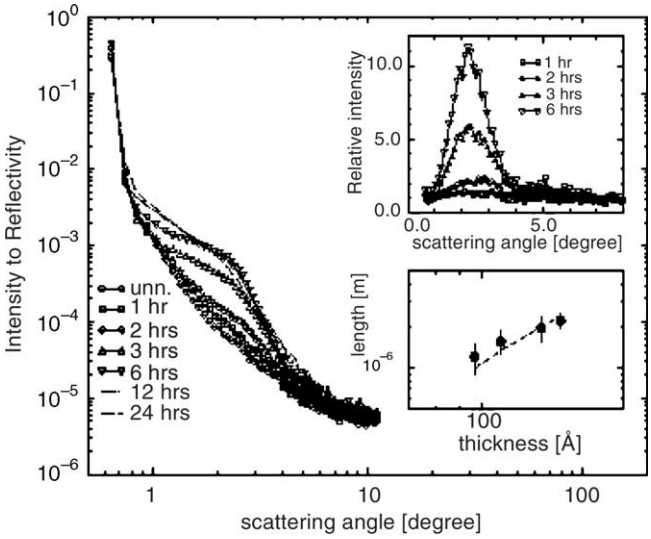

Fig. 12. Diffuse scattering versus angle away from the specular direction for a thin dPMMA film above a thick PS layer as a function if different annealing time at 155 °C. The inset at the top shows the excess scattering up to an annealing of 6 h while the inset at the bottom shows the characteristic wavelength and the theoretical prediction as a function of the dPMMA layer. Reproduced with permission from Ref. [185].

angle. This shows that there is a peak in intensity at a specific scattering angle (corresponding to a scattering object with a wavelength of ~1 μm) that grows with annealing time. Sferrazza et al. [185] interpreted the data as arising from diffraction from capillary waves at the polymer/polymer interface, with the peak arising from scattering from the fastest growing capillary wave, which is analogous to bulk spinodal decomposition. Sferrazza et al. also considered the thickness dependence and time dependence of the interfacial instability, the latter is an important feature of spinodal dewetting. It is this strong thickness dependence of the kinetics of dewetting that clearly distinguishes spinodal dewetting from, for example, nucleation and growth of holes. Fig. 13 shows the relative intensity at the maximum of the off-specular peak as a function of film thickness. At short times the growth of peak intensity is exponential, and only reaches an asymptotic value at later times. The rise times are shown in the inset to Fig. 13. They show the very strong dependence of rise time on the film thickness which is characteristic of spinodal dewetting. It was observed that a 50% increase in film thickness leads to a 770% increase in rise time.

Higgins et al. have used the dewetting mechanism of the liquid/liquid systems to probe the polymer viscosity of thin films to look for differences between thin film and bulk properties [201]. Differences between thin polymer films and bulk material have also been observed for properties such as glass transition temperatures [85,202–204] (summarised in a recent review by Forrest and Jones [205]), viscosity [173,206] and viscoelastic response [207,208]. Higgins et al. [201] used the dynamics of spinodal dewetting for the PS/PMMA system to probe possible changes in polymer viscosity as a function of annealing time and temperature for well defined film thicknesses. To follow the process in detail, they have performed in situ NR to follow continuously the change in the interface and top roughness of the PS/PMMA system. By using a narrow scattering q range coupled to a suitable choice of molecular weights and

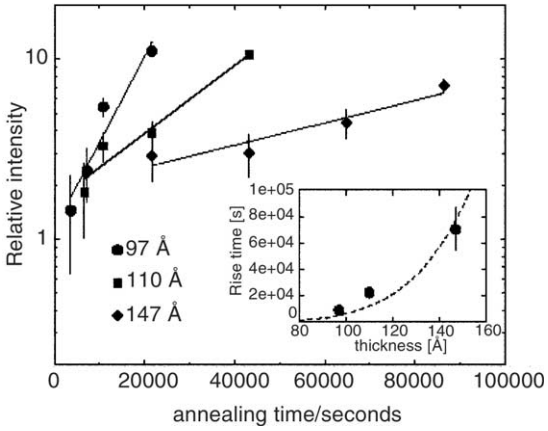

Fig. 13. Relative intensity of the off-specular peaks as a function of the annealing times for different thickness of the top PMMA film. The inset shows the rising time extracted from the data as a function of the thickness and a prediction based on the sixth power dependence on the thickness as predicted by theory. Reproduced with permission from Ref. [185].

temperature, in situ reflectivity at one angle was used to monitor the process closely. They showed that for the M_w's and temperatures used (the latter well above the glass transition temperature), the viscosity of thin PMMA film did not show any major deviation from the bulk behaviour. It was however not possible to say if the apparent low value of viscosity observed from the thin film in comparison to the bulk value were due to enhanced mobility in the thin films or to slippage at the PS/PMMA interface.

5.4. Controlled patterning of thin films

In the absence of mechanical confinement, thermal instabilities in thin polymer films can lead to dewetting of the films from the supported substrates (as discussed in the sections above) or hole formation in freely standing films [182,209]. As pointed out by Dalnoki-Veress et al. [210] control of these instabilities creates the possibility for unique self-assembled surface patterning systems from polymer films. Numerous studies have recently been carried out to capitalize on dewetting polymer films for producing patterned surfaces and some of these have been reviewed by Geoghegan and Krausch [211]. The patterns that dewetting processes produce have a huge potential since they are complementary to photo-lithographically produced microstructures. Patterning using dewetting would be most useful for large area applications where controlled lithographic methods are too time-consuming and costly to form these types of structures. An example of this is the production of nano-corrugated surface topographies as antireflective coatings on optical components such as display devices where light reflection can seriously impair legibility [212]. With the discovery of semi-conducting polymers for roles conventionally dominated by silicon based chip architectures, lithography is too costly and slow for these emerging technologies. Alternative methods such as stamping, screen-printing, ink-jet printing and even polymer dewetting are being developed at a rate where it is possible some may be used commercially [213].

A deceptively simple approach to controlling pattern formation is to induce a preferred orientation to the dewetting process by rubbing a polymer substrate before coating with a second polymer film that is unstable with respect to spinodal dewetting and forms aligned polymer lines (see Fig. 14) [188]. It is believed that the strong orientation of the dewetted pattern arises from the modulation of the thin top polymer layer thickness that is derived from the rubbing process. The thickness fluctuations with the correct wavelength are magnified by the spinodal dewetting process with the result that the orientation of the rubbed pattern is preserved in the final dewetted pattern. The width of these lines are well defined and can be controlled by the magnitude of the dispersion forces at the interface, which are controlled by the initial polymer film thickness. Even more control over the resulting dewetting pattern can be achieved through use of modified substrates, where the differences observed in interfacial energies can be utilised [167,168]. By chemically modifying the substrate to give heterogeneously striped wetting and non-wetting areas, theoretical modeling suggests that self-organized dewetted patterns can be produced [214,215], as long as the destabilising areas have a spacing that lies within a critical range, below which

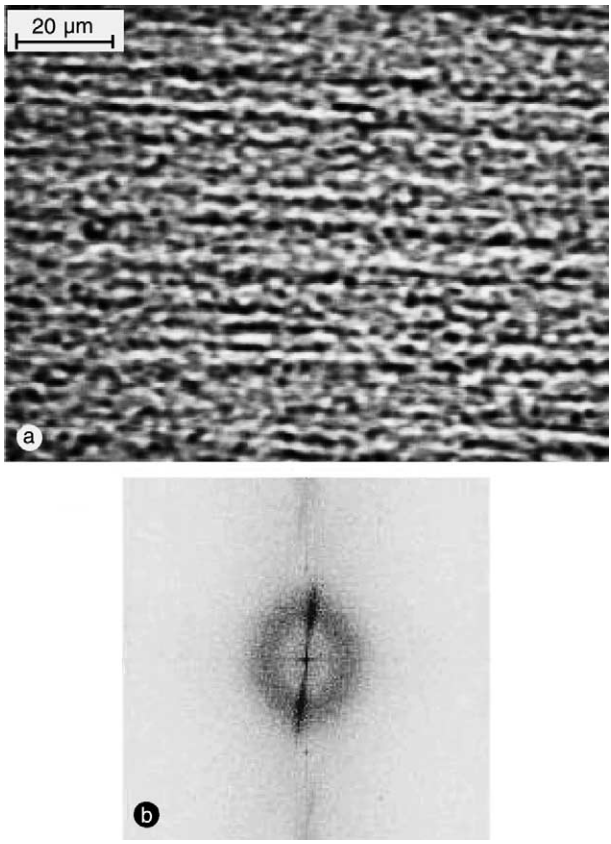

Fig. 14. Dewetted morphology of a Si/PS/PMMA sample, where the PMMA film was prepared on cleaved mica. (a) Optical micrograph of an annealed Si/PS/PMMA sample with a PS film thickness of 175.0 nm and a PMMA film thickness of 12.3 nm. (b) Fast Fourier transform of a red-colour-channel image. Reproduced with permission from Ref. [188].

dewetting does not occur and above which the surfaces features are not replicated [216]. Similarly, closely related theoretical modelling of the thin films of block copolymers on chemically heterogeneously patterned substrates has been published [217–219], although none of these studies have shown that surface topography would be observed on the surface of the copolymer film. Suh et al. have demonstrated that control over the resulting dewetting pattern can be produced by physically confining PS films spun cast on to silicon using a patterned PDMS mould in contact with the free surface of the PS [220]. Dewetting in this case is only observed if the wavelength of the capillary wave for the film, which initiates the dewetting process, is smaller than the pattern size in the mould.

The use of chemically heterogeneous surfaces that have been produced by microcontact printing monolayer alkanethiol patterns with hydrophobic and hydrophilic end groups (i.e. $-CH_3$ and –COOH, respectively) is able to perturb the phase

separation behaviour of blends of polymers in thin films in contact with these surfaces. These surfaces have been utilised by Karim et al. [117,119,221] to study phase separation in thin films of low molecular weight mixtures of dPS and PB and by Böltau et al. [121] investigated blends of PS with either PVP or brominated PS. In both these studies the authors demonstrated that the typical bulk spinodal decomposition behaviour one would expect is disrupted and by using an appropriate choice of surface chemical patterning a topographic surface is produced which replicates the chemical pattern. The surface chemical patterning is necessary if control over the resulting topography is required. If a random structure is sufficient, then simply controlling the blend film thickness and the common solvent used to spin cast the polymer mixture can be utilised to produce random topographic structures [222]. Distinct differences in surface topography and phase domain structure are observed depending of the thickness of the film, the substrate surface energy and the solubility of the two polymers in the mutual solvent. Simply spin casting thin films of PS under the appropriate conditions produces characteristic surface topography [223], through break-up of the film through instabilities.

An alternative approach to using modified substrates is to use polymer blends where the surface energies between the substrate and either of the polymers are very different. The result is to produce phase separation-induced surface patterns if the films are sufficiently thin so as to suppress surface-directed spinodal decomposition waves [224,225]. In the dPS-PVME and dPEP-PEP systems studied by Karim et al. [225] flattened droplets are formed at a very late stage of phase separation, with the substrate wetting polymer forming the continuous phase around the isolated phase domains of the other polymer. The aspect ratio of these droplets can be understood in terms of minimization in the interfacial free energy of the system [226]. Lateral surface structures have also been produced by mechanical confinement of the thin films of polymer blends, such as PS and PMMA between an SiO_x substrate and a SiO_x capping layer [227]. In this system there is a balance between the free energy increase associated with phase separation—through forming interfaces—and the free energy increase from the elastic bending of the capping layer. Consequently, there are critical thicknesses for the capping layer (L) and polymer blend layer (h) above which no lateral structure is observed, see Fig. 15. From experimental observation it was shown that when $L \geqslant (2.65 \pm 0.13)h^{2/3}$ (all units in nm), alternating layers of PS and PMMA are formed (lamellar) due to surface-directed spinodal decomposition [44,136,228]. Lateral structures are formed when values of L and h are below the critical layer thicknesses given in this relationship. The periodicity of the resulting lateral structures are approximately sinusoidal in one dimension with an average wavelength, λ, which depends on the polymer layer thickness through another experimentally determined relationship such that, $\lambda = (14.7 \pm 0.5)h$ (all units in nm). These structures are superficially similar to those seen by Dalnoki-Veress et al. for an unsupported mechanically confined polymer film (PS, PI and PMMA) capped on both sides by a range of materials (Au, SiO_x, and other polymers) [210].

Numerous studies of block copolymer films have demonstrated that symmetric diblock copolymers, for example, undergo an isotropic-to-lamellar transition below the order–disorder temperature if the product of the Flory–Huggins parameter and

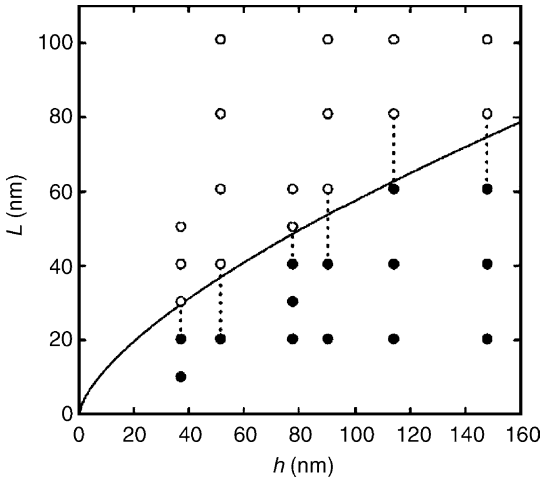

Fig. 15. Plot of the capping layer thickness L as a function of the PS–PMMA blend film thickness h for all of the samples used in the present study. The solid circles correspond to samples for which lateral morphology was observed, and the open circles correspond to samples for which lamellar morphology was observed. For each h value, dashed lines extend between the largest L value for which lateral morphology was observed and the smallest L value for which lamellar morphology was observed. The solid curve corresponds to calculated values of the transition capping layer thickness $L_c = Ch^{2/3}$ using the best fit value for $C = 2.65 \pm 0.13$ nm$^{1/3}$. Reproduced with permission from Ref. [227].

the total degree of polymerisation is greater than 10.5, i.e. $\chi N > 10.5$ [229]. In thin film geometries, the interfacial interactions impose restrictions on the local segmental concentration profiles, with the block possessing the lowest surface energy occupying the free surface [4]. Typically the copolymer lamellar form well ordered structures parallel to the substrate surface, with perfectly smooth surfaces formed if the copolymer layer thickness is commensurate with the lamellar repeat thickness. If the films thickness is not commensurate with the lamellar layer spacing, the system tries to minimise its free energy by creating a discontinuous layer. This minimisation produces isotropic distributions of topographical surface features including islands, holes and 'bicontinuous' patterns [230–232]. Most of the topographic structures observed in these copolymer films result as a consequence of thermal treatment. Wang et al. [233] recently demonstrated that thin films of alternating poly(styrene–maleic anhydride) copolymer (SMA) spontaneously forms well defined surface topography during the drying process at room temperature. Typical examples of the structures produced are shown in Fig. 16. These structures result from dissolving the SMA in a mixture of THF, H_2O and $HCl_{(aq)}$, so that the SMA is hydrolysed and acts as a surfactant to emulsify the water. On drying it is believed that the formation of the holes in the film is a consequence of the emulsified water droplets which evaporate on drying. Li and co-workers [234,235] have shown that propagation of patterned silicon substrates can be produced from both homopolymer and diblock copolymer thin films. In the latter case, modulation of the film surface of PS–P2VP copolymer films on periodic silicon surfaces (surface gratings), were found to be

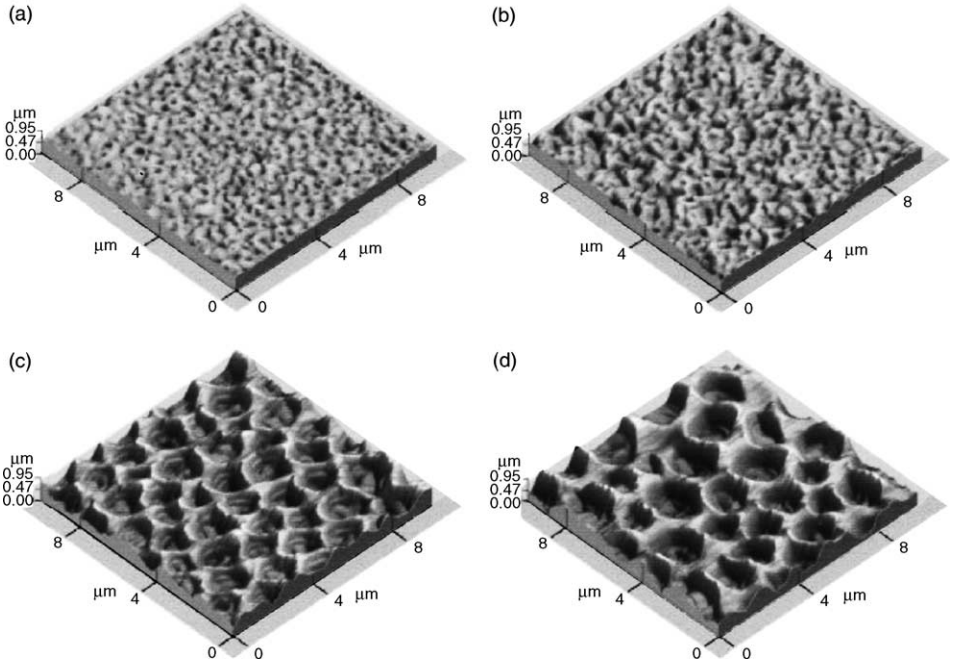

Fig. 16. AFM images of thin films cast from THF solutions with a SMA concentration of 2% g/ml and different weight ratio of H_2O/SMA: (a) SMA–H_2O with H_2O/SMA = 1/7, RMS = 23.7 nm; (b) SMA–H_2O with H_2O/SMA = 1/1, RMS = 43.7 nm; (c) SMA–H_2O–HCl with H_2O/SMA = 1/3, AFM depth $\approx$ 0.530 μm; (d) SMA–H_2O–HCl with H_2O/SMA = 1/1, AFM depth $\approx$ 0.670 μm. Reproduced with permission from Ref. [233].

either in phase (conformal) or out of phase (anti-conformal). A critical height of the surface grating was shown to define the transition from conformal behaviour to the anti-conformal conformation of the films that was found to be proportional to the lamellar height of the diblock copolymers. This can be quantitatively understood within a mean-field theory as a result of balancing the deformation and interfacial energies. Ordering in asymmetric diblock copolymers which form either spherical or cylindrical morphologies can be used to form topographic surfaces that have crystallographic ordering simply by controlling self-assembly [96,230,232,236–242], or by applying an electric field [104,243]. Similar surface patterns can also be observed in triblock copolymers thin films [244]. Although the surface topography is typically of the size of the copolymer spheres, i.e. a few tens of nanometers, these highly periodically defined structures can be used for subsequent processing to pattern the underlying substrate [245–248].

Some recent studies on the effect of an electric field applied across an ionomer film sandwiched between two aluminium layers and supported on a substrate produces the lateral structure shown in Fig. 17 is observed [249]. This result is particularly interesting since without the field applied the film is stable [210]. This is expected not only due to the capping layer but also due to the presence of ionic groups on the

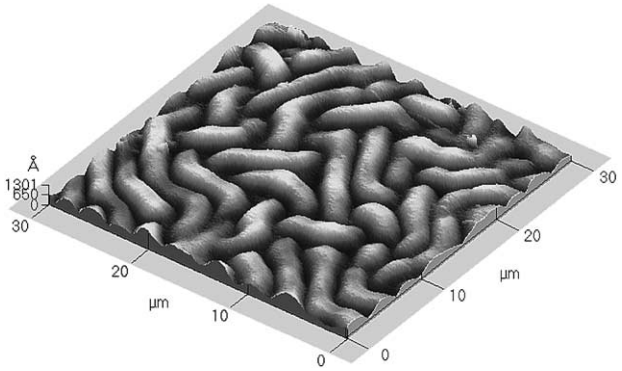

Fig. 17. AFM image of the lateral structure induced by an electric field applied across a zwitterionic–telechelic polystyrene film capped by an aluminium layer acting as an electrode. taken using a tapping mode scan of the lateral morphology showing the 3-D nature of the film surface. Reproduced with permission from Ref. [249].

chain ends which have been shown to form psuedo-networks which then stabilise such films [250]. A quantitative understanding of the observed morphology is obtained by considering the polymer film confined by a solid layer. As discussed by Dalnoki-Veress et al. [210] with reference to their model for a trilayer system which also undergoes microscopic deformation a number of simplifying assumptions are made. The resulting characteristic wavelength can be determined by analysing the total pressure within the polymer fluid film. The total pressure has contributions arising from the pressure induced by the dispersion force, the pressure induced by the electric field which drives the morphology, and the pressure due to the bending of the capping layer that resists the change in morphology.

When the film thickness is reduced due to the increased force between the aluminium layers, the fluid is squeezed out of these regions. Assuming as a first approximation a Poiseuille flow and the fluctuations have a sinusoidal functional form it can be shown that the growth of the deformation is expected to grow exponentially with a single dominant wave vector that grows most rapidly. The corresponding wavelength is:

$$\lambda = 2\pi\left[\left(\frac{A}{\pi(d+l)^4} + \frac{2\varepsilon_p\varepsilon_0 U^2}{d^3}\right)\Big/ 3D\right]^{-1/4} \tag{39}$$

where $D = (El^3)/(12(1-v^2))$, E and v are the Young's modulus and Poisson's ratio of the aluminium capping layer, respectively, A is the Hamaker constant associated with the aluminium–air interface, U is the voltage applied across the polymer film, and ε_p and ε_0 are the dielectric constant and permittivity of the polymer and vacuum, respectively. Considering the simplicity of model with no free parameters, the agreement with experimental the measurements is encouraging. It should also be noted that the second term within the inner bracket of Eq. (39), associated with the applied electric field is three orders of magnitude larger than the first term, and is the

dominate term. This confirms that the driving mechanism for the lateral structure observed is indeed dominated by the electric field.

Superficially similar micro-patterned surfaces can be produced by the buckling of a thin rigid layer on top of a mobile polymer film. Whitesides and co-workers demonstrated that by oxidizing the surface of a hot PDMS film to form a thin, stiff silicate layer and then cooling the system the silicate buckles with a characteristic wavelength [251,252]. The buckling results from the system relieving the compressive stress the silicate is put under. The wavelength, amplitude and pattern of the waves can be controlled by controlling the temperature of the PDMS and thickness of silicate layer formed. Far away from any steps on the substrate the PDMS is placed on the patterns are entirely isotropic, but become highly anisotropic and even linear near topographic features. Here the wavelength of the feature size is given in terms of the Young's modulus, Poisson's ratio of the PDMS (p) and silicate (m) and layer thickness (t) [252]:

$$\lambda \approx 4.36t\left(\frac{E_{\mathrm{m}}(1-\nu_{\mathrm{p}}^2)}{E_{\mathrm{p}}(1-\nu_{\mathrm{m}}^2)}\right)^{1/3} \tag{40}$$

A different approach to exploiting the dewetting behaviour of polymer films is to anneal polymer thin films in the presence of a solid surface placed very close to (typically less than a micron) but not initially touching the polymer surface. Amplification of destabilised capillary surface waves leads to formation of either periodic supramolecular pillar arrays [253] or mesa (terrace) replicas of a mask [254,255]. These deceptively simple but elegant methods of patterning surfaces have been termed as 'lithographically induced self-assembly' (LISA) and 'lithographically induced self-construction' (LISC), respectively. Since the polymer films are initially very thin, neither Rayleigh–Bernard (thermal convection) instabilities [256] or surface tension driven Bernard convection [257] could lead to the patterns formed. Chou et al. have proposed a model for LISA called the image charge-induced electrohydrodynamic-instability (ICE) model, which assumes that the electrostatic force is the driving force for the process [253]. The patterns formed as a result of the interplay and instability of charges in the polymer melt, image charges on the opposition surface and hydrodynamic forces in the polymer melt. Once the polymer film is in the melt there is a significant increase in both charge density and charge mobility in the polymer. Without a surface above the polymer film the charges in the polymer film would be evenly distributed due to the flat surface and symmetry. However, when a surface is present an electrohydrodynamic (EHD) instability due to charges in the polymer and image charges on the solid surface amplify polymer film capillary waves. This initially occurs at the corners of the protruding solid surface so that pillars form first at the sides and then propagate to the center of the solid surface. A similar process is thought to occur in the LISC process but the surface tension differences between the polymer film and the solid surface are arranged to be as small as possible [254]. When the difference between the surface tensions is minimised either by using surfactants or adjusting temperature then when polymer pillars are formed due to EHD instabilities in the initial phase of LISC they

will spread and merge with other pillars to form a single mesa under each solid surface. The resulting structure replicates exactly the protruding surface structure of the top mask.

EHD-driven instabilities and the use of applied electric fields to control destabilisation of thin polymer films have recently been demonstrated for polymer layers [258] as well oligomeric liquids [259]. Here we consider only the polymer case, but the results are equally valid for the oligomeric liquids, except that the features produced in the latter case occur 50 times quicker than for the polymer case [259]. To produce topographic features a thin polymer film was sandwiched between two solid electrodes with an air gap between the polymer surface and the top electrode. When the polymer film is annealed and an electric field is applied between the electrodes the net result is to produce columns with hexagonal order as predicted for two-dimensional systems if the top electrode is planar, see Fig. 18. If patterned top electrodes are used the polymer film replicates the electrode structure. Extension of EHD instability theory to include the applied electric field has achieved by analysing the overall pressure distribution at the film surface [260]. The total pressure can be described in terms of contributions from the atmospheric pressure, a Laplace pressure arising from the surface tension (γ), dispersive disjoining pressure and the electrostatic pressure arising from the electric field. At high enough field strengths only the Laplace and electrostatic terms need be considered. By assuming the surface perturbation to be sinusoidal with a characteristic wavelength and growth rate, it can be shown that the fastest growing fluctuation will dominate the growth of surface perturbations. By solving the appropriate equations for the Poiseuille flow within the polymer film the characteristic wavelength induced by applying an electric field across the polymer film is given by [260]:

$$\lambda = 2\pi E_{\mathrm{p}}^{-3/2}\sqrt{\frac{\gamma U}{\varepsilon_0\varepsilon_P(\varepsilon_P-1)^2}} \tag{41}$$

where U is the voltage applied, E_{p} is the field strength, and ε_0 and ε_{p} are the dielectric constants for a vacuum and the polymer, respectively. To compare the results of the dispersion relationship to experimental data reduced variables are used, so that:

$$\frac{\lambda}{\lambda_0} = 2\pi\left(\frac{E_{\mathrm{p}}}{E_0}\right)^{-3/2} \tag{42}$$

where $\lambda_0 = \varepsilon_0\varepsilon_{\mathrm{p}}(\varepsilon_{\mathrm{p}}-1)^2U^2/\gamma$ and $E_0 = U/\lambda_0$. A wide range of experimental results can be superposed to a single master curve using this reduced variable equation (see Fig. 19).

6. Diffusion in thin polymer films

Diffusion processes are important in many aspects of polymer understanding, and include areas such as adhesion, welding, membrane separation, and osmometry. There have been numerous attempts to understand diffusion processes in polymers

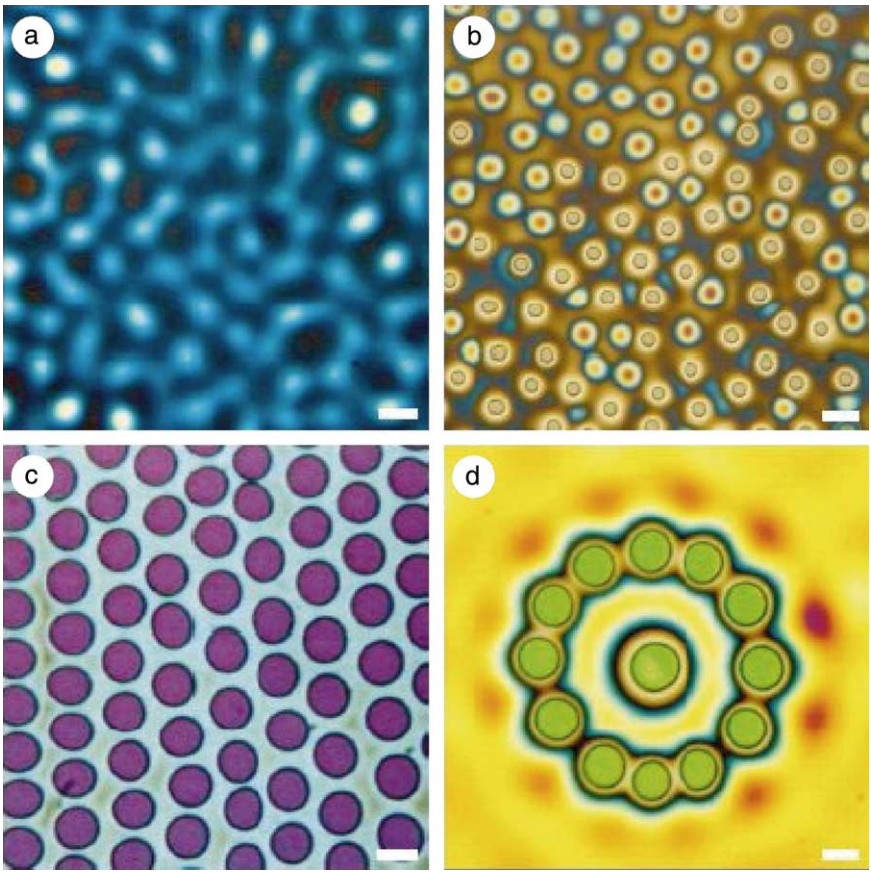

Fig. 18. Optical micrographs of polystyrene films which have been exposed to an electric field. In a and b, a 93-nm-thick polystyrene film was annealed for 18 h at 170 °C with an applied voltage $U = 50$ V. As the electrode spacing in a was larger than in b, corresponding to a lower electric field E_p, two different stages of the instability were observed, corresponding to a and b. In c and d, the thickness of the polystyrene film was doubled ($h = 193$ nm). This leads to a denser packing of the polymer columns and to an enhanced repulsion between the columns. As a result, we observe a more complete hexagonal order in c. In d a second-order effect is observed for a nucleated instability, where instead of a hexagonal symmetry which characterizes the nearest neighbours in c, a ring of 12 columns lies on a circle with a radius of 2λ. The scale bars correspond to 10 mm in a and b and to 5 μm in c and d. The colours arise from the interference of light, and correspond to the local thickness of the polymer structures (for example, in d, yellow corresponds to a film thickness of ~200 nm, green to ~450 nm). Reproduced with permission from Ref. [258].

and much of the terminology in terms of the classification derives from more classical mass transport phenomena, where diffusion processes can be defined according to the relative rates of diffusion and polymer relaxation [261]. Three classes of diffusion behaviour have been distinguished: Case I or Fickian diffusion, Case II diffusion and non-Fickian or anomalous diffusion. Experimentally the type of diffusion can be established by the observed dependency of time, t^n, where n is a constant.

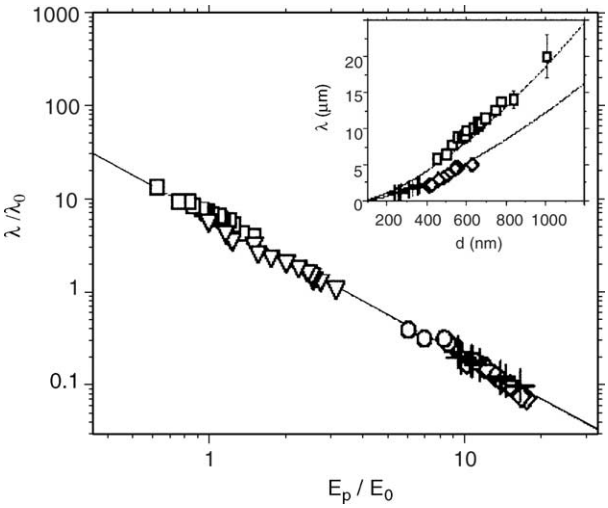

Fig. 19. Variation of λ versus the electric field in the polymer film E_p in reduced coordinates. The different symbols correspond to four data sets: (□) PS with $h_0 = 93$ nm, $d = 450$–1000 nm, $U = 30$ V; (▽) PS with $h_0 = 120$ nm, $d = 600$–1730 nm, $U = 50$ V; (○) PMMA with $h_0 = 100$ nm, $d = 230$–380 nm, $U = 30$ V; (◇) PBrS with $h_0 = 125$ nm, $d = 400$–620 nm, $U = 30$ V. The crosses correspond to an AC experiment (rectangular wave with a frequency of 1 kHz and an amplitude $U = 37$ V) using a PMMA film with $h_0 = 100$ nm, $d = 230$–360 nm. The line corresponds to calculated using Eq. (42). The inset shows some of the data in non-reduced coordinates versus d. Reproduced with permission from Ref. [260].

Case I systems are characterised by an exponent $n = 1/2$, Case II by $n = 1$ and non-Fickian systems by n taking an intermediate value between 1/2 and 1. The use of mass transport theories only provides a phenomenological description of the diffusion process, but only a complete understanding of the polymer behaviour can be derived by use of molecular based theories of polymer diffusion processes [262].

6.1. Polymer–polymer diffusion

There have been numerous experimental studies to test the applicability of the various models to diffusion of linear polymer melts. Many of these studies have used thin film geometries and the increase in interfacial width as a function of time between two miscible polymers to determine the diffusion behaviour. Among the most widely used techniques have been dynamic secondary ion mass spectroscopy (DSIMS) [263,264], RBS [80], FReS [42,265–267], ATR-FTIR [268], XR or NR [14,15,269–271] and NRA [272,273]. Developments in technique of NR to take very rapid reflectivity profiles is opening up the possibility to study small-molecule penetrant diffusion into polymers with sub-nanometer resolution [274–276]. An example of this is shown in Fig. 20 which illustrates reflectivity data collected from oligomeric (methyl methacrylate) (OMMA) of two different molecular weights diffusing into PMMA. These data are remarkable since in a traditional reflectivity measurement over an extended momentum transfer range, data collection times average

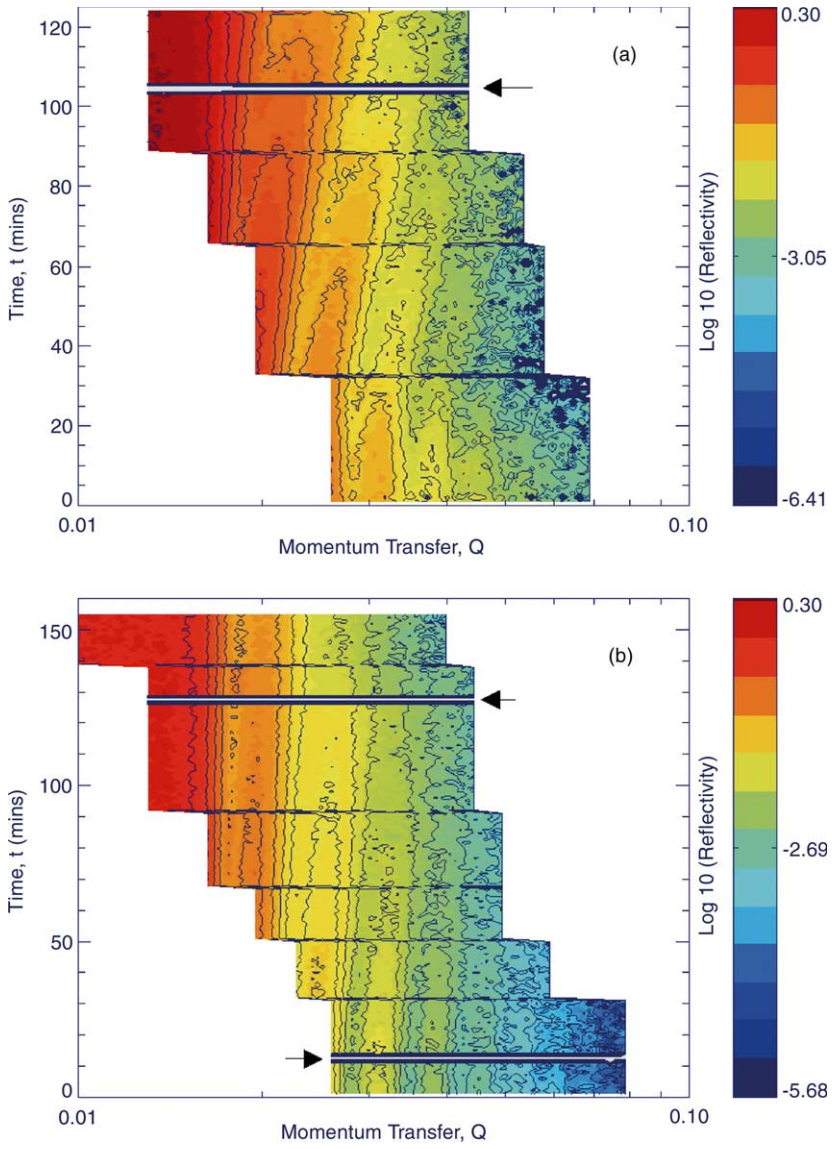

Fig. 20. Time dependent contour plots of real time reflectivity profiles for dPMMA–OMMA with $M_w = 510$ g/mol (a) and 1000 g/mol (b). The horizontal lines indicated by arrows are section of missing data due to 'down' time on the ISIS spallation source. The limited Q range at each angle is clearly observed. The loss of fringes at higher Q is also obvious, especially for the lower molecular weight oligomer (a). Reproduced with permission from Ref. [274].

about 1–2 h. Each reflectivity profile in these data were taken in 20 s in order to follow the relatively fast motion of the OMMA velocity front moving into the

PMMA [274]. A number of useful reviews comparing the various techniques and their application to polymers have been published [10,11,81,277].

Various theories have been proposed for the diffusion of polymers in melts. Perhaps the most widely accepted theory is the model of reptation proposed by de Gennes [2,278] and Doi and Edwards [261]. The basis of reptation is the snakelike motion of a polymer chain along its own contour formed by the constraint of neighbouring chains. The reptation model identifies distinct regions, which have characteristic power-law time dependencies with exponents (n) equal to 1/4 and 1/2. Chain diffusion in the bulk is different from the motion of the chain across an interface, as may occur in welding or adhesion processes. This welding process was evaluated theoretically by de Gennes [279,280], who first identified several distinct cases that depend on the time scale, magnitude of the molecular interactions and the initial configuration of the chain ends at the interface. More recent experimental studies of the welding process have confined the importance of the configuration of chain ends at the initial time of the diffusion process [281], as well as the effective number of monomers that have diffused across the interface [91,282].

For a situation where the molecular weight of the polymers is large compared to the moving polymer the motion of the neighbouring polymer chains are considered to be negligible. If the molecular weight of the matrix polymer is comparable to that of the polymer diffusing through it, then it is necessary to use the constraint release model [283] to take into account the motion of the matrix and diffusing polymer chains on similar time scales. The reptation and constraint release models provide an accurate description for the molecular weight dependencies of diffusion of linear PS in PS melts [284,285]. Other models used to describe polymer dynamics are the Rouse [286] and polymer mode-coupling (PMC) [287,288] models. Both these latter models equate the motion of a single chain in the bulk melt to the Brownian motion of a Gaussian chain in a structureless medium. The difference in these models derives from the description of the force exerted by the medium on a single polymer chain. In the Rouse model, the force is a 'local' friction given by the instantaneous velocity at a specific time on a particular monomer. In the PMC model, in addition to these local forces there are cumulative forces, so that the frictional force at any specific time depends on the entire previous trajectory of all the monomers. Incorporating this prior history explains why the Rouse model fails to describe adequately entangled polymer dynamics, whereas the PMC model can.

A very elegant series of experiments to test the reptation model have been the so-called 'ripple' experiments [94,289]. In these experiments both NR and DSIMS measurements were conducted on symmetrical PS triblock copolymer bilayers (made up of HDH and DHD layers) in order to probe directly the interdiffusion dynamics of the chains during welding of the interface. The HDH chains had their centres deuterated i.e. 50% of the chain deuterated, and the DHD chains had their ends deuterated (25% at each end) so that each chain contained approximately 50% deuterium. During the welding process, anisotropic motion of the chains was shown to produce a time-dependent oscillation (ripple) in the H and D concentration profiles at the interface, which bears the characteristic signature of the polymer dynamics (see Fig. 21). These 'ripple' experiments have subsequently been criticised

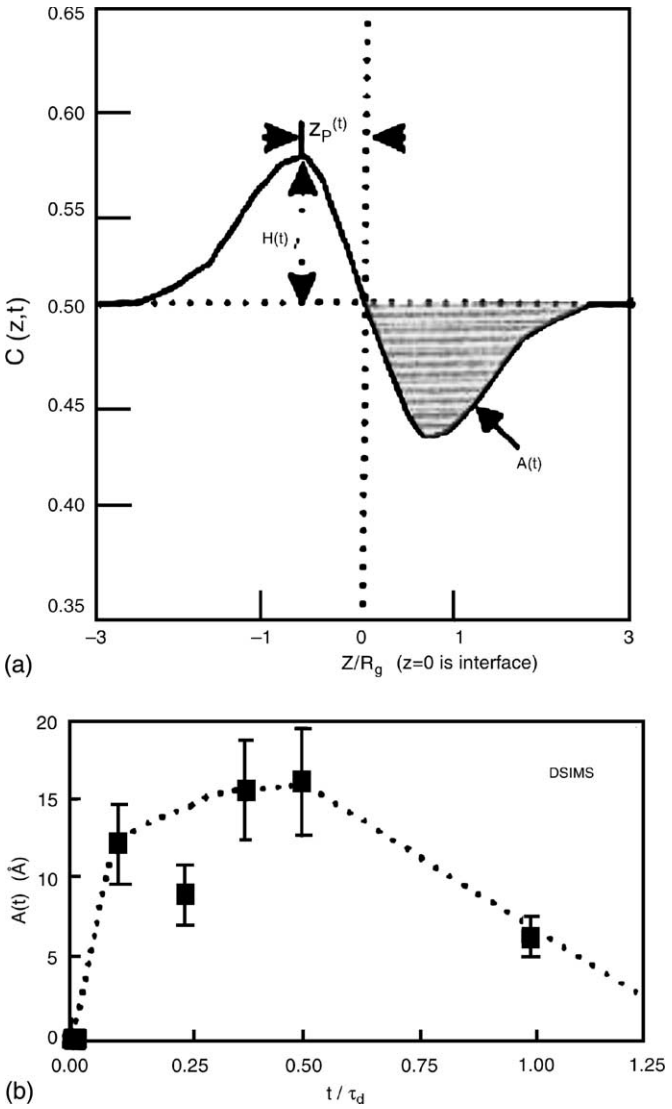

Fig. 21. (a) General 'ripple' profile observed using DSIMS measurements, with characteristic features of peak height, $H(t)$, peak area, $A(t)$, and peak position, $Z_p(t)$. (b) Normalised ripple peak area versus reduced time (t/τ_d) for a 400 kg/mol HDH/DHD bilayer, annealed at 131 °C ($\tau_d = 187$ min). Reproduced with permission from Ref. [91].

by Grayce et al. [290] who demonstrated that as well as the reptation model both the Rouse and PMC models could also explain the observed ripple behaviour. Further experimental work by Agrawal and co-workers [91,93,282] carefully compared experimental observations with those predicted by Rouse, PMC, and reptation dynamics. Their results produced clear support for reptation as a candidate mechanism

of interdiffusion at polymer–polymer interfaces, whilst the Rouse and PMC models did not explain all the experimental data in a number of key areas and were therefore thought not to be applicable mechanisms.

Bousmina and co-workers, have used small-amplitude oscillatory shear measurements to quantify the diffusion between PS–PS [281,291] and PMMA–SAN [292] interfaces. For the PS–PS interface systems they studied, it was observed that the complex shear modulus, G^*, at fixed oscillatory frequency, was shown to increase with diffusion time [281]. Two distinct time regimes were observed with initially $G^*(t) \propto t^{0.53}$ before there is a transition to a time dependence of $G^*(t) \propto t^{0.23}$. This transition between the two time regimes occurs at a time consistent with the calculated value for the Rouse time (τ_R). Since G^* is proportional to the mean displacement of the interface, these exponents are directly comparable to the predicted values of 1/2 and 1/4 expected from the reptation theory. Significantly though, the reptation theory predicts the opposite order for these exponents, indicating that initially the chain ends are not concentrated at the interface but mostly in the bulk, and diffuse to the interface with a $t^{1/2}$ dependence during the initial time regime. After reaching the interface, the dynamics change to a $t^{1/4}$ dependence as the chains diffuse across the interface. When these measurements were repeated by either pre-shearing or corona treating the sample to induce an increase number of chain ends at the interface, exponents of 0.32 and 0.34, respectively, for the comparable time regimes were observed instead of 1/4 or 1/2. These results suggest that this is closer to the case of diffusion starting with an excess of chain ends at the interface. The reverse was found to be true if the healing of fractured PS–PS interfaces was measured, where it was found that G^* increases with a time exponent of 0.29 that is close to the value of 1/4 predicted by de Gennes [279,280] and Prager and Tirrell [293].

There is considerable experimental evidence that shows a substantial difference in properties between the bulk polymer and those in thin films i.e. films less than approximately a few hundred nanometres. Polymer chains near interfaces have been shown to have substantially different properties to those in the bulk [294–296]. Property changes include those of glass transition behaviour [202–204,297–300], (for a recent review see [301]) dewetting [173,302], dynamics [303], chain conformation [304,305], crystallisation [306–309] and diffusion [310]. These changes in polymer behaviour in thin films derive from the enhanced effects of the interfacial regions as the thickness decreases. Studies of polymer diffusion near a solid substrate have indicated a reduction in polymer mobility close to the substrate [311], which has been associated with an increase in effective T_g. In comparison, experimental evidence has often shown that the free surface is a region of enhanced mobility [312–317]. Simulations have also shown it is a region of reduced density compared to the bulk [318], although experimental evidence using NR measurements on PMMA suggests that this may not always be true [319,320]. In supported polymer films (i.e. films deposited on a solid substrate), there is a subtle interplay between the competing interfacial effects, with the overall film properties determined by the dominant effect. Diffusion studies of PS on silicon substrates using DSIMS, have shown that diffusion rates perpendicular to the substrate were an order of magnitude slower than in the bulk even up to 80 nm, i.e. $10R_g$, away from the substrate [311]. Similarly, a

reduction in the lateral PS diffusion coefficient was found in films up to 150 nm (i.e. $50R_g$) thick [310].

Unlike linear polymers that exhibit an increase in viscosity as a power law of the molecular weight, entangled star polymers have a unique property where the viscosity increases exponentially with molecular weight [321,322]. If the reptation model is assumed then the dominating mechanism for translational motion is the retraction of ends of the arms along their average contour, with simultaneous projection of unentangled loops into the surrounding matrix [323,324]. Another complex system in terms of dynamics are ones where the polymers have cross-linked into networks. In this case the diffusion between networks and linear polymers or between two networks would be thought to be significantly slower and more complex than linear polymer dynamics. However, this is an over simplification of the situation, since networks can either be prepared as heterogeneous or in a swollen state, which would encourage diffusion as well as adhesion. The most widely studied polymer networks have been formed from PS. The kinetics of linear PS diffusion into crosslinked PS has been studied [325–327], as well as tethered polymer brush diffusion into PS [328] and PDMS [329,330] networks. The case of linear PS diffusion into a polymer network demonstrated an asymmetric interface with the linear polymer penetrating the network up to 20 nm [326], but also a high molecular weight cut-off for the linear PS above which diffusion could not proceed [325].

6.2. Small molecule penetrant diffusion into polymers

The understanding of diffusion of small-molecule penetrants such as gases and liquids into polymers is of vital importance in many areas, for instance, in order to identify chain architectures and mechanisms that could help develop new polymers for numerous barrier applications. However, the mechanisms that govern the diffusion behaviour are not fully understood despite continued research. Although numerous techniques have been applied to these diffusion studies, often the chosen techniques are restricted to particular length scales of measurement or resolution. This has meant experimental measurement of diffusion processes over the whole length scale from the atomic to the macroscopic have not been undertaken on the same system. This has produced anomalies from which theories founded on molecular behaviour do not adequately describe the observed macroscopic behaviour.

Small penetrants into molecules often retain a sharp diffusion front that moves through the polymer with a constant concentration of penetrant behind the front. This behaviour is often characterised by a Case II diffusion mechanism [331]. Classical approaches to diffusion associate the diffusion mechanism of small molecule penetrants into polymers in the rubbery state as being Fickian, whereas in the glassy state the time scale and diffusion lengths cannot be predicted by classical Fickian behaviour. The penetration of a solvent into a bulk polymer swells the chain network and introduces a supplementary stress that stretches the chains between their entanglements. This has the effect of modifying the chain relaxation mechanism, which in turn modifies the diffusion process of the solvent. Such behaviour can be described by a modified Fick's equation [332]:

$$\frac{\partial C}{\partial t} = \nabla \cdot [D(C)\nabla C + E(C)\nabla \sigma] \tag{43}$$

where C is the concentration, $D(C)$ is the diffusion coefficient, $E(C)$ is the stress coefficient and σ is the stress induced by the penetration of the solvent that causes the swelling of the polymer network and the displacement of entanglement points [333].

Theoretical treatment of small molecule diffusion through polymers has been investigated using both molecular modelling and simulation. The inability of traditional molecular dynamic simulation methods to span time scales relevant to diffusion in glassy polymers, i.e. micro-seconds and longer, has meant that these theories are not widely applicable to real systems. To overcome this problem, transition state theory (TST) based simulations have been developed [334–337]. More recently Greenfield and Theodorou have developed a coarse-grained model of small molecule diffusion within a glassy polymer using reverse and kinetic Monte Carlo simulations [338]. This method calculates molecular level jump rates between likely sorption states using multidimensional TST [337] and incorporates explicit chain motions that accompany each jump. In simulations of methane diffusion through glassy atactic polypropylene they found that at short to medium diffusion times, the mean-squared displacement $\langle r^2 \rangle$ of the methane increases sub-linearly, i.e. $\langle r^2 \rangle \propto t^n$ and $n < 1$ (i.e. anomalous diffusion), in structures with low to medium connectivity. This anomalous diffusion was attributed to confinement of the penetrant molecules to specific regions and pathways, and therefore similar to diffusion in percolating clusters [262,339,340]. For longer diffusion times the mean-squared displacement increases linearly with time for higher connectivity, but remains sub-linear ($< n < 1/2$) for the low connectivity matrix (see Fig. 22).

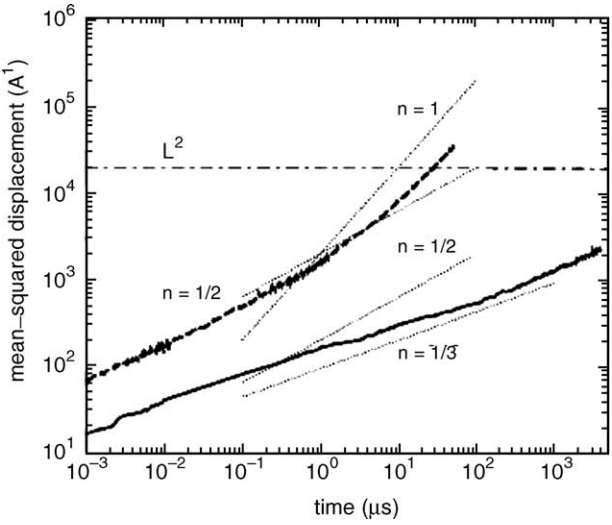

Fig. 22. Mean-squared displacement as a function of time for ghost particles on a network with realistic rate constants and sorption probabilities. Reproduced with permission from Ref. [338].

Polymer membranes of specific separation characteristics can be designed by appropriate blending of homopolymers or use of phase separated block copolymers. Transport properties of penetrant molecules in macroscopically phase separated polymer blends and micro-phase separated block copolymers are predominantly governed by molecular diffusion rates in either the continuous polymer phase or the more mobile phase if micro-domain co-continuity exists [341–345]. Zielinski and co-workers have studied the diffusion of a variety of penetrants into styrene–isoprene (SI) block copolymers including toluene [346,347], and the photochromic dye molecule tetrahydrothiophene–indigo (TTI) [342]. The results of the diffusion measurements of these small penetrant molecules into SI copolymers were analysed in terms of the free-volume (FV) theory of diffusion [348]. Within this theory the self-diffusion coefficient of the penetrant is evaluated in terms of the polymer jump size unit, $\widetilde{V}_{2j}$, which is a physical property of the polymer and sensitive to the chemical nature of the polymer. The self-diffusion coefficient of TTI in SI copolymer was determined by analysing the diffusion distance as a function of time using forced Rayleigh scattering. These observed diffusion rates were shown to be intermediate between those of the pure PS and polyisoprene (PI) homopolymers, although the dynamics appeared to be largely dominated by the PI component of the copolymer. The temperature dependence and TTI diffusion rates were analysed according to the FV theory, where $\widetilde{V}_{2j}$ was observed to be predominantly affected by the PS component of the copolymer. More recently, Tonge and Gilbert have compared the FV theory [348] to a 'typical jump' TST [349], against experimentally determined diffusion coefficients of camphorquinone and diactyl in PMMA [350]. The FV theory was seen to underestimate the experimental diffusion coefficient by many orders of magnitude at the temperatures studied. By contrast, the TST overestimated the diffusion coefficients of these penetrants, either because it underestimated the attractive potentials between the penetrant and the polymer matrix, or due to a breakdown of the model's assumption of linear elastic deformation for these relatively large penetrants. In systems where the penetrants are small and non-polar the TST model has successfully predicted the diffusion coefficients [349].

Penetration of organic vapour into polymers below their T_g has been modelled by Thomas and Windle [331], and refined by Kramer and co-workers [351], which stimulated some definitive experimental studies on case II sorption on a number of polymer-diluent systems by Kramer and co-workers [38,351–355]. This model assumes that the diffusion process is strongly coupled to the mechanical response of the polymer, where the rate of penetrant absorption must be compatible with the swelling rate controlled by creep deformation of the surrounding polymer. The creep deformation is dependent on both the osmotic pressure that drives the swelling of the polymer and the viscosity of the polymer. The penetrant therefore acts as a plasticiser and produces large decreases in segmental relaxation times corresponding to a glass–rubber transition if the concentration of penetrant is large enough. Although the theory of Thomas and Windle, together with later developments by Kramer is qualitatively successful in predicting the important mechanistic factors, it is unable to provide a quantitative prediction of the diluent kinetic penetration, which is characterised through the Deborah number [356]. However, the discovery

of diluent induced toughening effects in glassy PS [357], Argon et al. further refined the Thomas-Windle model of diluent penetration into polymers to take account of the kinetic factors quantitatively [358,359]. This latter model overcomes the limitations of previous theories by differentiating the driving forces resulting from chemical potential differences from material-misfit-induced pressures that counteract the diluent penetration. The 'pressure' which is caused by the chemical potential difference is considered to be an osmotic suction, which draws the diluent into the polymer. The sorbed diluent however, produces significant material misfit and results in the development of a real pressure that results in a stress that can initiate a process of visco-plastic extrusion of diluent-enriched polymer. The misfit induced pressure can exactly balance the osmotic suction so that diffusion comes to a standstill.

Studies on methanol diffusion in PMMA and dodecane in PS [360], and earlier work on MeOH diffusion in PET [361], have shown that existing diffusion theories using a concentration gradient or a swelling rate have difficulty explaining the measured data. In order to reconcile their data measured using macroscopic techniques (such as optical microscopy [360] and magnetic resonance imaging [362]) Vesely and coworkers have proposed a molecular sorption mechanism for solvent penetration into polymers [363]. In this mechanism, the attractive driving force for diffusion is the sorption of penetrant molecules into the polymer chains. Both the sorption process and the resistance of the matrix to the flow of penetrant are assumed to result directly from molecular interactions. The mechanism assumes the existence of density fluctuations between the polymer chains and the free volume, which therefore provides sufficient 'porosity' for sorption and permeability of small molecules. The driving force for diffusion in this porous media is molecular interaction, resulting in an internal pressure, similar to capillary pressure observed on a macroscopic scale. The rate of diffusion can therefore be expressed as $v = (\gamma_s/\eta) r \cos\alpha/x_0$, where $x_0 = B((kt+1)^{1/2} - 1)$ is the diffusion distance, B and k are temperature dependent diffusion constants, γ_s is the surface tension, η is the viscosity of the liquid in a capillary or radius r, making a contact angle α with the walls of the capillary.

Hall and Torkelson have studied the effect of film thickness and polymer affinity for the substrate on translational diffusion of decacylene and lophine penetrants in thin films of PS, poly(isobutyl methacrylate) (PBMA) and PVP [364]. These penetrants are large enough for their translational motion to be coupled to the segmental motion of the polymer matrix. The diffusion of penetrants in PS was shown to slow in comparison to bulk values as the film thickness was decreased below 150 nm. This slowing of the diffusion was interpreted as an effect of the interaction of the substrate on the polymer chains causing an apparent increase in T_g. This reduction in diffusion rate was not observed for the PBMA or PVP films as may be expected since they show a greater affinity for the quartz substrate, and would have been expected to cause a greater reduction in T_g. Hall and Torkelson assumed that the lack of reduction in diffusion rate for the PBMA and PVP films indicated that the range of influence of polymer-surface interactions is limited in extent, i.e. to approximately 40 nm, in modifying thin films behaviour.

7. Mechanical properties of polymer interfaces

The interfacial strength of a polymer–polymer interface is not only of academic interest but holds real technological relevance both in terms of applications but also for processing, such as adhesion, glues, coatings, welding, co-extrusion, polymer blends and so on. Control of these processes requires a detailed understanding of the relationship between the microscopic and molecular structure of the polymer and the macroscopic mechanical properties. For glassy polymers, the adhesion across the interface, or more precisely the toughness of the interface, is controlled through a combination of the chain coupling across the interface and the energy dissipation processes in the materials. The chain coupling is determined by the number of lengths of polymer chain between entanglements that cross the unit area of the interface, Σ. This is more often referred to in the literature as the areal chain density. Energy dissipation processes typically occur through growth of one or more crack tip crazes. Clearly, in terms of understanding and ultimately controlling adhesion, it is important to understand the role played by Σ. A glassy polymer has negligible fracture toughness if its number average molecular weight is less than approximately $2M_e$. This is because stress is mainly transferred by entanglements. The same argument has been shown to be true for immiscible polymer interfaces, where the interface fracture toughness, G_c, is negligible until the polymer chains on both sides are mutually entangled [365,366]. This principle also accounts for the effectiveness of diblock copolymers as compatibilisers at homopolymers–homopolymer interfaces, where the value of Σ can be controlled easily [367].

Two types of interface can be identified depending on whether the two polymers are the same or dissimilar, and are consequently called 'symmetric' and 'asymmetric' interfaces, respectively. Symmetric interfaces have proved less problematic experimentally and consequently there have been several detailed studies on these systems [368–370]. In these experiments sheets of the same polymer are held together under mild pressures and annealed at temperatures above T_g for varying lengths of time. After quenching to RT the fracture toughness between the two polymer sheets can be measured. An increase in fracture energy as a function of $t^{1/2}$ was observed for different kinds of polymers. This behaviour was shown to agree with diffusion predictions based on Fickian bulk motion. In interpreting these results assumptions about the dependence between G_c and interfacial width, w, were made and have variously been shown to be proportional to either w or w^2. However, these studies did not consider the relationship between G_c and micro-mechanisms of plastic deformation at the interface which are responsible for energy dissipation. A necessary condition for a strong adhesion is the formation of a plastic zone ahead of the propagating crack. This plastic zone will then fail through either chain scission or chain pullout.

Brown [371] has proposed a mechanism where the maximum width of the plastic zone and therefore the fracture toughness of the interface is controlled by the areal density of chains crossing the plane of the interface, Σ. In this model, plastic zone failure is exclusively via chain scission so that fracture toughness is predicted to be molecular weight independent. In this regime, which is valid for high M_w polymers,

G_c is predicted to scale with Σ^2. Fracture toughness measurements on PS–PS interfaces [372], showed that G_c only becomes molecular weight independent when M_w is greater than approximately 10–12M_e. Similarly, a PS–PVP interface reinforced by the corresponding block copolymer, G_c did not become independent of M_w until at least 5–6M_e [373]. Measurement of fracture toughness is easily achieved using an asymmetric double cantilever beam (aDCB). To ensure that the crack propagates along the interface and not into the more compliant polymer sheet, it is necessary to make this polymer thicker than the less compliant polymer. The precise thickness of the two sheets is usually determined by varying one relative to the other, until the fracture toughness reaches a minimum. The value of G_c can be determined from the crack length a using the equation proposed by Kanninen [374] which takes into account the finite elasticity of the material ahead of the crack tip:

$$G_c = \frac{3\Delta^2}{8a^4} \cdot \frac{E_1 h_1^3 E_2 h_2^3}{E_1 h_1^3 \alpha_2^2 + E_2 h_2^3 \alpha_1^2} \tag{44}$$

where Δ is the knife blade thickness used to force the crack to open, E_i and h_i are the Young's modulus and polymer thickness for material i and $\alpha_i = [(1 + 1.92(h_i/a)) + (1 + 1.22(h_i/a)^2) + (1 + 0.39(h_i/a)^3)](1 + 0.64(h_i/a))^{-1}$.

By combining aDCB and NR measurements Creton and co-workers have been able to directly correlate the fracture toughness of a number of polymer pairs with the interfacial width [375,376]. Since aDCB and NR measurements require different sample geometries, it is possible that geometry may have an effect [160]. By varying annealing temperatures for a PS-poly(*p*-methylstyrene) (P*p*MS) the width of the interface between the two polymers a direct relationship between G_c and w for values of $w \leqslant 11$ nm was observed, see Fig. 23 [375]. Clearly for such high M_w polymers the interfacial width is the main parameter controlling the interfacial fracture toughness. However, these workers were not able to determine whether G_c varied as a function of w or w^2 due to the limited range of interfacial widths obtained.

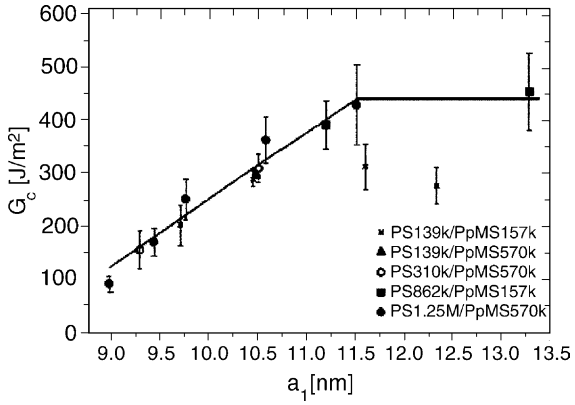

Fig. 23. Adhesion energy (G_c) of different samples of PS/P*p*MS plotted as a function of the interfacial width (a_i). The solid line is drawn as a guide to the eye. Reproduced with permission from Ref. [375].

Mechanical behaviour of the interface of miscible polymer blends are not widely studied with only limited examples in the literature, including poly(vinyl chloride) (PVC)/PMMA, [377,378], poly(vinylidene fluoride) (PVF)/PMMA [379] and poly(2,6-dimethyl-1,4-phenylene oxide) (PDMPO)/PS [380]. In such miscible systems the polymer–polymer interface has been shown to vanish at times greater than the reptation time (τ_r) as predicted by theory [2]. It is believed that crack healing (welding) in polymers involves the processes of chain rearrangement at the surface, diffusion and reorganisation. The latter two stages are controlled by reptation. Using this theory, the fracture stress, σ, of a healing polymer interface is predicted to increase as a function of the healing time to the reciprocal fourth power ($t^{-1/4}$) for a wide range of molecular weights [293,381,382] when welded together at temperatures well above T_g. Following the observation of craze healing in *a*-PS below T_g [383], Boiko and Prud'homme have subsequently shown that welding is also possible below the T_g of both polymers [380]. As seen for the cases of welding above T_g, crack healing below T_g also produces an interfacial strength as a function of $t^{1/4}$, see Fig. 24. This indicates that even at low temperatures relative to T_g the molecular chains and in particular the chain ends have more degrees of freedom and a higher mobility than those in the bulk due to the reduced entanglement density in the interfacial region [296].

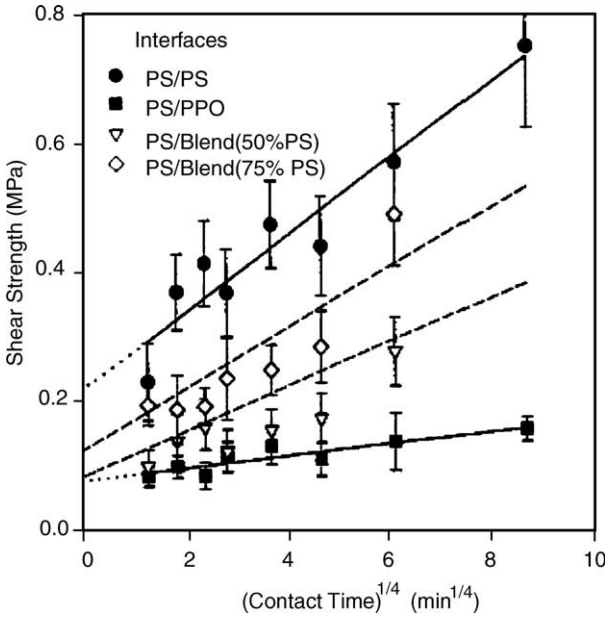

Fig. 24. Shear strength of several PS-containing polymer/polymer interfaces as a function of contact time (the error bars correspond to the standard deviation of the mean). The dashed lines represent calculations for shear strength based on volume fraction weighted shear strengths for the component interfaces whereas the solid lines correspond to a least-squares analysis. Reproduced with permission from Ref. [380].

7.1. Strengthening polymer–polymer interfaces

Since the strength of polymer blends depends largely on the strength of the polymer interface it is not surprising that mechanical failure of immiscible polymer blends occurs via crack propagation along the weak interface. The width of the interface and therefore the degree of intermixing and chain entanglement is a balance of the enthalpy and entropy which drive the extent of mixing. Use of polymer blends is a widely used technique for finding and extending polymer application capabilities by incorporating specific properties of the blend polymers. To ensure that these blends remain mechanically robust, it is necessary to strengthen the interfacial toughness. This can be achieved by a variety of methods such as reactive mixing and addition of compatibilising agents, such as triblock, random, combs or graft copolymers [47,373,384–393]. The use of diblock copolymers is wide spread for blend compatibilisation and has been used to great effect in high impact polystyrene (HIPS), where the PS and PB phases are blended with PS–b-PB diblock copolymers [394]. The copolymer is typically added in proportions of 5–30% and compatibilises the blend by segregating to the interface between the phases. The copolymer has to be chosen with care so that each block of the copolymer is compatible with one of the phases so that mixing occurs. The segregation behaviour of copolymers to immiscible polymer interfaces has been studied in detail using a combination of techniques such as NR, FReS and DSIMS. The mostly widely studied systems have been the diblock copolymers of PS–b-PMMA [371,387,388,395–397] and PS–b-PVP [373,398–402] used in a number of immiscible homopolymer blends.

The strength of immiscible polymer interfaces is determined as a function of the degree of polymerization of the blocks of the copolymer and the areal density of copolymer at the interface, Σ_c. As may be expected from studies of bulk homopolymers, the extent of entanglement of the blocks of the copolymer with the homopolymer, determines the strength of the interface and also the fracture mechanism. If the degree of polymerization of the blocks is below a critical value of approximately $2N_e$, the failure mode is via chain pullout. The energy involved in chain pullout is dependent on both the friction on the chain and the pullout rate. For glassy polymers the resistance to chains pulling out of a matrix is defined through the static monomer friction coefficient, ξ, with each monomer of length, b. It can be shown that for a low crack propagation rate the interfacial toughness due to chain pullout mechanisms is given by [403]:

$$G_c = \frac{\sum_c \xi N^2 b}{2} \tag{45}$$

When $N > N_e$ Brown and co-workers showed that the copolymers fail by chain scission [395], and consequently the interfacial toughness is independent of copolymer molecular weight [387,388]. In this case, if Σ_c is small, a limited amount of energy is dissipated since the copolymers break near their junction point. As Σ_c increases so does the stress on the interface, until at a critical value of Σ_c equal to Σ_c^*, a craze or yield zone can form at the interface, and the toughness increases rapidly [373]. Of course the interface can only accommodate a finite amount of copolymer,

which is equivalent to the density of chains within one lamella of pure diblock copolymer. If more copolymer is added to the system it must be accommodated within one of the homopolymer phases. Because of the miscibility of the different blocks and the homopolymer, diblock micelles are formed in the bulk of the homopolymer phase [47]. Indeed, the amount of copolymer at an interface has also been shown to decrease the fracture toughness once a critical value of $\Sigma_c = \Sigma_c^s$ has been exceeded (see Fig. 25) [399]. The optimal interfacial toughening by diblock copolymers is produced when they have a fairly low M_w, although of course M_w must be greater than M_e. Clearly for lower molecular weight copolymers, there will therefore be a significant density of chain ends, which are themselves a source of weakness, in close proximity to the interface.

Although the use of diblock copolymers for reinforcing interfaces can be understood quite intuitively, it is perhaps a little surprising that triblock and random

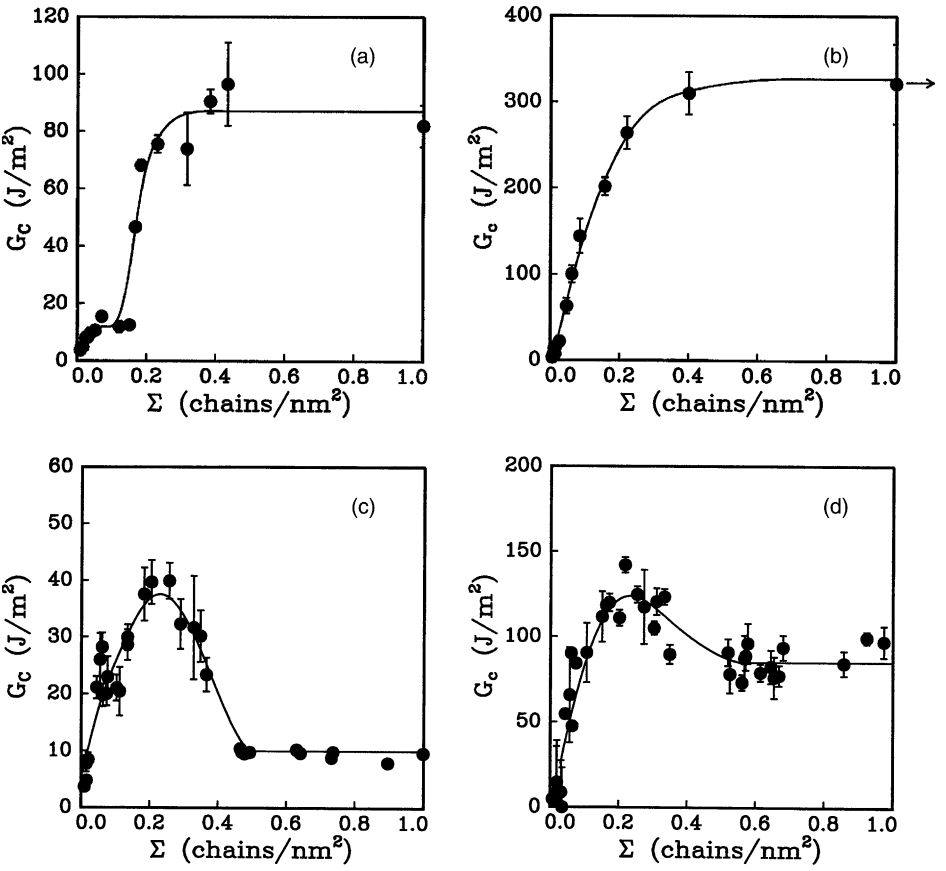

Fig. 25. Fracture toughness, G_c, of a PS–PVP interface, plotted as a function of areal chain density, Σ, of PVP–PS–PVP triblock and PS–PVP diblock copolymers. The interfaces are reinforced with triblock copolymers with $N_{PVP} - N_{PS} - N_{PVP}$ of (a) 290 – 470 – 290, (b) 580 – 1620 – 580; and diblock copolymers ($N_{PS} - N_{PVP}$) of (c) 540 – 510 and (d) 870 – 800. Reproduced with permission from Ref. [393].

copolymers are equally effective and often found to be better than the diblock equivalents [387,388,391,393]. As found for diblock copolymers the fracture toughness of triblock copolymer reinforced interfaces is controlled by Σ_c and the relative values of N of each of the blocks. Kramer and co-workers have shown that and interface between PS and PVP reinforced by the triblock copolymer PVP–b-PS–b-PVP fails by chain pullout, scission or crazing depending on the relative values of N_{PVP} and Σ_c [393]. For long PVP blocks ($N_{PVP} > N_e$) chain scission occurs at low values of Σ_c, with a transition to failure by crazing above a critical value of Σ_c ($= \Sigma_c^*$). The value of Σ_c^* for triblock copolymers in this regime, is approximately half that for diblock copolymers indicating that most of the triblock copolymers at the interface form a staple like structure with the PS middle block making a loop on the PS side of the interface. Within the crazing regime, but at values of $\Sigma_c < \Sigma_c^s$ the interfacial fracture toughness is controlled by the number density of copolymer excursions across the interface. Above Σ_c^s, the triblock copolymers reinforce the craze fibrils to an extent that the fracture toughness approaches that of the PS homopolymer. For short triblock copolymers, where $N_{PVP} < N_e$, the fracture mechanism changes from chain pullout to crazing with increasing Σ_c. For these short triblock copolymers, both staple and tail conformations are observed.

In diblock copolymer reinforced systems where χ is small, such as PS–b-PMMA diblock copolymer blends with PS and PMMA homopolymers, the high M_w copolymers tend to organize very slowly if Σ is large even when annealed well above the T_gs of the polymers [387]. Of particular interest was the observed decrease in fracture toughness as the diblock copolymer became more organised, with the highest values of G_c obtained for disorganised diblock copolymer. These findings have led to studies on random copolymers as interfacial reinforcement agents [387–389,391,392,404–409]. For immiscible polymer systems it may be expected that the random copolymer would form a phase separated thin layer at the homopolymer–homopolymer interface. If this were true there would be little penetration into either homopolymer, which would consequently lead to a weak interface. Random copolymers do however produce significant interfacial toughening and can produce G_c values, which are greater than the equivalent diblock copolymer. For small values of Σ, a strong confinement of random copolymers to the interface would necessarily require the chains to lie parallel with the interface. To do this would produce a very large loss in entropy. Therefore a compromise structure is speculated to exist in which although the copolymer is confined to the vicinity of the interface it forms relatively large loops into either homopolymer phase [391]. However, the mechanism is still unclear, because this simplistic argument does not explain the observed increase and saturation of G_c, without the decrease observed for diblock copolymer as Σ copolymer increases.

For a PS–PMMA interface reinforced with a PS–r-PMMA copolymer the measured fracture energy depends strongly on the degree of symmetry of the aDCB [389]. This symmetry is defined through the ratio of the layer thicknesses of the two polymer beams, a parameter often called the 'mixity'. In this system a minimum in G_c is observed for a mixity ($= h_{PS}/h_{PMMA}$) of 1.2, as shown in Fig. 26. For both lower and higher values of mixity extra energy was dissipated resulting in either forward or

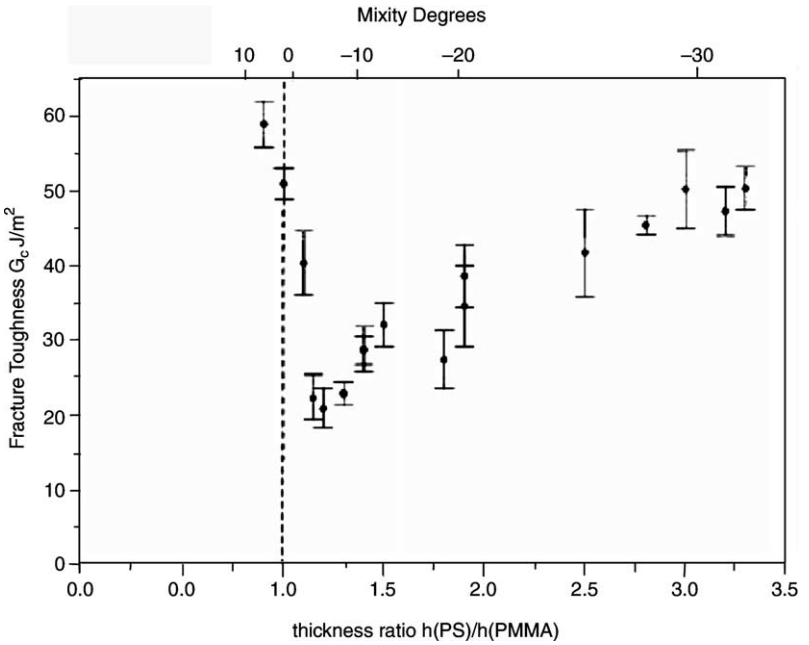

Fig. 26. Fracture toughness versus thickness ratio, h_{PS}/h_{PMMA} for 50 nm (nominal thickness) of 160 kg/mol random PS–r-PMMA copolymer consisting of 70% styrene at the PS/PMMA interface. The mixity is shown on the upper x-axis. Reproduced with permission from Ref. [389].

backward crazing, respectively. In addition, the molecular weight of the random copolymer plays a significant role in strengthening the interface, and increases in molecular weight of the copolymer were shown by Bernard et al. [389] to produce an increase in G_c. This observation is consistent with an increase in entanglement molecular weight at the interface.

Adhesion between immiscible polymers is known to be enhanced when the interface between them is roughened. This principle is well established for improving polymer adhesion to metals [410,411]. The adhesion mechanism between polyethylene (PE) and porous alumina is due to mechanical interlocking of the PE into the pores, giving a direct dependence of the adhesion properties to the pore size [412]. Similarly the adhesion between a Kevlar fibre and the polymer matrix can be enhanced by roughening the fibre surface by chemical etching, which increases the contact area between the two components [413]. More recent studies have shown that for the specific case of PC and SAN bilayers an increase in fracture toughness is observed from that of a smooth interface if macroscopic grooves are introduced either perpendicular or parallel to the crack propagation direction [414]. This method of oriented roughness to improve interface adhesion is rather novel. Crack propagation in this system was shown to follow a stick-slip mechanism, and the increase in fracture toughness is mainly due to cohesive failure and deformation of the polymers in the grooves.

7.2. Pressure sensitive adhesives

Pressure sensitive adhesives (PSAs) are materials, which can form an adhesive joint after only a short contact time under light pressure. The bonding interactions are generally limited to van der Waals bonds, but the energy necessary to break the joint, once established greatly exceeds the thermodynamic work of adhesion. The mechanisms for obtaining a good adhesion between the PSA and a hard surface are generally well understood [415–418]. A good physical contact needs to be achieved to achieve good adhesion between the PSA and the surface. Clearly surface roughness may make contact incomplete, producing a decrease in adhesive strength as the surface roughness is increased [419,420], although there is the possibility of an evolution with time [421]. The effects of the nature of probe surface in flat-probe adhesion tests has been studied by modifying the steel surface with poly(dimethyl siloxane) [422]. Zosel produced the first work discussing the effect of the molecular structure of the polymer on the adhesive properties and unambiguously demonstrated that fibril bridging during debonding detachment was essential for the adhesive to be of use [423,424]. However, Zosel did not explain the mechanism by which these fibrils form and it is only more recent work by Creton and co-workers that have identified cavitation occurring in the adhesive leading to the fibrils forming [415], in an analogous way to fibril formation in crazes [394]. The micro-mechanisms associated with the debonding process however, are still not well understood on a quantitative basis [425], although a series of recent experimental and theoretical studies have begun to shed some light on the details of the mechanisms occurring at a microscopic level [415–418,426,427].

The debonding mechanisms have been studied using flat-probe adhesion tests in styrenic block copolymers [425] and acrylic polymers [428]. In the case of styrene–isoprene–styrene (SIS) triblock copolymer PSAs, Brown et al. [425] have identified four micro-mechanisms of adhesive detachment from the substrate, each corresponding to characteristic stress–strain behaviour. Analysis of samples during the debonding process has shown that these failure mechanisms are a result of either interfacial cavitation at low debonding rates or cavitation within the bulk of the polymer matrix, as observed at higher debonding rates. Although, the debonding process can be qualitatively understood from these micro-mechanisms the maximum debonding stress and adhesion energy could not be predicted using the visco-elastic properties of the polymers alone [425]. Debonding studies of poly(*n*-butyl acrylate) (PnBA), poly(*n*-butyl acrylate-*co*-acrylic acid) (PnBA-AA) and poly(ethylhexyl acrylate-*co*-acrylic acid) (PEHA-AA) can be distinguished by three micro-mechanisms which depend on an effective Deborah number (*De*) [428]. In this case *De* is defined as the terminal relaxation time of the polymer multiplied by the temperature shifted initial strain rate imposed during the debonding process. The maximum stress carried by the adhesive bonds is dependent on the nucleation of cavities, which is therefore directly affected by the amplitude of the surface roughness [420]. Air pockets trapped at the interface between the PSA and the hard surface act as nucleation sites for cavities in the early stages of the failure process [427]. Surface roughness increases the size of the air pockets trapped during the contact stage,

which consequently initiates cavity growth at lower levels of stress on debonding. Chiche et al. [420] have studied the effect on the PSA adhesive poly(2-ethylhexyl acrylate) (PEHA) as a function of controlled amplitude of roughness on a steel surface. Their studies have confirmed that the nucleation of cavities is the dominant process and a smooth surface gives a higher adhesive energy. The nucleation of cavities on rough surfaces means that the adhesive layer cannot store as much elastic energy as a smooth surface, which in turn also slows down the growth of the cavities once they are nucleated.

8. Closing remarks

This paper summarises some of the most recent but nevertheless still very substantial body of work on the molecular understanding that currently exists about polymer interfaces and their influence in modifying the behaviour of thin film. As we have demonstrated the interface, which is either free or confined can have a dominating effect on the behaviour of polymers that are located well away from the interface. It has been shown that theoretical developments have been coupled with increasingly sophisticated experiments, not only in terms of the continual improvement in techniques and equipment but also through well designed and elegant experiments. An example of this is the diffusion 'ripple' experiment described in Section 6.1 [93,94], where not only the use of clever isotopic substitution schemes have been employed, but a number of highly sensitive depth profiling techniques have been used. Clearly with the continual developments in current techniques, with better spatial resolution or faster dynamic range, theories associated with interfaces at interfaces are also being critically tested and themselves being re-evaluated. A case in point is the interfacial width of an interface between two immiscible polymers. As we discussed above, the theoretical description has had to be modified to account for experimentally observed interfacial roughness, which is now described under the framework of thermally excited capillary waves.

Given that the area of polymer interfaces is such a large one, a review of any sort is not going to cover all the possible related topics. This is true of this review not only to try to limit the final size of the paper, but also because some important critical reviews have recently appeared that cover extremely well aspects of related issues on thin polymer films. For instance, wetting behaviour and T_g effects have recently been reviewed by Geoghegan and Krausch [211], and Forrest and Jones [301], respectively. Some significant areas we have deliberately not covered include polymer brush behaviour, chemical surface modification, and solution behaviour. Similarly, although we have included some important aspects of the most powerful and more popular techniques used to study experimentally the behaviour of polymer surfaces and interfaces, a significant body of work in the literature describes the detail of techniques in greater detail (see relevant references in the main text above).

Despite the obvious vigorous activity both in the theoretical and experimental communities in this area of research, the field continues to develop both fundamental understanding as well as challenge long standing concepts. In some areas this

understanding and application to real systems is showing huge potential within technological applications. A case in point is the defined patterning of surfaces. This is approached in numerous ways, but commercially is dominated by photolithography. This domination in specific sectors is now being seriously questioned by a number of different approaches, such as dewetting methods and self-assembly of organic or in many case polymeric materials. In this paper although we have described some of the exciting work associated with patterning by controlling thin polymer film behaviour, other work using polymers as a method to pattern also exists. Whitesides has developed a number of approaches to what is commonly known as 'soft lithography' where patterning is achieved through use of polymer materials—hence the use of the term 'soft'. Although the soft lithography term has come to mean either the use of PDMS in the cross-linked state for rapid pattern transfer (micro-contact printing) or as an initially un-cross-linked fluid to replicate a define structure once cross-linked (replica moulding). The different strategies to patterning on a sub-micron level using soft-lithography have been extensively reviewed by Whitesides and co-workers [429,430].

References

[1] Helfand E, Tagami Y. J Chem Phys 1972;56:3592.
[2] de Gennes PG. Scaling concepts in polymer physics. 5th ed. Ithaca, NY, USA: Cornell University Press; 1996.
[3] Binder K. Adv Polym Sci 1994;112:181.
[4] Jones RAL, Richards RW. Polymers at surfaces and interfaces. Cambridge: Cambridge University Press; 1998.
[5] Sanchez IC. Physics of polymer surfaces and interfaces. London: Butterworth-Heinemann; 1992.
[6] Edwards SF. Proc Phys Soc London 1965;85:613.
[7] Stamm M, Schubert DW. Ann Rev Mater Sci 1995;25:325.
[8] Kramer EJ. Physica B 1991;173:189.
[9] Schwarz SA, Wilkens BJ, Pudensi MAA, Rafailovich MH, Sokolov J, Zhao X, et al. Mol Phys 1992;76:937.
[10] Russell TP. Ann Rev Mater Sci 1991;21:249.
[11] Russell TP. MRS Bull 1996;21:49.
[12] Zhou XL, Chen SH. Phys Rep Rev Sect Phys Lett 1995;257:223.
[13] Lekner J. Theory of reflection. Dordrecht: Martinus Nijhoff; 1987.
[14] Russell TP. Physica B 1996;221:267.
[15] Bucknall DG, Higgins JS. Polymers and surfaces—a versatile combination. In: Hommell H, editor. Trivandrum, India: Research Signpost; 1998. p. 161–99.
[16] Squires GL. Introduction to the theory of thermal neutron scattering. Cambridge: Cambridge University Press; 1978.
[17] Richards RW, Penfold J. Trends Polym Sci 1994;2:5.
[18] Bucknall DG. In: Pethrick RA, Dawkins JV, editors. Experimental methods in polymer characterisation. Chichester, UK: John Wiley & Sons, Ltd; 1999. p. 109–40.
[19] Born M, Wolf E. Principles of optics. 6th ed. Oxford: Pergamon Press; 1980.
[20] Lekner J. Physica B 1991;173:99.
[21] Lovell MR, Richardson RM. Curr Opin Colloid Interface Sci 1999;4:197.
[22] Higgins JS, Benoit BC. Polymers and neutron scattering. Oxford: Clarendon Press; 1993.
[23] Golub R, Richardson D, Lamoreaux SK. Ultra-cold neutrons. Bristol: A. Hilger; 1991.
[24] Lovesey SW. Theory of neutron scattering from condensed matter. Oxford: Oxford University Press; 1984.

[25] Penfold J, Webster JRP, Bucknall DG, Sivia DS. Colloids Surf A: Physicochem Eng Aspects 1994;86:165.
[26] Sivia DS, Hamilton WA, Smith GS. Physica B 1991;173:121.
[27] Sivia DS, Hamilton WA, Smith GS, Rieker TP, Pynn R. J Appl Phys 1991;70:732.
[28] Sferrazza M, Xiao C, Jones RAL, Bucknall DG, Webster J, Penfold J. Phys Rev Lett 1997;78:3693.
[29] Zhao W, Zhao X, Rafailovich MH, Sokolov J, Mansfield T, Stein RS, et al. Physica B 1991;173:43.
[30] Seeck OH, Kaendler ID, Tolan M, Shin K, Rafailovich MH, Sokolov J, et al. Appl Phys Lett 2000;76:2713.
[31] Dailland G, Gibaud A. X-ray and neutron reflectivity—principles and applications. Berlin: Springer; 1999.
[32] Mallegol J, Gorce JP, Dupont O, Jeynes C, Mcdonald PJ, Keddie JL. Langmuir 2002;18:4478.
[33] Dennler G, Houdayer A, Segui Y, Wertheimer MR. J Vac Sci Technol A: Vac Surf Films 2001;19:2320.
[34] Roe KJ, Kolodzey J, Swann CP, Tsao MW, Rabolt JF, Chen J, et al. Appl Surf Sci 2001;175:468.
[35] Cole DH, Shull KR, Rehn LE, Baldo PM. Nucl Instrum Meth Phys Res B: Beam Interact Mater Atoms 1998;138:283.
[36] Cole DH, Shull KR, Rehn LE, Baldo P. Phys Rev Lett 1997;78:5006.
[37] Schone H, Walsh D, Mcgrath RT, Burkhart JH, Doyle BL. Nucl Instrum Meth Phys Res B: Beam Interact Mater Atoms 1997;130:543.
[38] Gall TP, Kramer EJ. Polymer 1991;32:265.
[39] Dai KH, Kramer EJ. Polymer 1994;35:157.
[40] Kim E, Kramer EJ, Osby JO, Walsh DJ. J Polym Sci B: Polym Phys 1995;33:467.
[41] Stoffel NC, Chandra S, Kramer EJ, Volksen W, Russell TP. Polymer 1997;38:5073.
[42] Sokolov J, Rafailovich MH, Jones RAL, Kramer EJ. Appl Phys Lett 1989;54:590.
[43] Zhao X, Zhao W, Sokolov J, Rafailovich MH, Schwarz SA, Wilkens BJ, et al. Macromolecules 1991;24:5991.
[44] Jones RAL, Norton LJ, Kramer EJ, Bates FS, Wiltzius P. Phys Rev Lett 1991;66:1326.
[45] Shull KR, Dai KH, Kramer EJ, Fetters LJ, Antonietti M, Sillescu H. Macromolecules 1991;24:505.
[46] Shull KR, Kramer EJ, Bates FS, Rosedale JH. Macromolecules 1991;24:1383.
[47] Shull KR, Winey KI, Thomas EL, Kramer EJ. Macromolecules 1991;24:2748.
[48] Calcagno L, Foti G. J Appl Phys 1992;71:3216.
[49] Composto RJ, Kramer EJ, White DM. Macromolecules 1992;25:4167.
[50] Yokoyama H, Kramer EJ. Macromolecules 1998;31:7871.
[51] Yokoyama H, Kramer EJ, Hajduk DA, Bates FS. Macromolecules 1999;32:3353.
[52] Heier J, Kramer EJ, Revesz P, Battistig G, Bates FS. Macromolecules 1999;32:3758.
[53] Oslanec R, Genzer J, Faldi A, Composto RJ, Garrett PD. Macromolecules 1999;32:4098.
[54] Genzer J, Composto RJ. Polymer 1999;40:4223.
[55] Wang H, Composto RJ. Phys Rev E 2000;61:1659.
[56] Schulze JS, Cernohous JJ, Hirao A, Lodge TP, Macosko CW. Macromolecules 2000;33:1191.
[57] Oslanec R, Composto RJ, Vlcek P. Macromolecules 2000;33:2200.
[58] Wang H, Composto RJ. Europhys Lett 2000;50:622.
[59] Pellegrini NN, Composto RJ, Winey KI. J Polym Sci B: Polym Phys 2000;38:1547.
[60] Geoghegan M, Boue F, Menelle A, Abel F, Russ T, Ermer H, et al. J Phys: Condens Matter 2000;12:5129.
[61] Wang H, Composto RJ. J Chem Phys 2000;113:10386.
[62] Schulze JS, Moon B, Lodge TP, Macosko CW. Macromolecules 2001;34:200.
[63] Oslanec R, Brown HR. Macromolecules 2001;34:9074.
[64] Wang H, Composto RJ. Macromolecules 2002;35:2799.
[65] Composto RJ, Walters RM, Genzer J. Mater Sci Eng R: Rep 2002;38:107.
[66] Payne RS, Clough AS, Murphy P, Mills PJ. Nucl Instrum Meth Phys Res B: Beam Interact Mater Atoms 1989;42:130.
[67] Rysz J, Bernasik A, Ermer H, Budkowski A, Brenn R, Hashimoto T, et al. Europhys Lett 1997;40:503.

[68] Hopkinson I, Kiff FT, Richards RW, Bucknall DG, Clough AS. Polymer 1997;38:87.
[69] Shearmur TE, Clough AS, Drew DW, Vandergrinten MGD, Jones RAL. Phys Rev E 1997;55:R3840–3.
[70] Yerushalmirozen R, Klein J. J Phys: Condens Matter 1997;9:7753.
[71] Kerle T, Scheffold F, Losch A, Steiner U, Schatz G, Klein J. Acta Polym 1997;48:548.
[72] Shearmur TE, Clough AS, Drew DW, Vandergrinten MGD, Jones RAL. Polymer 1998;39:2155.
[73] Kerle T, Yerushalmi-Rozen R, Klein J. Macromolecules 1998;31:422.
[74] Kerle T, Klein J, Binder K. Eur Phys J B 1999;7:401.
[75] Geoghegan M, Ermer H, Jungst G, Krausch G, Brenn R. Phys Rev E 2000;62:940.
[76] Russ T, Brenn R, Abel F, Boue F, Geoghegan M. Eur Phys J E 2001;4:419.
[77] Hutchings LR, Richards RW, Thompson RL, Bucknall DG, Clough AS. Eur Phys J E 2001;5:451.
[78] Hutchings LR, Richards RW, Thompson RL, Clough AS, Langridge S. J Polym Sci B: Polym Phys 2001;39:2351.
[79] Steiner U, Chaturvedi UK, Zak O, Krausch G, Schatz G, Klein J. Makromol Chem: Macromol Symp 1991;45:283.
[80] Composto RJ, Kramer EJ. J Mater Sci 1991;26:2815.
[81] Geoghegan M. In: Richards RW, Peace SK, editors. Polymer surfaces and interfaces III. Chichester: John Wiley and Sons Ltd; 1999. p. 43–73.
[82] Endisch D, Rauch F, Gotzelmann A, Reiter G, Stamm M. Nucl Instrum Meth Phys Res B: Beam Interact Mater Atoms 1992;62:513.
[83] Maldener J, Giessler KH, Becht T, Rauch F, Stamm M, Arai E. Nucl Instrum Meth Phys Res B: Beam Interact Mater Atoms 1995;99:444.
[84] White H, Pu Y, Rafailovich M, Sokolov J, King AH, Giannuzzi LA, et al. Polymer 2001;42:1613.
[85] Kajiyama T, Kawaguchi D, Sakai A, Satomi N, Tanaka K, Takahara A. High Perform Polym 2000;12:587.
[86] Noolandi J. Annu Rev Phys Chem 1992;43:237.
[87] Mattsson J, Forrest JA, Krozer A, Soddervall U, Wennerberg A, Torell LM. Electrochim Acta 2000;45:1453.
[88] Kajiyama T, Satomi N, Tanaka K, Takahara A. Macromol Symp 1999;143:171.
[89] Fodor JS, Briber RM, Russell TP, Carter KR, Hedrick JL, Miller RD, et al. Polymer 1999;40:2547.
[90] Slep D, Asselta J, Rafailovich MH, Sokolov J, Winesett DA, Smith AP, et al. Langmuir 1998;14:4860.
[91] Welp KA, Wool RP, Satija SK, Pispas S, Mays J. Macromolecules 1998;31:4915.
[92] Stoffel NC, Dai CA, Kramer EJ, Russell TP, Deline V, Volksen W, et al. Macromolecules 1996;29:6880.
[93] Agrawal G, Wool RP, Dozier WD, Felcher GP, Zhou J, Pispas S, et al. J Polym Sci B: Polym Phys 1996;34:2919.
[94] Russell TP, Deline VR, Dozier WD, Felcher GP, Agrawal G, Wool RP, et al. Nature 1993;365:235.
[95] Bucknall DG, Grovenor CRM, Henry B, Dark C, Smart K, Hillion F. Unpublished results.
[96] Harrison C, Cheng ZD, Sethuraman S, Huse DA, Chaikin PM, Vega DA, et al. Phys Rev E 2002;66:011706.
[97] Sharp JS, Jones RAL. Phys Rev E 2002;66:011801.
[98] Schonherr H, Wiyatno W, Pople J, Frank CW, Fuller GG, Gast AP, et al. Macromolecules 2002;35:2654.
[99] Park C, De Rosa C, Fetters LJ, Thomas EL. Macromolecules 2000;33:7931.
[100] Loo YL, Register RA, Adamson DH. Macromolecules 2000;33:8361.
[101] Hong S, Bushelman AA, Macknight WJ, Gido SP, Lohse DJ, Fetters LJ. Polymer 2001;42:5909.
[102] Wirnsberger G, Yang PD, Huang HC, Scott B, Deng T, Whitesides GM, et al. J Phys Chem B 2001;105:6307.
[103] Miyata T, Yamada H, Uragami T. Macromolecules 2001;34:8026.
[104] Boker A, Knoll A, Elbs H, Abetz V, Muller AHE, Krausch G. Macromolecules 2002;35:1319.
[105] Chang MY, Abuzaina FM, Kim WG, Gupton JP, Garetz BA, Newstein MC, et al. Macromolecules 2002;35:4437.

[106] Fukunaga K, Hashimoto T, Elbs H, Krausch G. Macromolecules 2002;35:4406.
[107] Bendejacq D, Ponsinet V, Joanicot M, Loo YL, Register RA. Macromolecules 2002;35:6645.
[108] Thomas S, Groeninckx G. Polymer 1999;40:5799.
[109] Huang E, Mansky P, Russell TP, Harrison C, Chaikin PM, Register RA, et al. Macromolecules 2000;33:80.
[110] Fang AP, Ng H, Su XD, Li SFY. Langmuir 2000;16:5221.
[111] Hillborg H, Ankner JF, Gedde UW, Smith GD, Yasuda HK, Wikstrom K. Polymer 2000;41:6851.
[112] Oh KW, Kim SH, Kim EA. J Appl Polym Sci 2001;81:684.
[113] Bandopadhay D, Panda AB, Pramanik P. J Appl Polym Sci 2001;82:406.
[114] Newby BMZ, Wakabayashi K, Composto RJ. Polymer 2001;42:9155.
[115] Schulz BM, Huber MR, Bieringer T, Krausch G, Zilker SJ. Synth Met 2001;124:155.
[116] Hasegawa M, Ikawa T, Tsuchimori M, Watanabe O, Kawata Y. Macromolecules 2001;34:7471.
[117] Karim A, Douglas JF, Lee BP, Glotzer SC, Rogers JA, Jackman RJ, et al. Phys Rev E 1998;57:R6273–6.
[118] Cabral JT, Higgins JS, Mcleish TCB, Strausser S, Magonov SN. Macromolecules 2001;34:3748.
[119] Ermi BD, Nisato G, Douglas JF, Rogers JA, Karim A. Phys Rev Lett 1998;81:3900.
[120] Sharp JS, Jones RAL. Adv Mater 2002;14:799.
[121] Boltau M, Walheim S, Mlynek J, Krausch G, Steiner U. Nature 1998;391:877.
[122] Cech V, Horvath P, Trchova M, Zemek J, Matejkova J. J Appl Polym Sci 2001;82:2106.
[123] Pijpers AP, Meier RJ. J Electron Spectrosc Relat Phenom 2001;121:299.
[124] Sodhi RNS, Sahi VP, Mittelman MW. J Electron Spectrosc Relat Phenom 2001;121:249.
[125] Zhu XX, Wang F, Nivaggioli T, Winnik MA, Macdonald PM. Macromolecules 1993;26:6397.
[126] Wang P, Tan KL, Kang ET, Neoh KG. J Membrane Sci 2002;195:103.
[127] Tannenbaum R, Hakanson C, Zeno A, Tirrell M. Langmuir 2002;18:5592.
[128] Keddie JL. Curr Opin Colloid Interface Sci 2001;6:102.
[129] Elwing H. Biomaterials 1998;19:397.
[130] Styrkas D et al. In: Peace SK, Richards RW, editors. Polymer surfaces and interfaces III. London: John Wiley and Sons; 1999. p. 1.
[131] Anastasiadis SH, Russell TP, Satija SK, Majkrzak CF. J Chem Phys 1990;92:5677.
[132] Fernandez ML, Higgins JS, Penfold J, Ward RC, Shackleton C, Walsh DJ. Polymer 1988;29:1923.
[133] Higashida N, Kressler J, Yukioka S, Inoue T. Macromolecules 1992;25:5259.
[134] Kressler J, Higashida N, Inoue T, Heckmann W, Seitz F. Macromolecules 1993;26:2090.
[135] Anastasiadis SH, Gancarz I, Koberstein JT. Macromolecules 1988;21:2980.
[136] Geoghegan M, Jones RAL, Payne RS, Sakellariou P, Clough AS, Penfold J. Polymer 1994;35:2019.
[137] Stone VW, Arys X, Legras R, Jonas AM. Macromolecules 2000;33:3031.
[138] Jones RAL. Curr Opin Solid State Mater Sci 1997;2:673.
[139] Hermes HE, Higgins JS, Bucknall DG. Polymer 1997;38:985.
[140] Bucknall DG, Butler SA, Hermes HE, Higgins JS. Physica B 1998;241–243:1071.
[141] Hermes HE, Bucknall DG, Butler SA, Higgins JS. Macromol Symp 1998;126:331.
[142] Bucknall DG, Butler SA, Higgins JS. J Phys Chem Solids 1999;60:1273.
[143] Bucknall DG, Butler SA, Higgins JS. Scattering from polymers. In: Hsiao BS, Lohse DJ, Cebe P, editors. ACS Symposium Series, Washington, DC, vol. 739, 2000. p. 57–73.
[144] Butler SA, Higgins JS, Bucknall DG, Sferrazza M. Macromol Chem Phys 2001;202:2275.
[145] Shull KR, Mayes AM, Russell TP. Macromolecules 1993;26:3929.
[146] Pershan PS. J Phys: Condens Matter 1994;6:A37–50.
[147] Buff FP et al. Phys Rev Lett 1965;15:621.
[148] Rowlinson JS, Widom B. Molecular theory of capillarity. Oxford: Clarendon Press; 1992.
[149] Davis HT. J Phys Chem 1977;67:3636.
[150] Bedeaux D, Weeks JD. J Chem Phys 1985;82:972.
[151] Braslau A, Pershan PS, Swislow G, Ocko BM, Alsnielsen J. Phys Rev A 1988;38:2457.
[152] Weeks JD. J Chem Phys 1977;67:3106.
[153] Evans R. Adv Phys 1979;28:143.
[154] Schubert DW, Stamm M. Europhys Lett 1996;35:419.

[155] Israelachvili J. Intermolecular and surface forces. London: Academic Press; 1992.
[156] Doerr AK, Tolan M, Prange W, Schlomka JP, Seydel T, Press W, et al. Phys Rev Lett 1999;83:3470.
[157] Seeck OH, Hupfeld D, Krull H, Doerr AK, Schlomka JP, Tolan M, et al. Phys Rev B 1999;59:3474.
[158] Wang J, Tolan M, Seeck OH, Sinha SK, Bahr O, Rafailovich MH, et al. Phys Rev Lett 1999;83:564.
[159] Tolan M, Seeck OH, Schlomka JP, Press W, Wang J, Sinha SK, et al. Phys Rev Lett 1998;81:2731.
[160] Kerle T, Klein J, Binder K. Phys Rev Lett 1996;77:1318.
[161] Degennes PG. Rev Modern Phys 1985;57:827.
[162] Reiter G. Phys Rev Lett 1992;68:75.
[163] Silberzan P, Leger L. Phys Rev Lett 1991;66:185.
[164] Silberzan P, Leger L. Macromolecules 1992;25:1267.
[165] Krausch G. J Phys: Condens Matter 1997;9:7741.
[166] Reiter G. Phys Rev Lett 2001;87 [art. no. 186101].
[167] Seemann R, Herminghaus S, Jacobs K. J Phys: Condens Matter 2001;13:4925.
[168] Seemann R, Herminghaus S, Jacobs K. Phys Rev Lett 2001;86:5534.
[169] Redon C, Brochardwyart F, Rondelez F. Phys Rev Lett 1991;66:715.
[170] Zhao W, Rafailovich MH, Sokolov J, Fetters LJ, Plano R, Sanyal MK, et al. Phys Rev Lett 1993;70:1453.
[171] Reiter G. Langmuir 1993;9:1344.
[172] Brochard-Wyart F, Martin P, Redon C. Langmuir 1993;9:3682.
[173] Reiter G. Macromolecules 1994;27:3046.
[174] Redon C, Brzoska JB, Brochardwyart F. Macromolecules 1994;27:468.
[175] Liu Y, Rafailovich MH, Sokolov J, Schwarz SA, Zhong X, Eisenberg A, et al. Phys Rev Lett 1994;73:440.
[176] Yerushalmirozen R, Klein J, Fetters LJ. Science 1994;263:793.
[177] Shull KR, Karis TE. Langmuir 1994;10:334.
[178] Lambooy P, Phelan KC, Haugg O, Krausch G. Phys Rev Lett 1996;76:1110.
[179] Qu S, Clarke CJ, Liu Y, Rafailovich MH, Sokolov J, Phelan KC, et al. Macromolecules 1997;30:3640.
[180] Sharma A, Reiter G. J Colloid Interface Sci 1996;178:383.
[181] Mullerbuschbaum P, Vanhoorne P, Scheumann V, Stamm M. Europhys Lett 1997;40:655.
[182] Debregeas G, Martin P, Brochardwyart F. Phys Rev Lett 1995;75:3886.
[183] Brochardwyart F, Debregeas G, Fondecave R, Martin P. Macromolecules 1997;30:1211.
[184] Xie R, Karim A, Douglas JF, Han CC, Weiss RA. Phys Rev Lett 1998;81:1251.
[185] Sferrazza M, Heppenstallbutler M, Cubitt R, Bucknall DG, Webster J, Jones RAL. Phys Rev Lett 1998;81:5173.
[186] Kim HI, Mate CM, Hannibal KA, Perry SS. Phys Rev Lett 1999;82:3496.
[187] Reiter G, Khanna R, Sharma A. Phys Rev Lett 2000;85:1432.
[188] Higgins AM, Jones RAL. Nature 2000;404:476.
[189] Jacobs K, Herminghaus S, Mecke KR. Langmuir 1998;14:965.
[190] Brochard-Wyart F, Daillant J. Can J Phys 1990;68:1084.
[191] Faber TE. Fluid dynamics for physicists. Cambridge: Cambridge University Press; 1995.
[192] Vrij A. Discuss Faraday Soc 1966;42:23.
[193] Ruckenstein E, Jain RK. J Chem: Faraday Trans 1974;II:132.
[194] Koplik J, Banavar JR. Phys Rev Lett 2000;84:4401.
[195] Sharma A, Reiter G. Met Mater Processes 1998;10:287.
[196] Bischof J, Scherer D, Herminghaus S, Leiderer P. Phys Rev Lett 1996;77:1536.
[197] Herminghaus S, Jacobs K, Mecke K, Bischof J, Fery A, Ibn-Elhaj M, et al. Science 1998;282:916.
[198] Faldi A et al. Mater Sci Soc Proc 1995;366:71.
[199] Martin P, Buguin A, Brochardwyart F. Europhys Lett 1994;28:421.
[200] Konnur R, Kargupta K, Sharma A. Phys Rev Lett 2000;84:931.
[201] Higgins AM, Sferrazza M, Jones RAL, Jukes PC, Sharp JS, Dryden LE, et al. Eur Phys J E 2002;8:137.
[202] Keddie JL, Jones RAL, Cory RA. Europhys Lett 1994;27:59.

[203] Forrest JA, Dalnoki-Veress K, Stevens JR, Dutcher JR. Phys Rev Lett 1996;77:2002.
[204] Keddie JL, Jones RAL, Cory RA. Faraday Discuss 1994:219.
[205] Forrest JA, Jones RAL. In: Alamgir K, Kumar S, editors. Polymer surfaces, interfaces and thin films. Singapore: World Scientific Publishing; 2000.
[206] Horn RG, Israelachvili JN. Macromolecules 1988;21:2836.
[207] Hammerschmidt JA, Gladfelter WL, Haugstad G. Macromolecules 1999;32:3360.
[208] Luengo G, Schmitt FJ, Hill R, Israelachvili J. Macromolecules 1997;30:2482.
[209] Dalnoki-Veress K, Nickel BG, Roth C, Dutcher JR. Phys Rev E 1999;59:2153.
[210] Dalnoki-Veress K, Nickel BG, Dutcher JR. Phys Rev Lett 1999;82:1486.
[211] Geoghegan M, Krausch G. Prog Polym Sci 2003;28:261.
[212] Ibn-Elhaj M, Schadt M. Nature 2001;410:796.
[213] Service RF. Science 1997;278:383.
[214] Kargupta K, Konnur R, Sharma A. Langmuir 2000;16:10243.
[215] Zope M, Kargupta K, Sharma A. J Chem Phys 2001;114:7211.
[216] Kargupta K, Sharma A. Phys Rev Lett 2001;86:4536.
[217] Petera D, Muthukumar M. J Chem Phys 1998;109:5101.
[218] Petera D, Muthukumar M. J Chem Phys 1997;107:9640.
[219] Chen H, Chakrabarti A. J Chem Phys 1998;108:6897.
[220] Suh KY, Park J, Lee HH. J Chem Phys 2002;116:7714.
[221] Nisato G, Ermi BD, Douglas JF, Karim A. Macromolecules 1999;32:2356.
[222] Walheim S, Boltau M, Mlynek J, Krausch G, Steiner U. Macromolecules 1997;30:4995.
[223] Shapovalov V, Zaitsev VS, Strzhemechny Y, Choudhery F, Zhao W, Schwarz SA, et al. Polym Int 2000;49:432.
[224] Tanaka K, Takahara A, Kajiyama T. Macromolecules 1996;29:3232.
[225] Karim A, Slawecki TM, Kumar SK, Douglas JF, Satija SK, Han CC, et al. Macromolecules 1998;31:857.
[226] Keblinski P, Kumar SK, Maritan A, Koplik J, Banavar JR. Phys Rev Lett 1996;76:1106.
[227] Dalnoki-Veress K, Forrest JA, Dutcher JR. Phys Rev E 1998;57:5811.
[228] Geoghegan M, Jones RAL, Clough AS. J Chem Phys 1995;103:2719.
[229] Hamley IA. The physics of block copolymers. Oxford: Oxford University Press; 1998.
[230] Limary R, Green PF. Macromolecules 1999;32:8167.
[231] Limary R, Green PF. Langmuir 1999;15:5617.
[232] Masson JL, Limary R, Green PF. J Chem Phys 2001;114:10963.
[233] Wang MT, Zhu XG, Wang SX, Zhang LD. Polymer 1999;40:7387.
[234] Li Z, Qu S, Rafailovich MH, Sokolov J, Tolan M, Turner MS, et al. Macromolecules 1997;30:8410.
[235] Li Z, Tolan M, Hohr T, Kharas D, Qu S, Sokolov J, et al. Macromolecules 1998;31:1915.
[236] Loo YL, Register RA, Ryan AJ. Phys Rev Lett 2000;84:4120.
[237] Loo YL, Register RA, Ryan AJ, Dee GT. Macromolecules 2001;34:8968.
[238] Loo YL, Register RA, Ryan AJ. Macromolecules 2002;35:2365.
[239] Harrison C, Adamson DH, Cheng ZD, Sebastian JM, Sethuraman S, Huse DA, et al. Science 2000;290:1558.
[240] Knoll A, Horvat A, Lyakhova KS, Krausch G, Sevink GJA, Zvelindovsky AV, et al. Phys Rev Lett 2002;89 [art. no. 035501].
[241] Sivaniah E, Genzer J, Fredrickson GH, Kramer EJ, Xiang M, Li X, et al. Langmuir 2001;17:4342.
[242] Green PF, Limary R. Adv Colloid Interface Sci 2001;94:53.
[243] Ashok B, Muthukumar M, Russell TP. J Chem Phys 2001;115:1559.
[244] Boker A, Muller AHE, Krausch G. Macromolecules 2001;34:7477.
[245] Harrison C, Park M, Chaikin PM, Register RA, Adamson DH. J Vac Sci Technol B 1998;16:544.
[246] Park M, Harrison C, Chaikin PM, Register RA, Adamson DH. Science 1997;276:1401.
[247] Mansky P, Harrison CK, Chaikin PM, Register RA, Yao N. Appl Phys Lett 1996;68:2586.
[248] Park M, Chaikin PM, Register RA, Adamson DH. Appl Phys Lett 2001;79:257.
[249] Bucknall DG, Briggs GAD. MRS Symp Proc 2002;705:151.
[250] Henn G, Bucknall DG, Stamm M, Vanhoorne P, Jerome R. Macromolecules 1996;29:4305.

[251] Bowden N, Huck WTS, Paul KE, Whitesides GM. Appl Phys Lett 1999;75:2557.
[252] Bowden N, Brittain S, Evans AG, Hutchinson JW, Whitesides GM. Nature 1998;393:146.
[253] Chou SY, Zhuang L. J Vac Sci Technol B 1999;17:3197.
[254] Chou SY, Zhuang L, Guo LJ. Appl Phys Lett 1999;75:1004.
[255] Schift H, Heyderman LJ, Maur MAD, Gobrecht J. Nanotechnology 2001;12:173.
[256] Rayleigh R. Philos Mag 1916;32:529.
[257] Bernard H. Rev Gen Sci Pure Appl 1900;11:1261.
[258] Schaffer E, Thurnalbrecht T, Russell TP, Steiner U. Nature 2000;403:874.
[259] Lin ZQ, Kerle T, Baker SM, Hoagland DA, Schaffer E, Steiner U, et al. J Chem Phys 2001;114:2377.
[260] Schaffer E, Thurn-Albrecht T, Russell TP, Steiner U. Europhys Lett 2001;53:518.
[261] Doi M, Edwards SF. The theory of polymer dynamics. Oxford: Oxford University Press; 1986.
[262] Havlin S, Ben-Avraham D. Adv Phys 2002;51:187.
[263] Whitlow SJ, Wool RP. Macromolecules 1989;22:2648.
[264] Whitlow SJ, Wool RP. Macromolecules 1991;24:5926.
[265] Mills PJ, Green PF, Palmstrom CJ, Mayer JW, Kramer EJ. J Polym Sci B: Polym Phys 1986;24:1.
[266] Romanelli JF, Mayer JW, Kramer EJ, Russell TP. J Polym Sci B: Polym Phys 1986;24:263.
[267] Mills PJ, Palmstrom CJ, Kramer EJ. J Mater Sci 1986;21:1479.
[268] Jabbari E, Peppas NA. Macromolecules 1993;26:2175.
[269] Stamm M, Reiter G, Kunz K. Physica B 1991;173:35.
[270] Liu Y, Reiter G, Kunz K, Stamm M. Macromolecules 1993;26:2134.
[271] Russell TP. Mater Sci Rep 1990;5:171.
[272] Reiter G, Steiner U. J Phys II 1991;1:659.
[273] Geoghegan M, Jones RAL, Van Der Grinten MGD, Clough AS. Polymer 1999;40:2323.
[274] Bucknall DG, Higgins JS, Butler SA. Chem Eng Sci 2001;56:5473.
[275] Bucknall DG, Butler SA, Higgins JS. Macromolecules 1999;32:5453.
[276] Higgins JS, Butler SA, Bucknall DG. Macromol Symp 2002;190:1.
[277] Stamm M. Adv Polym Sci 1992;100:357.
[278] de Gennes PG. J Chem Phys 1971;55:572.
[279] de Gennes PG. CR Hebd Acad Sci Serie B 1980;291:219.
[280] de Gennes PG. CR Acad Sci, Ser IIb: Mec, Phys Sciences De L Univers Sciences De La Terre 1988;307:1841.
[281] Bousmina M, Qiu H, Grmela M, Klemberg-Sapieha JE. Macromolecules 1998;31:8273.
[282] Welp KA, Wool RP, Agrawal G, Satija SK, Pispas S, Mays J. Macromolecules 1999;32:5127.
[283] Graessley WW. Adv Polym Sci 1982;47:67.
[284] Green PF, Mills PJ, Palmstrom CJ, Mayer JW, Kramer EJ. Phys Rev Lett 1984;53:2145.
[285] Green PF, Kramer EJ. Macromolecules 1986;19:1108.
[286] Grayce C. J Chem Phys 1993;98:9916.
[287] Fuchs M, Schweizer KS. Macromolecules 1997;30:5133.
[288] Fuchs M, Schweizer KS. Macromolecules 1997;30:5156.
[289] Agrawal G, Wool RP, Dozier WD, Felcher GP, Russell TP, Mays JW. Macromolecules 1994;27:4407.
[290] Grayce CJ, Szamel G, Schweizer KS. J Chem Phys 1995;102:2222.
[291] Qiu H, Bousmina M. J Rheol 1999;43:551.
[292] Qiu H, Bousmina M. Macromolecules 2000;33:6588.
[293] Prager S, Tirrell M. J Chem Phys 1981;75:5194.
[294] Baschnagel J, Binder K. Macromolecules 1995;28:6808.
[295] Baschnagel J, Binder K. J Phys I 1996;6:1271.
[296] Brown HR, Russell TP. Macromolecules 1996;29:798.
[297] Beaucage G, Composto R, Stein RS. J Polym Sci B: Polym Phys 1993;31:319.
[298] Dalnoki-Veress K, Forrest JA, De Gennes PG, Dutcher JR. J Phys IV 2000;10:221.
[299] Forrest JA, Dalnoki-Veress K, Dutcher JR. Phys Rev E 1997;56:5705.
[300] Forrest JA, Dalnoki-Veress K, Stevens JR, Dutcher JR. Phys Rev Lett 1996;77:4108.
[301] Forrest JA, Dalnoki-Veress K. Adv Colloid Interface Sci 2001;94:167.

[302] Reiter G. Europhys Lett 1993;23:579.
[303] Hall DB, Hooker JC, Torkelson JM. Macromolecules 1997;30:667.
[304] Despotopoulou MM, Frank CW, Miller RD, Rabolt JF. Macromolecules 1995;28:6687.
[305] Grohens Y, Brogly M, Labbe C, Schultz J. Polymer 1997;38:5913.
[306] Frank CW, Rao V, Despotopoulou MM, Pease RFW, Hinsberg WD, Miller RD, et al. Science 1996;273:912.
[307] Sutton SJ, Izumi K, Miyaji H, Miyamoto Y, Miyashita S. J Mater Sci 1997;32:5621.
[308] Despotopoulou MM, Frank CW, Miller RD, Rabolt JF. Macromolecules 1996;29:5797.
[309] Srinivas S, Babu JR, Riffle JS, Wilkes GL. J Macromol Sci, Phys 1997;36:455.
[310] Frank B, Gast AP, Russell TP, Brown HR, Hawker C. Macromolecules 1996;29:6531.
[311] Zheng X, Rafailovich MH, Sokolov J, Strzhemechny Y, Schwarz SA, Sauer BB, et al. Phys Rev Lett 1997;79:241.
[312] Lin EK, Wu WI, Satija SK. Macromolecules 1997;30:7224.
[313] Tanaka K, Takahara A, Kajiyama T. Macromolecules 1997;30:6626.
[314] Kajiyama T, Tanaka K, Takahara A. Macromolecules 1997;30:280.
[315] Tanaka K, Taura A, Ge SR, Takahara A, Kajiyama T. Macromolecules 1996;29:3040.
[316] Kajiyama T, Tanaka K, Takahara A. Macromolecules 1995;28:3482.
[317] Toney MF, Russell TP, Logan JA, Kikuchi H, Sands JM, Kumar SK. Nature 1995;374:709.
[318] Mansfield KF, Theodorou DN. Macromolecules 1991;24:6283.
[319] Fernandez ML, Higgins JS, Penfold J, Shackleton CS. Polym Commun 1990;31:124.
[320] Wu WL, Orts WJ, Vanzanten JH, Fanconi BM. J Polym Sci B: Polym Phys 1994;32:2475.
[321] Kraus G, Gruver JT. J Polym Sci A 1965;3:105.
[322] Fetters LJ, Kiss AD, Pearson DS, Quack GF, Vitus FJ. Macromolecules 1993;26:647.
[323] Barkema GT, Baumgaertner A. Macromolecules 1999;32:911.
[324] Mcleish TCB, Allgaier J, Bick DK, Bishko G, Biswas P, Blackwell R, et al. Macromolecules 1999;32:6734.
[325] Wu WL, Wallace WE, Vanzanten JH, Bauer BJ, Liu DW, Wong A. Polymer 1997;38:2583.
[326] Geoghegan M, Boue F, Bacri G, Menelle A, Bucknall DG. Eur Phys J B 1998;3:83.
[327] Zheng X, Rafailovich MH, Sokolov J, Zhao X, Briber RM, Schwarz SA. Macromolecules 1993;26:6431.
[328] Geoghegan M, Clarke CJ, Boue F, Menelle A, Russ T, Bucknall DG. Macromolecules 1999;32:5106.
[329] Deruelle M, Leger L, Tirrell M. Macromolecules 1995;28:7419.
[330] Deruelle M, Tirrell M, Marciano Y, Hervet H, Leger L. Faraday Discuss 1994:55.
[331] Thomas NL, Windle AH. Polymer 1982;23:529.
[332] Edwards DA. J Polym Sci B: Polym Phys 1996;34:981.
[333] Grmela M, Ottinger HC. Phys Rev E 1997;56:6620.
[334] June RL, Bell AT, Theodorou DN. J Phys Chem 1991;95:8866.
[335] Snurr RQ, Bell AT, Theodorou DN. J Phys Chem 1994;98:5111.
[336] Greenfield ML, Theodorou DN. Mol Simul 1997;19:329.
[337] Greenfield ML, Theodorou DN. Macromolecules 1998;31:7068.
[338] Greenfield ML, Theodorou DN. Macromolecules 2001;34:8541.
[339] Havlin S, Ben-Avraham D. Adv Phys 1987;36:695.
[340] Haus JW, Kehr KW. Phys Rep: Rev Sect Phys Lett 1987;150:263.
[341] Kinning DJ, Thomas EL, Ottino JM. Macromolecules 1987;20:1129.
[342] Zielinski JM, Heuberger G, Wiesner U, Zhang YM. J Polym Sci B: Polym Phys 1998;36:1739.
[343] Rein DH, Csernica J, Baddour RF, Cohen RE. Macromolecules 1990;23:4456.
[344] Rein DH, Baddour RF, Cohen RE. J Appl Polym Sci 1992;45:1223.
[345] Zielinski JM, Heuberger G, Sillescu H, Wiesner U, Heuer A, Zhang YM, et al. Macromolecules 1995;28:8287.
[346] Hong SU, Laurer JH, Zielinski JM, Samseth J, Smith SD, Duda JL, et al. Macromolecules 1998;31:2174.
[347] Hong SU, Stolken S, Zielinski JM, Smith SD, Duda JL, Spontak RJ. Macromolecules 1998;31:937.
[348] Vrentas JS, Vrentas CM. Eur Polym J 1998;34:797.

[349] Grayweale AA, Henchman RH, Gilbert RG, Greenfield M, Theodorou DN. Macromolecules 1997;30:7296.
[350] Tonge MP, Gilbert RG. Polymer 2001;42:501.
[351] Hui CY, Wu KC, Lasky RC, Kramer EJ. J Appl Phys 1987;61:5137.
[352] Lasky RC, Kramer EJ, Hui CY. Polymer 1988;29:673.
[353] Lasky RC, Kramer EJ, Hui CY. Polymer 1988;29:1131.
[354] Hui CY, Wu KC, Lasky RC, Kramer EJ. J Appl Phys 1987;61:5129.
[355] Gall TP, Lasky RC, Kramer EJ. Polymer 1990;31:1491.
[356] Wu JC, Peppas NA. J Polym Sci B: Polym Phys 1993;31:1503.
[357] Gebizlioglu OS, Beckham HW, Argon AS, Cohen RE, Brown HR. Macromolecules 1990;23:3968.
[358] Argon AS, Cohen RE, Patel AC. Polymer 1999;40:6991.
[359] Argon AS, Cohen RE, Patel AC. Comput Theor Polym Sci 1999;9:339.
[360] Morrissey P, Vesely D. Polymer 2000;41:1865.
[361] Billovits GF, Durning CJ. Polymer 1988;29:1468.
[362] Dutheillet Y, Mantle M, Vesely D, Gladden L. J Polym Sci B: Polym Phys 1999;37:3328.
[363] Vesely D. Polymer 2001;42:4417.
[364] Hall DB, Torkelson JM. Macromolecules 1998;31:8817.
[365] Creton C, Brown HR, Shull KR. Macromolecules 1994;27:3174.
[366] Brown HR. Macromolecules 2001;34:3720.
[367] Shull KR, Kramer EJ. Macromolecules 1990;23:4769.
[368] Jud K, Kausch HH. Polym Bull 1979;1:697.
[369] Kausch HH, Tirrell M. Ann Rev Mater Sci 1989;19:341.
[370] Wool RP, Yuan BL, Mcgarel OJ. Polym Eng Sci 1989;29:1340.
[371] Brown HR. Macromolecules 1991;24:2752.
[372] Wool RP. Polymer interfaces—structure and strength. Munich, Germany: Hanser Verlag; 1995.
[373] Creton C, Kramer EJ, Hui CY, Brown HR. Macromolecules 1992;25:3075.
[374] Kanninen MF. Int J Fract 1973;9:83.
[375] Schnell R, Stamm M, Creton C. Macromolecules 1998;31:2284.
[376] Schnell R, Stamm M, Creton C. Macromolecules 1999;32:3420.
[377] Vorenkamp EJ, Vanruiten J, Kroesen FA, Meyer JG, Hoekstra J, Challa G. Polym Commun 1989;30:116.
[378] Boven G, Mlcm O, Challa G, Schouten AJ. Polymer 1990;31:2377.
[379] Siqueira DF, Galembeck F, Nunes SP. Polymer 1991;32:990.
[380] Boiko YM, Prud'homme RE. Macromolecules 1998;31:6620.
[381] de Gennes PG. J Chem Phys 1980;72:4756.
[382] Kim YH, Wool RP. Macromolecules 1983;16:1115.
[383] Wool RP, Oconnor KM. Polym Eng Sci 1981;21:970.
[384] Shull KR, Kramer EJ, Hadziioannou G, Tang W. Macromolecules 1990;23:4780.
[385] Thomas S, Prudhomme RE. Polymer 1992;33:4260.
[386] Russell TP, Anastasiadis SH, Menelle A, Felcher GP, Satija SK. Macromolecules 1991;24:1575.
[387] Brown HR, Char K, Deline VR, Green PF. Macromolecules 1993;26:4155.
[388] Char K, Brown HR, Deline VR. Macromolecules 1993;26:4164.
[389] Bernard B, Brown HR, Hawker CJ, Kellock AJ, Russell TP. Macromolecules 1999;32:6254.
[390] Boucher E, Folkers JP, Hervet H, Leger L, Creton C. Macromolecules 1996;29:774.
[391] Dai CA, Dair BJ, Dai KH, Ober CK, Kramer EJ, Hui CY, et al. Phys Rev Lett 1994;73:2472.
[392] Dai CA, Dair BJ, Dai KH, Ober CK, Kramer EJ, Hui CY, et al. Phys Rev Lett 1995;74:2837.
[393] Dai CA, Jandt KD, Iyengar DR, Slack NL, Dai KH, Davidson WB, et al. Macromolecules 1997;30:549.
[394] Bucknall CB. Toughened plastics. London: Applied Science Publishers; 1977.
[395] Brown HR, Deline VR, Green PF. Nature 1989;341:221.
[396] Brown HR. Macromolecules 1989;22:2859.
[397] Creton C, Brown HR, Deline VR. Macromolecules 1994;27:1774.
[398] Creton C, Kramer EJ, Hadziioannou G. Macromolecules 1991;24:1846.

[399] Washiyama J, Creton C, Kramer EJ, Xiao F, Hui CY. Macromolecules 1993;26:6011.
[400] Washiyama J, Kramer EJ, Hui CY. Macromolecules 1993;26:2928.
[401] Washiyama J, Kramer EJ, Creton CF, Hui CY. Macromolecules 1994;27:2019.
[402] Dai CA, Kramer EJ, Washiyama J, Hui CY. Macromolecules 1996;29:7536.
[403] Xu DB, Hui CY, Kramer EJ, Creton C. Mech Mater 1991;11:257.
[404] Dai CA, Osuji CO, Jandt KD, Dair BJ, Ober CK, Kramer EJ, et al. Macromolecules 1997;30:6727.
[405] Kulasekere R, Kaiser H, Ankner JF, Russell TP, Brown HR, Hawker CJ, et al. Physica B 1996;221:306.
[406] Kulasekere R, Kaiser H, Ankner JF, Russell TP, Brown HR, Hawker CJ, et al. Macromolecules 1996;29:5493.
[407] Edgecombe BD, Frechet JMJ, Xu ZH, Kramer EJ. Chem Mater 1998;10:994.
[408] Edgecombe BD, Stein JA, Frechet JMJ, Xu ZH, Kramer EJ. Macromolecules 1998;31:1292.
[409] Xu ZH, Kramer EJ, Edgecombe BD, Frechet JMJ. Macromolecules 1997;30:7958.
[410] Chen YM, Kalyon DM, Bayramli E. J Appl Polym Sci 1993;50:1169.
[411] Stralin A, Hjertberg T. J Appl Polym Sci 1993;49:511.
[412] Malpass. J Appl Polym Sci 1974;18:3249.
[413] Breznick M, Banbaji J, Guttmann H, Marom G. Polym Commun 1987;28:55.
[414] Janarthanan V, Garrett PD, Stein RS, Srinivasarao M. Polymer 1997;38:105.
[415] Lakrout H, Sergot P, Creton C. J Adhes 1999;69:307.
[416] Crosby AJ, Shull KR, Lakrout H, Creton C. J Appl Phys 2000;88:2956.
[417] Crosby AJ, Shull KR. J Polym Sci B: Polym Phys 1999;37:3455.
[418] Creton C, Lakrout H. J Polym Sci B: Polym Phys 2000;38:965.
[419] Zosel A. J Adhes Sci Technol 1997;11:1447.
[420] Chiche A, Pareige P, Creton C. CR Acad Sci Serie Iv Phys Astrophys 2000;1:1197.
[421] Creton C, Leibler L. J Polym Sci B: Polym Phys 1996;34:545.
[422] Creton C, Hooker J, Shull KR. Langmuir 2001;17:4948.
[423] Zosel A. Colloid Polym Sci 1985;263:541.
[424] Zosel A. J Adhes 1989;30:135.
[425] Brown K, Hooker JC, Creton C. Macromol Mater Eng 2002;287:163.
[426] de Gennes PG. Langmuir 1996;12:4497.
[427] Gay C, Leibler L. Phys Rev Lett 1999;82:936.
[428] Lakrout H, Creton C, Ahn DC, Shull KR. Macromolecules 2001;34:7448.
[429] Xia YN, Rogers JA, Paul KE, Whitesides GM. Chem Rev 1999;99:1823.
[430] Whitesides GM, Ostuni E, Takayama S, Jiang XY, Ingber DE. Ann Rev Biomed Eng 2001;3:335.